Microtubule Plus-End Tracking Protein and Polymerase, XMAP215, affects the Neuronal Microtubule and Actin Cytoskeletons to control Axon Outgrowth and Guidance Mechanisms

Garrett Cammarata

A dissertation submitted to the Faculty of the Biology Department

in partial fulfillment of the requirements for the degree of Doctor

of Philosophy

Boston College

Morrissey College of Arts and Sciences

Graduate School

August 2020

Abstract

While XMAP215 (CKAP5 / ch-TOG) has been best characterized for its microtubule polymerase function, recent studies have highlighted a novel role for XMAP215 in facilitating an interaction between microtubules and F-actin in the embryonic neuronal growth cone, a critical structure involved in neuronal outgrowth and guidance mechanisms. Microtubule and F-actin cytoskeletal cross talk and reorganization are important aspects of axonal guidance mechanisms, but how associated proteins facilitate this function largely remains a mystery. In addition, it has long been established that neuronal growth cone navigation depends on changes in microtubule (MT) and F-actin architecture downstream of guidance cues. However, the mechanisms by which MTs and F-actin are dually coordinated remain a fundamentally unresolved question.

Here, I report that the well-characterized MT polymerase, XMAP215 (also known as ch-TOG / CKAP5), plays an important role in mediating MT–F-actin interactions within the growth cone. I demonstrate that XMAP215 regulates MT–F-actin alignment through its N-terminal TOG 1–5 domains. Additionally, I show that XMAP215 directly binds to F-actin in vitro and co-localizes with F-actin in the growth cone periphery. By working with lab colleagues, we also find that XMAP215 is required for regulation of growth cone morphology and response to the guidance cue, Ephrin A5. Our findings provide the first strong evidence that XMAP215 coordinates MT and F-actin interaction in vivo. It is here that I suggest a model in which XMAP215 regulates MT extension along F-actin bundles into the growth cone periphery and that these interactions may be important to control cytoskeletal dynamics downstream of guidance cues.

Furthermore, I then go on to study this dual microtubule and F-actin role, diving deeper into the mechanism behind this novel ability of XMAP215. Here, I report that XMAP215 is capable of spatially localizing populations of microtubules into distinct domains in the growth cone through its less well-characterized microtubule-lattice binding activity. In addition, through the use of purified proteins and biochemical assays, I show that XMAP215 is capable of binding directly to F-actin, facilitated by its unique TOG5 domain. Finally, through biochemical means and super resolution imaging, I show that this novel function of XMAP215 is mediated by polymerase-incompetent mutants of XMAP215. Taken together, my findings show strong evidence of a non-microtubule-polymerase function of XMAP215, providing mechanistic insights into how microtubule populations can be guided by interaction with the F-actin cytoskeleton.

In conclusion, I explore a novel and functionally important role for XMAP215 in facilitating interactions between microtubule and actin cytoskeletons, bridging the two structural components of the cell together. In this way, XMAP215 is now known as a distinct microtubule/F-actin regulator that governs microtubule exploration through the help of actin in neurons, in addition to its previously characterized function as a microtubule polymerase. While this thesis explores the very groundwork of XMAP215's new novel function, there is still a great deal more to learn about the overall mechanism occurring, as well as an understanding of its role in various cell types.

Portions of abstract were adapted:

(Adapted from Slater and Cammarata et al., 2019 – Journal of Cell Science)

(Adapted from Cammarata et al., 2020 – Molecular Biology of the Cell (In Submission))

Table of Contents

Chapter 5. Appendix

I. The microtubule plus-end-tracking protein TACC3 promotes persistent axon outgrowth and mediates responses to axon guidance signals during development

II. Abelson-induced phosphorylation of TACC3 modulates its interaction with microtubules and affects its impact on axon outgrowth and guidance

III. Characterization of Xenopus laevis Guanine Deaminase reveals new insights for its expression and function in the embryonic kidney

Acknowledgements

I would like to thank everyone who has helped me along this journey, through all of the hardships, mistakes, and successes of graduate school. I think most importantly, and the only reason that I have made it this far, is from all of the kind support of everyone around me during my time at Boston College.

The first person that I have to thank is my girlfriend, Mary Alice. You have been the most wonderful source of support for me. Even though you have heard my research a million times, and could probably recite much of it better than me, you were always so attentive and an amazing source of motivation for me. Similarly, I have to thank my wonderful family members and friends. Each of you have kept me motivated (and sane) until the very end of my graduate career.

I also have to acknowledge my PI, Laura Anne, my Thesis Committee members, Sangmook Lee, my collaborators, as well as my friends and graduate student colleagues, Micaela, Beth, and Burcu. Each one of you has provided me the environment to become a great scientist, and enjoy every day that I come to work. My favorite part about graduate school has always been the friends that I have made along the way, and I will always be thankful for that.

Finally, I wanted to thank the BC Biology Dept., Animal Care Facility, and the entire faculty. There are too many people to list, but so many people have left their mark on this transformative process for me. Specifically, I wanted to thank Eric Folker for being like a secondary PI to me this last year. I am forever grateful for the help you have extended to me. Finally, I wanted to thank Welkin, Dina, Colette, Diane, and Walter, for always having the time to chat with me and make my day a little brighter.

List of Figures

List of Symbols and Abbreviations

MT = microtubule

F-actin = filamentous actin

XMAP215 = Xenopus microtubule associated protein 215

chTOG = colorectal and hepatic Tumor Overexpressed Gene

CKAP5 = Cytoskeletal Associated Protein 5

KD = knockdown

OE = overexpression

+TIP = plus end tracking protein

MAP = microtubule associated protein

EB1 = End binding protein 1

TACC3 = Transforming acidic coiled-coil 3 protein

CLASP = Cytoplasmic linker associated protein

GDA = guanine deaminase

Chapter 1. Introduction

(Adapted from Cammarata et al., 2016 – Cytoskeleton Reviews)

I. The Growth Cone

The growth cone is a dynamic structure found on the ends of growing axons, which allows axons to navigate through their environment by intercepting a myriad of extracellular cues and translating them into mechanical behaviors [1]. The structure of the growth cone is thus suitably complex, containing several compartments each with unique cytoskeletal arrangements (**Figure 1.I.1.**). The structure of the growth cone is chiefly divided into three domains (central, transitional and peripheral), which contain distinct cytoskeletal arrangements of actin filaments (F-actin) and microtubules [2]. Both of these polymers form complex arrays to create traction, transduce force, and facilitate trafficking, in order to permit proper elongation and navigation of the axon. Along the axon shaft, microtubules are tightly bundled [3–6]. Upon arrival at the growth cone central domain, their dynamic plus-ends splay more freely, growing and shrinking as they come into contact with F-actin arcs [7]. Many microtubule plus-ends are sequestered here and undergo both looping and catastrophe. Some microtubules, commonly referred to as "pioneer microtubules", break through to the peripheral domain, where they traverse through the crisscrossing F-actin lamella [6–9]. Once they have reached the periphery, these pioneer microtubules intersect and then crosslink with F-actin bundles, which are thought to guide the microtubules out to the ends of filopodia [10] (**Figure 1.I.2.**). As they journey out to the far reaches

of the growth cone together, these interacting microtubule and F-actin networks are exposed to signaling events downstream of extracellular guidance cues.

These guidance-signaling pathways directly and indirectly modify filopodial actin and microtubule networks, catalyzing mechanical movements of the growth cone. Initially, precise mechanistic interactions between signaling molecules and the growth cone cytoskeleton were not clear, and early studies focused mainly on how these cascades may specifically impact the remodeling of F-actin [11,12]. However, it had long been established that microtubules are also important for successful axon guidance [6,13–16]. Approximately a decade ago, an important set of

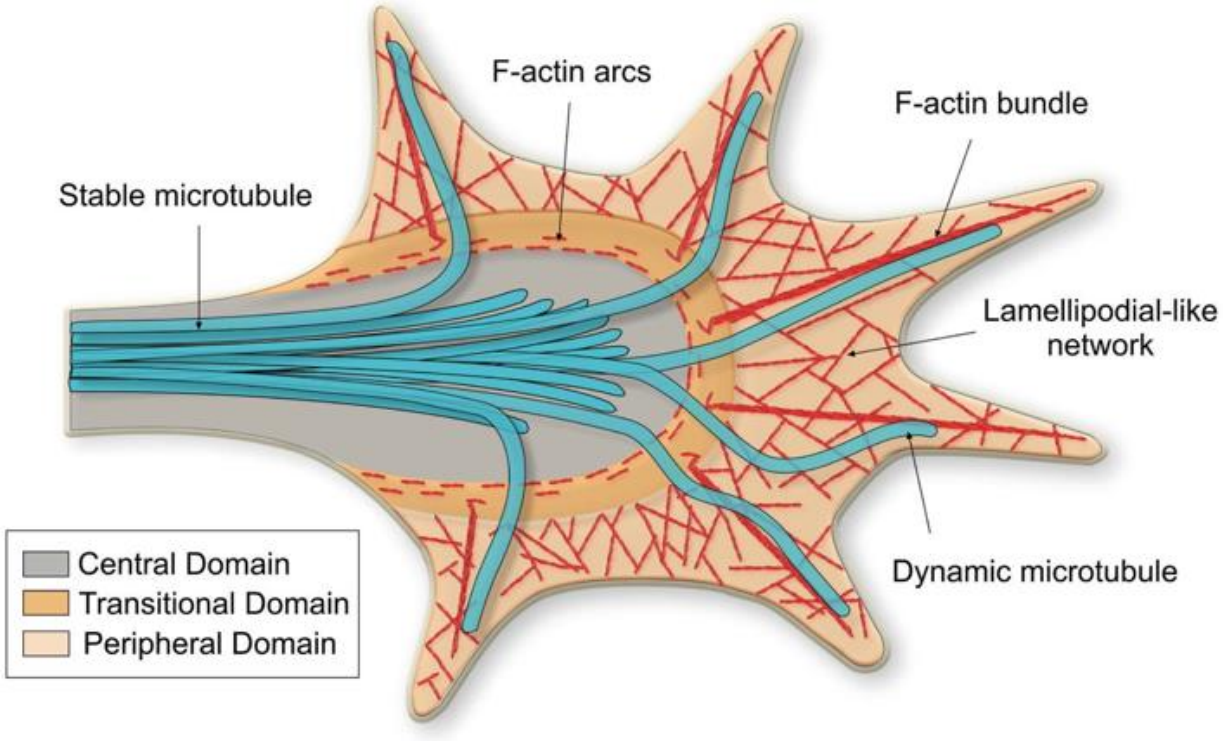

Figure 1.I.1. Overview of the different compartments of the neuronal growth cone. The growth cone is made up of several distinct compartments, each containing unique microtubule (blue) and F-actin (red) structural elements. The central domain (gray) is comprised of stable microtubules that have entered through the axon shaft and are then consolidated. These stable microtubules are hindered by F-actin arcs; structures located in the transitional domain (tan) that act as barriers for microtubule growth. Microtubules that do emerge from the transitional domain into the peripheral domain (peach) are called "pioneer microtubules". It is in this domain that pioneer microtubules are guided along F- actin bundles and traverse through a lamellipodial-like F-actin network. F-actin is orientated so that their barbed plus-ends are directed towards the leading edge of the growth cone while their pointed minus-ends are directed towards the central domain. These pioneer microtubules follow the F-actin tracks as they reach the ends of filopodia.

studies revealed that guidance signaling pathways could evoke changes in growth cone guidance by direct modification of a specific set of proteins found on the distal tips of dynamic microtubules, the plus-end tracking proteins (+TIPs) (**Figure 1.I.2.**) [17,18]. Since then, increasing evidence has accumulated that +TIPs may be important for axon guidance and turning [19]. However, their participation in these behaviors may stem from more than a single ability to interact with and regulate microtubules; many +TIPs interact with actin as well [20–23]. This affinity for both cytoskeletal networks makes +TIPs intriguing candidates as 'bilingual' networking facilitators, positioned to interact at the intersection of signaling pathway transduction and cytoskeletal remodeling. Understanding this precise junction is a dominant focus in the cell biological study of the growth cone; thus, more information is needed about how microtubules and actin work downstream of these signals and about how +TIPs may be regulating these behaviors.

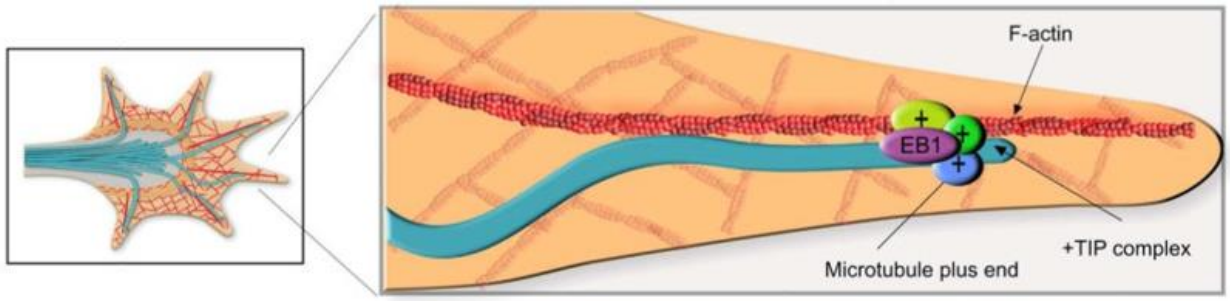

Figure 1.I.2. Microtubule and F-actin functioning in the periphery of the growth cone. A +TIP complexes allow pioneer microtubules to interact with F-actin bundles in the periphery. +TIP complex is not drawn to scale.

II. Actin Networks in the Growth Cone

Actin dynamics have classically been credited with generating the major driving force behind growth cone steering and motility. Early on, the "clutch" hypothesis was put forth [8], later described as the substrate-cytoskeletal coupling model [12,24,25], which links actin dynamics to

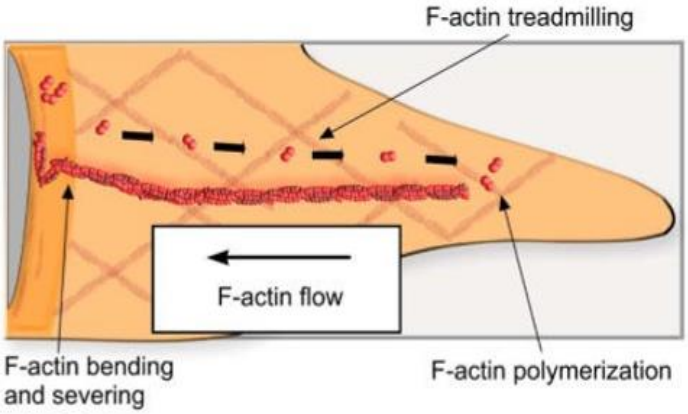

Figure 1.II.1. F-actin polymerization and retrograde flow provide a constant treadmilling of actin towards the central domain. In the transitional domain, F-actin bundles are contracted and bent by myosin motor proteins while ADF/ cofilin severs actin filaments into a pool of actin monomers. This pool provides G-actin that is then recycled back to the plus-end for F-actin polymerization.

growth cone protrusion. F-actin bundles found in the peripheral domain are oriented such that their barbed plus-ends point towards the cell membrane, while their pointed minus ends are directed towards the central domain of the growth cone (**Figure 1.II.1.**). F-actin lamellar networks are comprised of crisscrossed actin filaments, which are located in the peripheral domain (**Figure 1.I.1.**). Under the effects of F-actin retrograde flow [2,26,27], the actin filaments are simultaneously in a constant state of polymerization (at the plus-ends) and severing/depolymerization (at the minus ends). This affects protrusion and retraction of the actin filaments and corresponding protrusion and retraction of the growth cone [26,28] (**Figure 1.II.1.**). While polymerization occurs in the peripheral domain of the growth cone, F-actin buckling and severing occurs in the transition zone, likely due to mechanical strain applied by either myosin II contraction or by the pushing of F-actin assembly. F-actin severing is followed by depolymerization of F-actin fragments [27], thus allowing free actin subunits to be recycled back to the plus-end (**Figure 1.II.1.**). The interaction of actin with an adhesive substrate causes the filaments to be stabilized, reducing the rate of retrograde flow and allowing polymerization at the plus-end to dominate, resulting in net growth toward the edge of the cell [24]. However, this stability is counterbalanced by a need for dynamicity within the growth cone; developing and specified axons demonstrate an intrinsically less-stable actin network compared to developing

dendrites, and this instability is critical for rapid axonal outgrowth. This unstable actin cytoskeleton facilitates extension of microtubules into the periphery of the growth cone [29].

III. Microtubule Dynamics in the Growth Cone

Although it is widely accepted that the actin cytoskeleton provides a majority of the motile function in the growth cone, microtubules certainly do play an extensive role in axon guidance and outgrowth. This was initially shown by studies that demonstrated that microtubules were required for growth cone forward progression [6,13]. Microtubules are dynamic structures by nature, constantly undergoing periods of polymerization followed by periods of shrinking [30], which seem to assist exploratory microtubules in "feeling" around the peripheral domain and making functional connections [31]. Tubulin subunits (α/β tubulin heterodimers) are either added or removed at the microtubule plus-end by certain classes of +TIPs uniquely suited to this task (**Figure 1.II.1.**) [32,33]. (However, note that interaction of different types of +TIPs with microtubule plus-ends is quite complex and involves various processes and regulatory mechanisms. For review, see [32,34–38]). Importantly, it was demonstrated that guidance cues could affect microtubule turning behavior of the growth cone and predict overall direction of outgrowth [6,9,39–41]. Following careful local application of a microtubule stabilizing drug, Taxol, or a depolymerizing drug, Nocodazole, a growth cone could be encouraged to turn towards or away from a specific axis [16] (**Figure 1.III.1**). This led

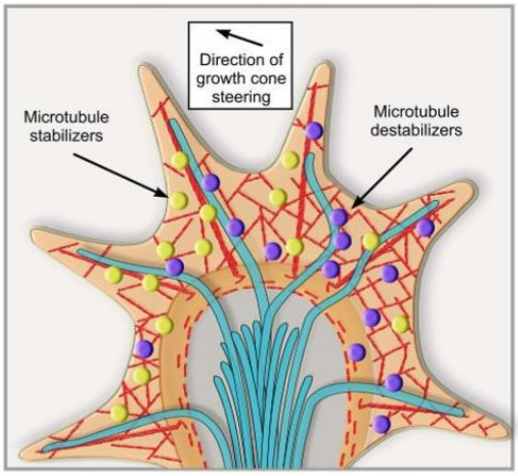

Figure 1.III.1. Microtubule stabilizers and destabilizers are able to control growth cone steering. Microtubules that bind stabilizers on a specific side of the growth cone will cause growth cone turning towards that axis (left). Conversely, destabilizing compounds, or regulated removal of stabilizing molecules, can cause repulsion or retraction from that area (right).

to the hypothesis that individual peripheral domain microtubules act as guidance sensors of the growth cone, helping to govern growth cone advancement and directionality [42].

IV. The Coupling of Microtubules to Actin Dynamics

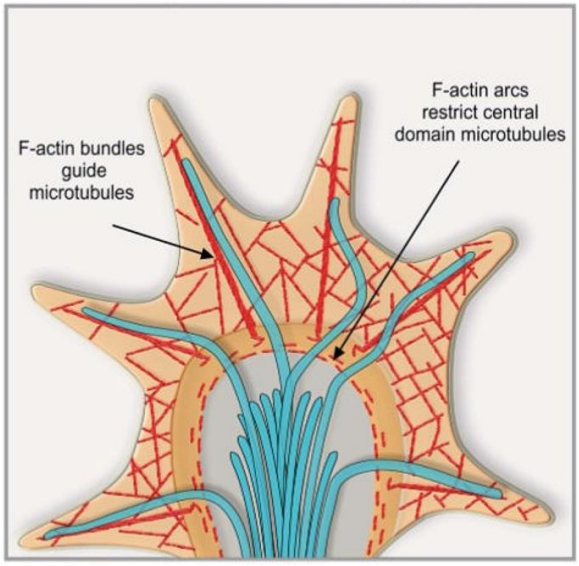

Figure I.IV.1. Microtubules interact with several distinct F-actin structures throughout the growth cone. F-actin arcs surround the central domain and restrict microtubules from exploring the periphery. F-actin bundles provide tracks for growing microtubules to follow into growth cone filopodia.

Several studies have shown a clear connection between the role of microtubules in interaction with the actin cytoskeleton and overall growth cone steering [10,43–45]. Microtubules usually follow the same path as F-actin bundles in the peripheral zone of the growth cone, leading to the idea that F-actin provides tracks for the microtubules to follow into the periphery [46] (**Figure I.IV.1.**). When actin networks were manipulated with ML-7, a myosin kinase inhibitor that produces selective loss of actin bundles and resultant growth cone collapse without significantly disrupting actin lamellipodial veils [10,41], microtubules seemed to be completely removed from the peripheral domain. In addition, growth cone turning in response to guidance cues was impaired when the F- actin structure was altered under treatment of ML-7 and cytochalasin D, an actin depolymerizer [41]. By acting as predetermined tracks for microtubule growth, actin networks may regulate or even limit microtubule advancement into the periphery [45,47] (**Figure I.IV.1.**).

Microtubules are transiently coupled to these F-actin tracks, leaving them susceptible to F-actin retrograde flow [7,48,49]. Coupling of exploratory microtubules to F-actin retrograde flow

caused a reduction in the number of microtubules to advance into the periphery [10,26,41], and furthermore, caused looping of microtubules back towards the central domain [49]. In a separate study, uncoupling of F-actin- microtubule interactions caused microtubules to progress further into the periphery [47]. The absence of F-actin bundles was not found to influence central domain microtubules; however, when F-actin arcs located in the transitional domain were disrupted, central domain microtubules were abnormally broad and irregular in appearance [47]. This suggests that the F-actin arcs create a selective barrier in the transitional zone to limit microtubule escape into the periphery (**Figure I.IV.1.**). These data indicate that F- actin-microtubule interactions can profoundly affect growth cone morphology and extension, which, in turn, suggest that regulation of these interactions may take place downstream of guidance cue interception. We postulate that +TIPs act as signaling pathway intermediates that can affect these cytoskeletal-coupling events.

V. +TIPs act as signaling transduction elements to alter cytoskeletal dynamics

Within the context of closely coupled actin and microtubule networks at the 'sensory' ends of growth cone filopodia, +TIPs are in the perfect location to act as cytoskeletal "social networking" agents. +TIPs can interact with a multitude of molecules and structures including microtubules, actin filaments, and regulatory kinases, which can induce microtubule-actin crosslinking [18,20–22,32,50]. In addition, +TIPs are very dynamic molecules and share a large interaction network with each other [32]. Furthermore, +TIPs have been demonstrated to mediate some of the F-actin-microtubule interactions that were shown to affect growth cone guidance in seminal works [21,22,50–53]. +TIPs can orchestrate transient coupling events to F-actin during microtubule polymerization, thought to guide microtubules progressing into the periphery [22] (**Figure 1.V.1.**). Excessive or enduring coupling to F-actin, through +TIP complexes, can cause

microtubules to undergo retrograde flow, and thus effectively oppose microtubule outgrowth [51–53] (**Figure 1.V.1.**). Asymmetric or spatially regulated accumulations of these +TIPs could therefore be imagined to couple microtubules to F-actin in a way that leads to axial steering of the growth cone. In this next section, we discuss some of the current evidence showing that +TIPs may work to influence growth cone guidance, in part, through the regulation of microtubule-F-actin interactions.

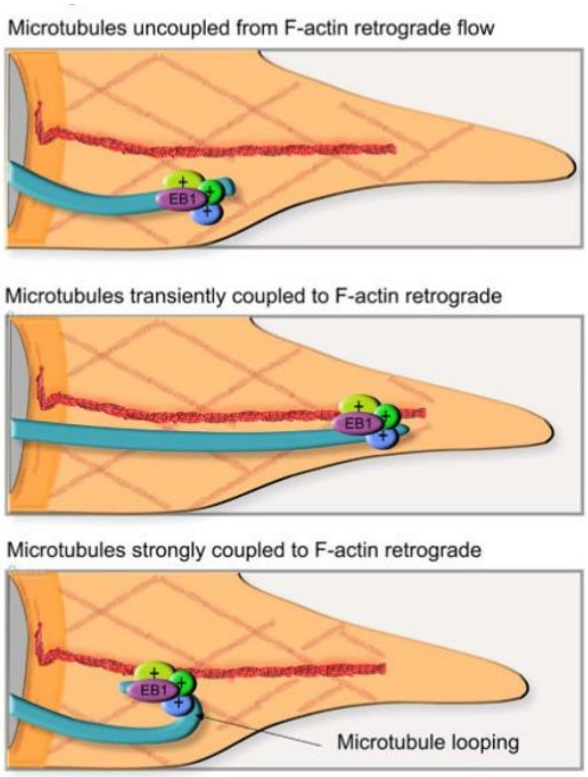

Figure 1.V.1. Microtubule protrusion and advancement into the periphery can be altered through coupling with F-actin retrograde flow. When uncoupled from retrograde F-actin flow, microtubules may progress further into the periphery through polymerization and translocation/sliding. When microtubules are transiently coupled to F-actin retrograde flow, through +TIP complexes, they follow F-actin bundles towards the ends of the filopodia. However, if microtubules are coupled strongly enough, or undergo enduring coupling, then microtubules can be translocated by F-actin retrograde flow, causing microtubule looping.

VI. Proteins Linking Microtubules to F-actin and Retrograde Flow

The first axon guidance-relevant +TIPs: CLASP/APC—The first +TIPs that were identified in directing axon guidance mechanisms were CLASP and APC [17,18]. Lee et al. showed that the CLASP1 homolog in *Drosophila* is downstream of Abl tyrosine kinase pathways [17], a signaling effector known to function downstream of repellent guidance cues. This initial study highlighted the localization of CLASP on "pioneer microtubules" in the growth cone peripheral domain,

which were previously exhibited to follow actin filaments [7–9,54] (**Figure 1.VI.1.**). Furthermore, when CLASP was overexpressed in *Xenopus laevis* growth cones, microtubules remained sequestered in the central domain and exhibited a peculiar looping phenotype [17] (**Figure 1.VI.1.**). This finding suggested that Abl signaling, in addition to its known role in actin remodeling [55–57], could affect microtubule dynamics in the growth cone periphery via its interaction with CLASP. However, whether there was any direct communication between the actin and microtubule cytoskeletons by way of CLASP regulation was not completely clear.

Later studies alluded to a more direct link between CLASP, F-actin, and microtubule behaviors. Marx et al. first demonstrated that depletion of CLASP in Xenopus leads to slower velocities of microtubules growth as they exit the axonal shaft into the growth cone [52]. This phenotype was intriguing when coupled to evidence from earlier studies that had shown CLASP's ability to bind actin and microtubules through a shared domain, and CLASP's ability to undergo retrograde flow [21]. This led them to question whether it was CLASP that might be affecting microtubule coupling to F- actin retrograde flow, in turn affecting microtubule forward velocities. While speckle microscopy did not illustrate any marked change in actin retrograde flow following CLASP depletion, both the microtubule advance in filopodial and overall actin network morphology in the lamellae were disrupted. This resulted in weakened F-actin structure as well as impaired axon outgrowth [52]. These experiments supported a functional role for CLASP-mediated microtubule-F-actin crosslinking in the growth cone.

Additional studies showed that CLASP-mediated cytoskeletal coupling could be regulated downstream of both Abl and GSK3 signaling mechanisms. Engel et al. indicated that Abl possesses the ability to phosphorylate CLASP within its microtubule and F-actin binding domain [51]. When a constitutively active form of Abl was overexpressed, CLASP localization to the plus-

end of the microtubule was decreased, and its interaction with actin rich structures in the central domain increased. Thus, it was postulated that Abl activity could trigger a 'switch' between the microtubule and actin binding properties of CLASP; when CLASP is heavily phosphorylated, microtubule plus-end affinity could be reduced, and CLASP may then be targeted to the microtubule lattice where it could facilitate microtubule-F-actin crosslinking. Similarly, GSK3, a serine/threonine kinase and Wnt downstream effector, was also demonstrated to regulate CLASP localization and actin-microtubule binding in both a positive and negative manner. It was found that highly active GSK3 caused phosphorylation of multiple sites along CLASP, prompting CLASP to dissociate from the plus-ends and reduce overall axon outgrowth [53]. The same study indicated that a moderate GSK3 kinase activity allowed CLASP plus-end binding to promote axon elongation, while low GSK3 kinase activity promoted CLASP accumulation to the lattice, thereby promoting association with F-actin retrograde flow and causing characteristic microtubule looping. CLASP lattice localization could be effectively mitigated by treatment with blebbistatin, a myosin II inhibitor that affects F-actin retrograde flow, thus permitting microtubules to extend into the periphery once again [53]. Together, these studies illustrate a critical role for dynamic, +TIP-mediated cytoskeletal crosslinking during axon outgrowth. Further evidence reveals that this role is not unique to CLASP, but is also shared by other +TIPs.

APC is another +TIP that emerged early on as an important mediator of microtubule-F-actin coupling during growth cone steering. APC promotes axon outgrowth by acting at the plus- end to stabilize microtubules [18]. Also, APC undergoes phosphorylation by GSK3 in a CLASP-like manner, and its different phosphorylation states can change its interactions with the cytoskeleton. In one study, when GSK3 was inactive, APC bound to the plus-ends of microtubules, where it stabilized and promoted their outgrowth [18]. This study demonstrated that APC-bound

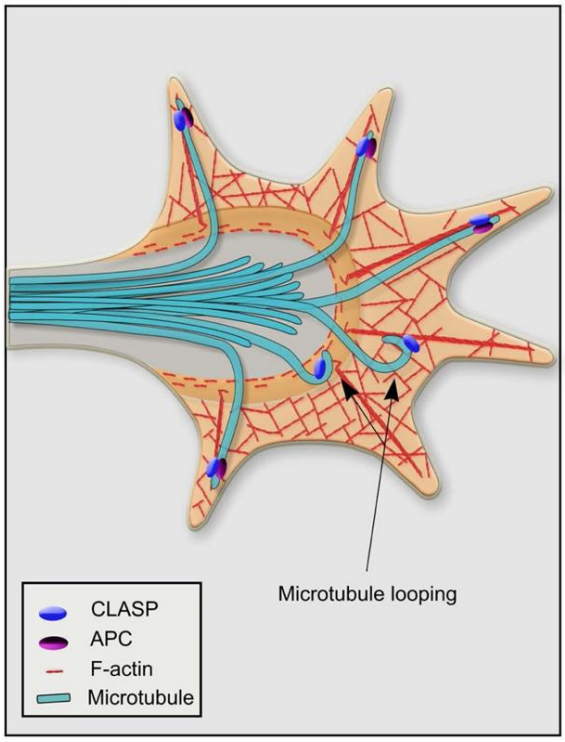

Figure 1.VI.1. Example +TIP proteins affect MT attachment to F-actin bundles. The +TIPs, CLASP and APC, are found on the plus-ends of microtubules located in the periphery of the growth cone. Asymmetric localization of both CLASP (dark blue) and APC (purple) can alter microtubule protrusion and interaction with F-actin. Together, APC and CLASP bind to the plus-end, resulting in extension of the microtubule to the ends of the filopodia.

microtubules are located primarily in the actin-rich growth cone periphery, where GSK3 activity is repressed (**Figure 1.VI.1.**). Later observations indicated that this colocalization with actin structures might be a product of APC-mediated interaction, as APC was shown to interact with actin filaments in vitro and colocalize to actin structures in fibroblasts [58]. Interestingly, APC's ability to interact with the microtubule plus-end or potentially facilitate microtubule-F-actin coupling may not only affect axon outgrowth, but also guidance and growth cone turning. APC's localization to a particular side of the growth cone caused axonal direction to change towards that side of the axis [59]. It could be speculated that spatially restricted phosphorylation downstream of a localized signaling cascade may preferentially cause APC plus-end binding and microtubule stabilization, whereas separate signaling events on the opposite side of the growth cone may prompt microtubule-F-actin coupling and slowed microtubule velocities. Furthering this notion, loss of APC localization to the MT through GSK3 signaling presented large increases in microtubule looping and loss of growth cone progression [60]. While this data supports a role for APC in microtubule-F-actin coupling, the more intricate details of its regulation within the growth cone remain to be elucidated, as studies that have examined F-actin interactions with APC focused primarily on

non-neuronal cells [58,61]. Looking beyond CLASP and APC, a number of +TIPs have also been affiliated with cytoskeletal coupling functions apart from their classical roles as microtubule regulators.

EB1/3 can connect actin-binding proteins to the plus-end and are some of the best characterized +TIPs that regulate microtubule dynamics. The binding of EB proteins in an autonomous manner at the microtubule plus-end is sufficient to affect microtubule growth speeds and catastrophe rates [62,63]. However, perhaps their most powerful regulatory role centers on their ability to act as scaffolding proteins for other +TIPs, as well as some known actin binding proteins. This ability stems from EB1's well-known SXIP motif, which acts as a microtubule tip localization signal for a variety of proteins [64]. Indeed, EB1 is necessary to recruit two of the aforementioned +TIPs, APC and CLASP, to the plus-end, in addition to recruiting other known actin modulators, such as Formins and Spectraplakins [32,64]. In addition to +TIPs, EB1/3 have been recently shown in the growth cone to interact with the classic microtubule associated protein, MAP1B [65], which, in conjunction with Tau, have been shown to interact with actin filaments and alter actin dynamics [66–68]. Interaction with MAP1B caused sequestering of EB1 and EB3 into the cytosol of the growth cone. When overexpressed, MAP1B caused reduced EB binding to plus-ends, which in turn affected microtubule dynamics [65]. Therefore, it is important to note that EB proteins may play a central role in connecting classical MAPs and +TIPs to the regulation of actin dynamics in the growth cone.

There is also strong evidence that EB3 is involved in coupling microtubules to F-actin in the growth cone through an affiliation with the actin binding protein Drebrin [22,69,70]. EB3-bound microtubules were demonstrated to follow the tracts of F-actin bundles into peripheral filopodia, closely associating with Drebrin-bound actin. When a form of EB3 was expressed that could

bind microtubules but lacked a Drebrin-interacting domain, growth cones showed arrested forward extension [22]. One recent study disputed this, indicating that a loss of Drebrin-binding caused only minimal effects [71]; but others have illustrated that a loss of this interaction could affect axon extension and actin-microtubule coupling in the growth cone [22,69,70,72]. These studies indicated that Drebrin is regulated downstream of Cdk5 and potentially PTEN phosphorylation [69,70,72,73]. Cdk5 was shown to phosphorylate Drebrin on Ser142, causing an open conformation that allowed both binding to actin filaments and EB3-microtubule interactions. Phosphorylated Drebrin was associated to a larger extent with actin filaments in the filopodia of growth cones [69,70]. Not surprisingly, phospho-mimetic mutants of Drebrin increased microtubule association with filopodial actin, while phospho-dead mutants reduced this association [69]. These data point towards an EB3-Drebrin interaction that may allow exploratory microtubules to be guided into the filopodia through their dynamic interface with F-actin bundles.

Recent data in non-neuronal cells points to another possible role for coupling of EB3 and Drebrin to F-actin. Namely, Drebrin has recently been found to compete with the actin severing protein, cofilin. Although not demonstrated in vivo or in neuronal growth cones presently, Drebrin was able to compete with cofilin for binding to actin filaments in several studies [74–76]. Mikati et al. indicated that using the neuron specific isoform, Drebrin A, could alter actin polymerization dynamics in vitro. One likely role of cofilin in the growth cone is to contribute to F-actin recycling following the severing of F-actin bundles, a process that is promoted through myosin II contractility in the transition zone and through mechanical forces created during F-actin assembly [27]. Therefore, coupling of EB3 and Drebrin to F-actin in the growth cone may potentially inhibit cofilin-severing activity. This might indirectly affect how coupled microtubules may progress into the periphery and into filopodia, though this speculative function

still needs rigorous growth cone-specific substantiation, as growth cone cytoskeletal dynamics may undergo unique regulation compared to other types of directed cell migration.

Spectraplakins are a class of proteins long shown to interact with both microtubules and actin cytoskeletons [77–82]. However, such interactions have only recently been documented to occur at microtubule plus-ends [50,80,83] and shown to do so within the growth cone [50]. Several studies have demonstrated that Spectraplakins are required for microtubule protrusion and axon outgrowth [50,84,85], as well as filopodial formation [86]. Structure-function studies of one such Spectraplakin, actin crosslinking factor 7 (ACF7), showed that it can impact microtubule organization in the growth cone, an effect that requires both microtubule and actin interaction domains [86]. Spectraplakins are guided to the plus-ends of microtubules by EB1 [50], and furthermore, actin-microtubule interactions are controlled by Spectraplakin binding through this EB1 interaction [50,87]. EB1 interactions at the plus-end conformationally change Spectraplakin shape, thus opening domains for microtubule attachment, and once in its conformationally active form, Spectraplakins preferentially bind to the microtubule lattice, where it may interact with actin filaments [50,87]. While there is much known about how Spectraplakins regulate F-actin-microtubule interactions, several aspects of this specific mechanism have not been explicitly examined in growth cones.

While interactions of Spectraplakins with other classes of +TIPs have not been rigorously examined in neurons, non-neural data indicate that such interactions may take place to modulate F-actin-microtubule coupling. There is evidence that ACF7 may act in a manner upstream of the +TIP, CLASP [88]. Furthermore, a deficiency in ACF7 resulted in disorganization of peripheral microtubule bundles [89,90], an effect that was comparable to a CLASP deficiency [91]. Similarly, Spectraplakins were also shown to interact with APC near cortical focal adhesions [92]. Taken

together with the F-actin-microtubule coupling role of these proteins individually, these data may support a more elaborate or collaborative mechanism for Spectraplakins in regulating cytoskeletal coordination.

Finally, the microtubule polymerase, XMAP215, is a +TIP protein that has only been speculated to be a potential MT/F-actin interacting protein, but no clear evidence has been put forward before now. Early on, XMAP215 was classically characterized as a microtubule growth enhancement protein [93] and, more recently, as a processive microtubule polymerase [94]. First showing some initial hints that XMAP215 could possibly interact in some way with F-actin, msps (minispindles), a Drosophila orthologue to XMAP215, was shown to genetically interact with and antagonize the activity of the actin binding +TIP, CLASP, during axon outgrowth events [95]. Subsequent studies led to the discovery that ch-TOG, the XMAP215 mammalian orthologue, interacted with the +TIPs, SLAIN1/2, CLASP and CLIPs, to increase microtubule growth rates and reduce catastrophe rates [96,97] and that the +TIP, TACC3, promoted the microtubule polymerization function of XMAP215 [98]. It has been shown more recently that TACC3, the well-known XMAP215 interactor, may interact with the branched actin modulator ENA/Vasp [99], which could potentially alter actin in the growth cone to affect axon outgrowth and guidance behaviors [100], although how this could function in combination with XMAP215 is entirely unknown.

While much of XMAP215's role as a MT polymerase has been mapped out to its various pentameric TOG (Tumor Overexpressed Gene) domains [34,94,101,102], nothing is known about how a suspected F-actin related function would be facilitated by these regions, or its less well characterized C-terminal domain [97,103,104]. In addition, it is entirely unknown if any suspected F-actin related function could co-function alongside its main polymerase function. It has been

noticed that the suspected F-actin interacting TOGL domain of CLASP shares a high sequence similarity to that of one of the TOG domains of XMAP215 [21,105]. Given that microtubule exploration of the growth cone periphery is suggested to result from frequent transient coupling with F-actin retrograde flow [106,107], it is possible that XMAP215 directly or indirectly mediates the coupling and uncoupling of microtubules to actin flow, although whether this could be independent of EB1/other +TIPs is entirely unknown. The evidence presented in this thesis work will focus on outlining the distinctive discoveries involving XMAP215's role in growth cones, and highlights a novel interaction with F-actin, governing the organization of microtubules to affect overall outgrowth and guidance mechanisms as a whole.

VII. Models for how Microtubules Interact with F-actin to Control Coupling

Although evidence for how +TIPs control axon guidance through microtubule/F-actin interaction remains in its early stages, a basic model may be put forward. While microtubules actively extend into the periphery of the growth cone, they are in regular contact with F-actin. Depending on the specific configuration of +TIPs localizing to the plus-end [18,21,22,32,50], as well as the accumulation of localized signaling molecules [6,9,41], microtubules may couple with F-actin retrograde flow through both F-actin bundles in the periphery and F-actin arcs in the transitional domain [7,41,45,47,49]. While prevention of microtubule extension through the coupling to retrograde flow would cause an inhibition of forward growth cone progression [10,26,41], it may be that an asymmetrical coupling of microtubules to F-actin throughout the growth cone causes some microtubules to progress forward while others retract, which can result in altered steering of the growth cone [108].

Some +TIPs that do couple microtubules to actin, like EB1 and the actin binding protein Drebrin, or XMAP215, may not cause microtubule looping back to the central domain, but instead allow transient coupling of microtubules along F-actin bundles [22]. This may effectively guide microtubules out alongside F-actin, thereby allowing polymerization to dominate and extend microtubules further into the periphery. This may well be the case with the MT polymerase, XMAP215, and it's specific F-actin related function in growth cones[109]. There is some evidence that the appropriate balance of these persistent or transient coupling behaviors (or alternatively, complete dissociation from the plus-end) is influenced by +TIP modifications downstream of signaling kinases [17,18,51,110], thus linking microtubule and actin behaviors to the guidance molecules encountered by the remodeling growth cone. However, as future studies investigate additional details of microtubule and F-actin interactions, more advanced models will undoubtedly be put forward.

VIII. Outline of Research Presented on XMAP215 Functioning

In this thesis work presented here, I show specifically how XMAP215, a microtubule polymerase, is capable of correctly localizing populations of microtubules in the embryonic neuronal growth cone through a previously unknown MT/F-actin interaction. Chapter 1 has focused on the background of the growth cone, the roles that MTs and F-actin play individually in growth cones, as well as how MTs and F-actin dually coordinate each other to facilitate proper cytoskeletal functioning internally. Bringing together work that was started by my collaborator, Paula Slater, in Chapter 2, I combine super resolution microscopy imaging and growth cone analysis, with biochemical assays and structure/function analysis. In this way, I determined a novel mechanism for how XMAP215 is positioning populations of MTs in the growth cone

through F-actin interaction, leading to insights into the role XMAP215 plays during axon outgrowth and guidance mechanisms. In Chapter 3, I explored more deeply this novel mechanism, highlighting the domains responsible for XMAP215/F-actin interaction, as well as how XMAP215 is utilizing this function through an uncharacterized MT lattice based localization. Finally, I show that XMAP215's function in coordinating MT populations through F-actin interactions is separate from its characteristic MT polymerase capabilities, establishing an entirely new role for XMAP215, and providing a new light in which XMAP215 can be studied from in the future.

Chapter 2. XMAP215 promotes microtubule–F-actin interactions to regulate growth cone microtubules during axon guidance

(Adapted from Slater and Cammarata et al., 2019 – Journal of Cell Science)

I. Introduction

The growth cone is a structure at the tip of the growing axon that is responsible for directing neuronal extension and guidance. Growth cone motility depends upon actin filament (F-actin) dynamics in the periphery, while growth cone steering occurs as microtubules (MTs) from the axon shaft advance in the direction of new outgrowth [111–113]. There are also dynamic MTs that explore the F-actin-rich periphery, and these MTs appear to probe along filopodial F-actin bundles as if they were tracks to follow [7,46]. There is a complicated interplay between these two cytoskeletal systems during axonal extension and guidance, and coordination between MTs and F-actin is essential for the axon to mechanically respond to extracellular guidance cues. Thus, crosstalk between these two systems is a critical component of axonal pathfinding.

Recent work has increasingly shown the importance of canonically described MT-associated proteins in facilitating regulation of interactions between MTs and F-actin within the growth cone. These studies have ascribed these roles in cytoskeletal coordination to well-characterized MT regulators TAU (also known as MAPT) and CLASP family proteins, among others, and sought to identify motifs and binding partners that facilitate MT–F-actin coordination

[19,22,52,110,114–117]. Nevertheless, many of the molecular mechanisms underlying this cytoskeletal crosstalk during axonal growth are still largely unresolved. Elucidating these mechanisms is essential for understanding how neuronal development occurs in both normal and pathological conditions.

It was shown that Xenopus microtubule associated protein 215 (XMAP215, also known as CKAP5) is important for promoting axon outgrowth as well as regulating MT trajectories within the growth cone [112]. However, it was unclear how changes in XMAP215 activity affected MT behaviors within the growth cone, although it was apparent that XMAP215 must have additional functions beyond catalyzing MT polymerization. Given that MT advancement into the growth cone periphery depends upon MT extension along F-actin bundles, I wondered whether XMAP215 might be specifically involved in the regulation of MT–F-actin interactions within the growth cone. XMAP215 family members have received significant attention as critical regulators of MT polymerization and nucleation [94,101,118–121], but there were no previous studies that examine whether XMAP215 can bind directly to F-actin or mediate MT–F-actin interactions in any system.

In this study, I used a combination of approaches, ranging from super-resolution microscopy of cultured neurons to in vitro assays with purified proteins. Here, I uncovered a critical role for XMAP215, and specifically the N-terminal TOG 1–5 domains, in regulating MT–F-actin interactions within the growth cone in Xenopus laevis embryos. In addition, with the help of imaging taken by a lab colleague, we show that XMAP215 is required for maintaining normal growth cone morphology and its accurate response to guidance cues. Finally, I demonstrate that XMAP215 can directly bind to F-actin. Thus, the work here highlights a newly discovered role

for XMAP215 in cytoskeletal coordination and steering of the axonal growth cone during embryonic development.

II. RESULTS

XMAP215 knockdown leads to global morphological changes in the growth cone and defects in axon guidance

Previous studies demonstrated that XMAP215 is important for promoting axon outgrowth but did not provide thorough characterization of the growth cone phenotype after XMAP215 knockdown [112]. It was at this point that Paula Slater, a collaborator on this work, utilized neuronal explant culturing and microscopy to determine morphological changes in the growth cone. When XMAP215 levels were knocked down by 70% in X. laevis embryos (XMAP215 KD hereafter) (**Fig. 2.S.1A**), it was observed that distinct and unexpected phenotypic changes in the growth cone occurred (**Fig. 2.S.1B**). The most noticeable effect of XMAP215 KD was increased area of the growth cone by 52% (**Fig. 2.II.1A**; **Fig. 2.S.1B, C**). Additionally, while the number of growth cone filopodia was not significantly altered (**Fig. 2.II.1B**), XMAP215 KD resulted in increased filopodia mean length by 43% (**Fig. 2.II.1C**). These phenotypes were rescued by concomitant expression of XMAP215–GFP mRNA in the KD condition (**Fig. 2.II.1A, C**), suggesting that the XMAP215 is necessary and sufficient to maintain normal growth cone morphology.

Axon pathfinding is a dynamic process consisting of growth cone exploratory movements, in which the growth cone pauses before advance, retraction or turning. Growth cone pauses are characterized by an increase in growth cone area and filopodia length, compared to rapidly

advancing growth cones [6,122]. As XMAP215 KD also results in larger growth cones and longer filopodia, it was next investigated whether XMAP215 KD leads to changes in parameters of

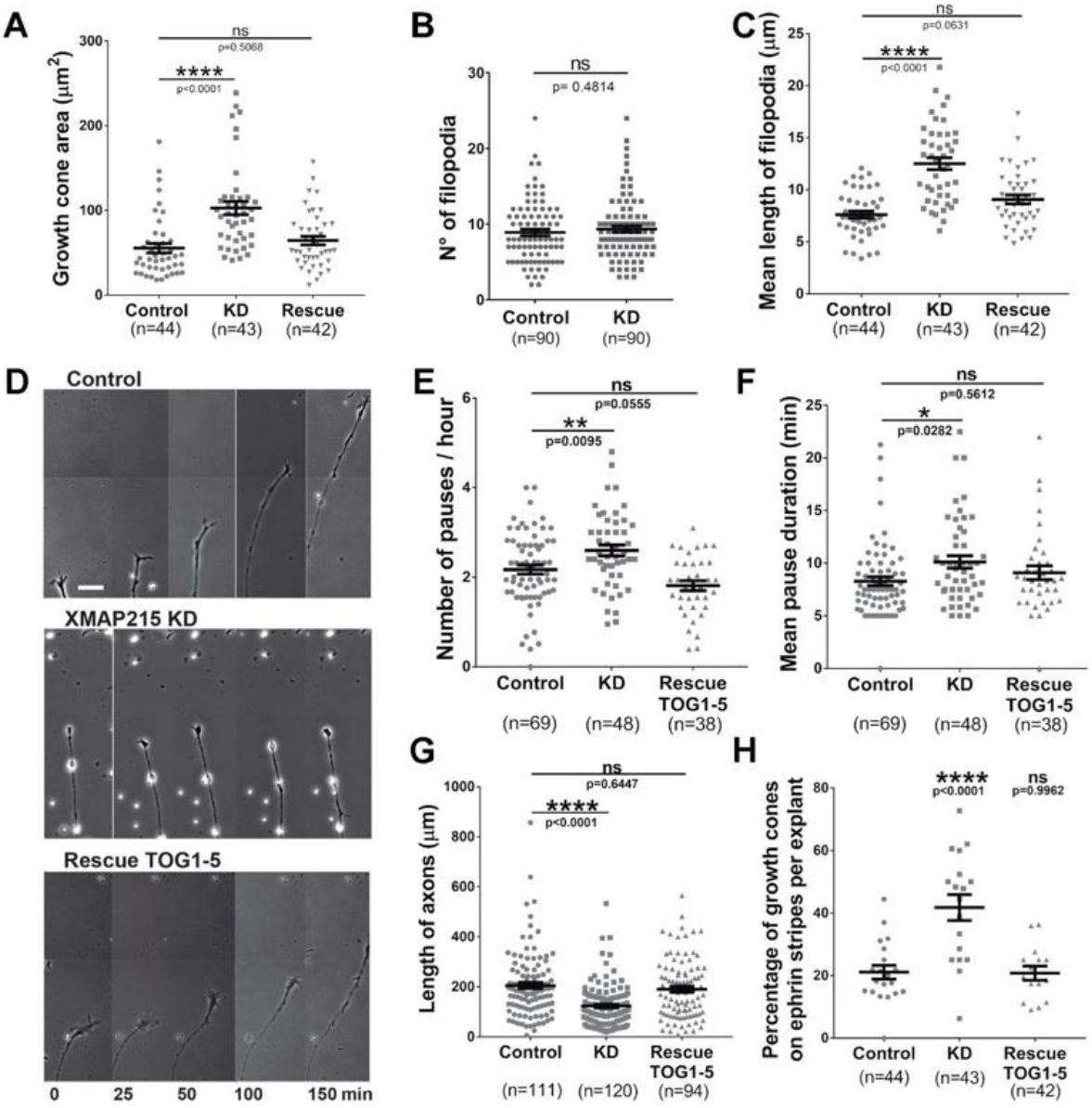

Figure 2.II.1. XMAP215 KD leads to global growth cone phenotypic changes and guidance defects. (A–C). XMAP215 KD induces growth cone pausing-like morphology. XMAP215 KD increases growth cone area (A), has no effect on number of filopodia (B), and increases the mean length of filopodia (C). See Fig. S1C for more information regarding how the quantifications were performed. (D–F). XMAP215 KD increases number and duration of growth cone pauses. (D) Time- lapse montage of representative axons from control, XMAP215 KD and XMAP215 KD rescued by expression of TOG1–5. Scale bar: 25 μm. XMAP215 KD increases the number of pauses per hour (E) and the mean pause duration (F). (G,H) TOG1–5 rescues the axon outgrowth parameters affected by XMAP215 KD.(G) XMAP215 XMAP215 KD increases the percentage of growth cones on Ephrin A5 stripes per explant. See Fig. S2C for representative images. *P<0.05; **P<0.01; ****P<0.0001; ns, not significant, from a one-way ANOVA analysis comparing multiple conditions, and from a Student's t-test when comparing XMAP215 KD to control. Data presented as mean±s.e.m.

growth cone pausing (**Fig. 2.II.1D-F**). It was determined that XMAP215 KD led to a 20% increase in the number of growth cone pauses per hour (**Fig. 2.II.1E**) and a 22% increase in the duration of the pauses (**Fig. 2.II.1F**) compared to a control condition. In addition, we were able to rescue these phenotypes by concomitant expression of the XMAP215 N-terminal TOG1–5 domains (TOG1–5 hereafter) to the KD condition (**Fig. 2.II.1E, F**). Furthermore, it was determined that expression of the XMAP215 N-terminus could rescue the decrease in overall axon length and axon outgrowth that is observed with XMAP215 KD (**Fig. 2.II.1G**).

Next, I wanted to determine whether XMAP215 KD might affect axon guidance in addition to outgrowth. Stripe assays have been widely used to study the responsiveness of growing axons to external cues [123–125]. My collaborator investigated the effect of XMAP215 KD on axon guidance by determining whether cultured axons avoided stripes containing the repellent guidance cue Ephrin A5. There was a twofold increase in the number of growth cones per explant that were trespassing on Ephrin A5 stripes when comparing XMAP215 KD cells to controls (**Fig. 2.II.1H**). Importantly, this guidance defect was rescued by concomitant expression of exogenous TOG1–5 along with XMAP215 KD (**Fig. 2.II.1H**). These results suggest that normal levels of XMAP215 expression are necessary for axons to be responsive to Ephrin A5 and, thus, for correct axon guidance.

XMAP215 KD disrupts MT organization in the growth cone

It was previously demonstrated that partial XMAP215 KD led to abnormal MT trajectories within the neuronal growth cone [112]. The mechanism by which this occurred was unclear, but it seemed likely that XMAP215 might display another function in growth cones other than simply acting as a catalytic MT polymerase [112]. Thus, we sought to further investigate and quantify

several MT parameters in axonal growth cones after XMAP215 KD. Because X. laevis neurons express very high levels of XMAP215 compared to other cell types, knocking down XMAP215 by 70% still allows for sufficient XMAP215 to facilitate MT polymerization, while also resulting in abnormal MT behaviors specifically in growth cones [112]. MT dynamics vary depending on axonal behaviors [126]; during pausing periods, growth cones present looped or bundled MTs,

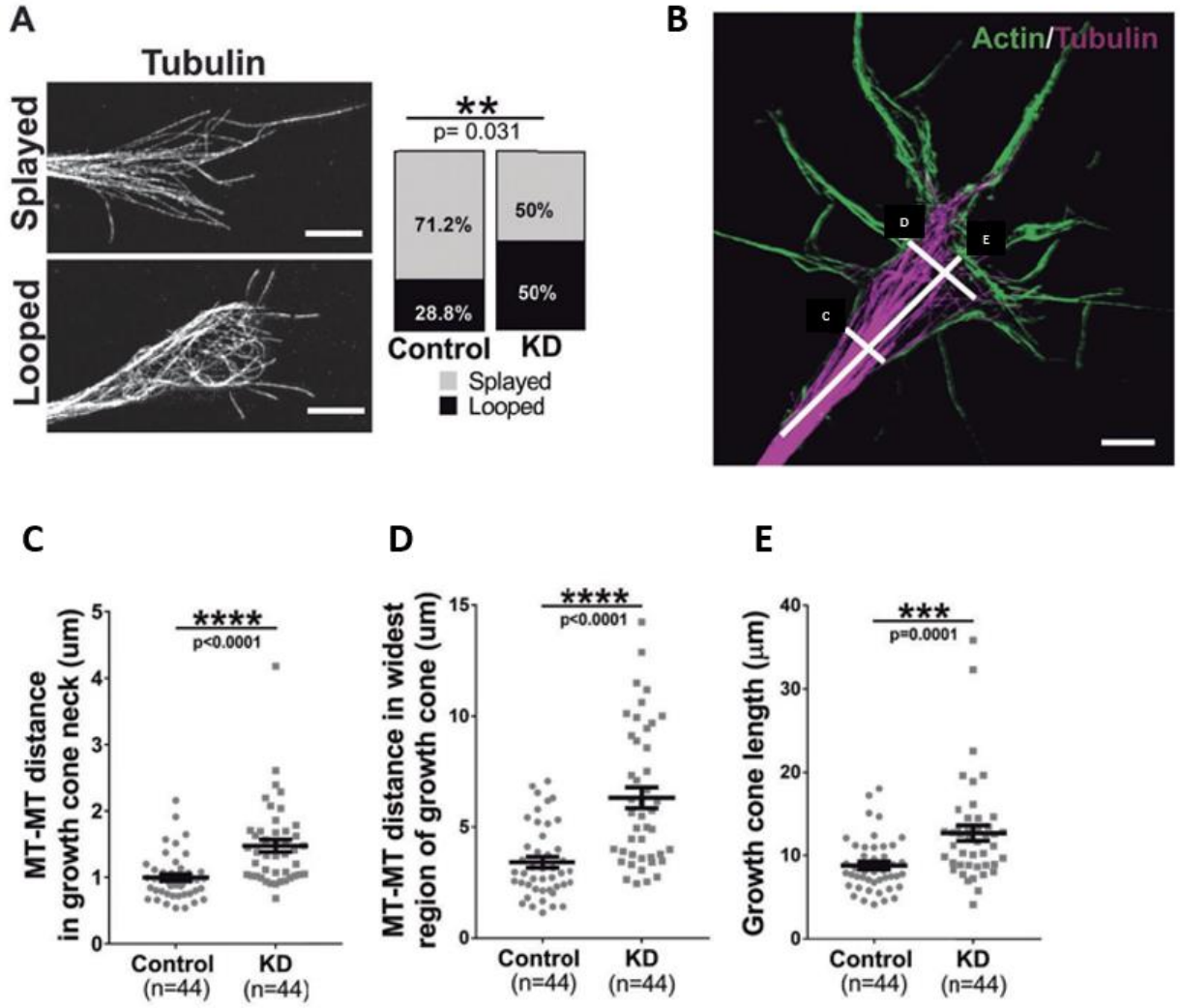

Figure 2.II.2. XMAP215 KD disrupts MT organization in the growth cone. (A) Representative SIM images of growth cone MTs considered as 'splayed' and 'looped'. XMAP215 KD increases the MT looped morphology compared to controls. Scale bar: 3 μm. (B) Representative SIM image of growth cones stained for actin and tubulin. The labeled lines letter indicate how the MT measurements were performed for the corresponding plots in C-E. Scale bar: 8 μm. (C-E) Quantification of the different MT parameters. XMAP215 KD increases the MT–MT distance in growth cone neck (C), the MT–MT distance in the growth cone's widest region (D), as well as the growth cone length (E). **P<0.01; ***P<0.001; ****P<0.0001; ns, not significant, from a Student's t-test comparing XMAP215 KD to control. Data presented as mean±s.e.m.

which then reorganize into splayed MTs during growth cone advance [127,128]. MT morphology was then quantified by Paula Slater, and the percentage of growth cones presenting 'splayed' versus 'looped' MTs after tubulin staining was counted, as previously described [14]. XMAP215 KD axons displayed a significant increase in the number of growth cones presenting a looped morphology (almost twice as many as in controls) (**Fig. 2.II.2A**). Finally, the distribution of MTs within the growth cone was assayed using structured illumination microscopy (SIM) imaging. There was an observed 48% increase in MT spreading within the growth cone neck after XMAP215 KD and an 85% increase in the widest part of the central domain (**Fig. 2.II.2B-E**). Moreover, XMAP215 KD resulted in a 44% increase in the overall length of the growth cone, from axon shaft to end of the central domain (**Fig. 2.II.2E**). These results demonstrate that XMAP215 regulates MT organization in terms of morphology, dynamicity and distribution throughout the growth cone.

XMAP215 promotes penetration of MTs into growth cone filopodia

We next wanted to investigate whether XMAP215 regulates MT penetration into the peripheral domain of the growth cone. We overexpressed (OE), and knocked down XMAP215 in X. laevis embryos and analyzed axonal growth cone MTs and F-actin. We collected SIM images after immunostaining for F-actin and tubulin and counted the number of 'exploring' MTs, which are defined as MTs that extend beyond the central domain of the growth cone, into the actin-rich peripheral domain (**Fig. 2.II.3A**; **Fig. 2.S.2A, B**). To determine whether these exploring MTs were able to enter filopodia, the number of MTs present in filopodia were counted (**Fig. 2.II.3D-**

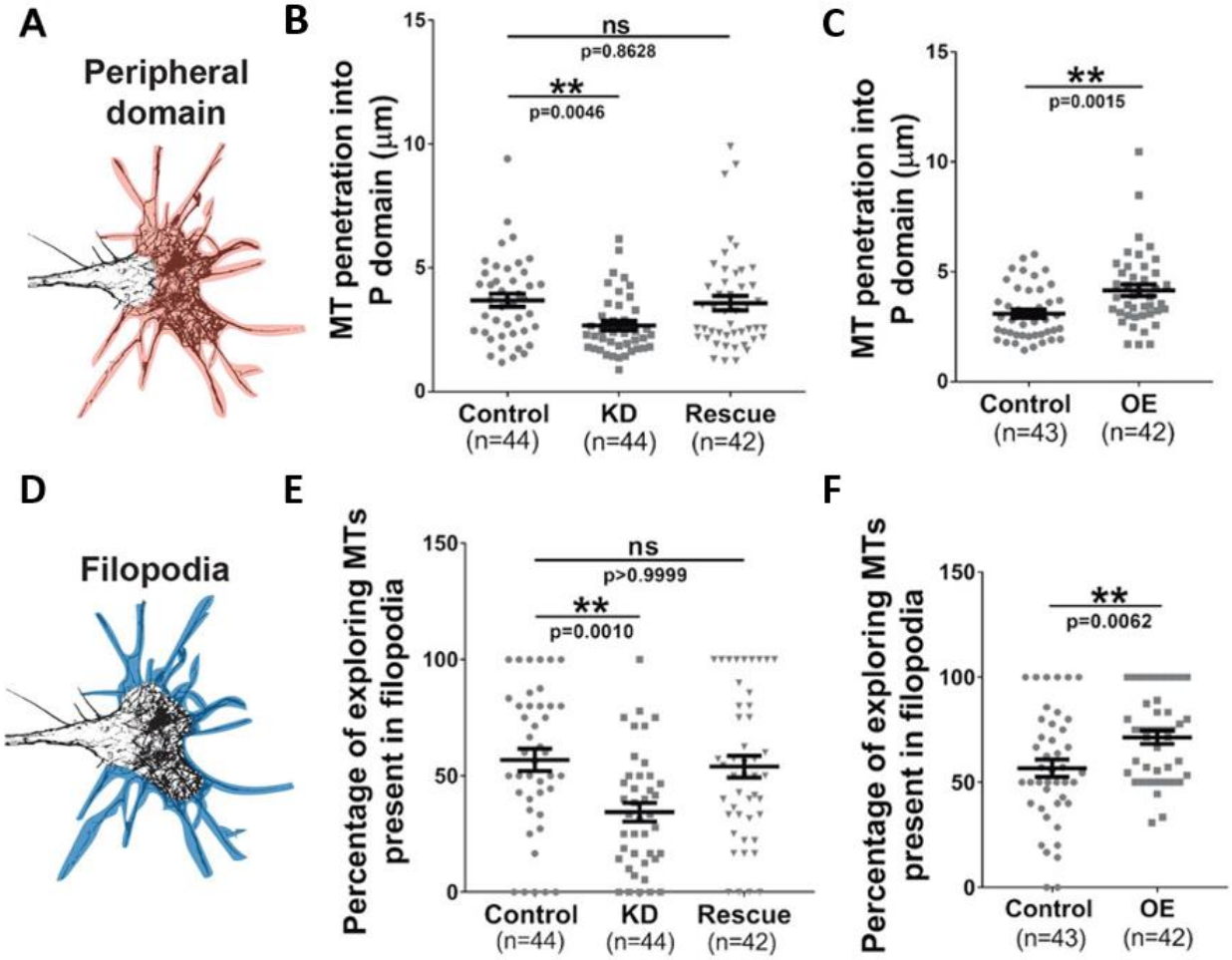

Figure 2.II.3. XMAP215 promotes penetration of MTs into growth cone filopodia. (A,B) Growth cone mask images outlining the growth cone peripheral domain colored in orange (A), and the filopodia colored in blue (B). C) Quantification of MT penetration into the actin-rich peripheral domain of the growth cone after XMAP215 knockdown (KD) or overexpression (OE). D) Quantification of the percentage of exploring microtubules present in filopodia after KD or OE. XMAP215 KD effects were rescued by co-expression of KD-resistant XMAP215–GFP mRNA. **P<0.01; ****P<0.0001; ns, not significant, from a one-way ANOVA analysis comparing XMAP215 KD, XMAP215 rescue and control, and from a Student's t-test comparing XMAP215 OE to control.

F), as well as measured the extent of penetration of these MTs into the peripheral domain (**Fig. 2.S.2A-C**). With XMAP215 KD, there was a 23% decrease in the number of MTs that were present specifically within filopodia (**Fig. 2.II.3E**). By contrast, the data showed a 26% increase in the number of MTs within filopodia upon XMAP215 OE (**Fig. 2.II.3F**). MT penetration into the peripheral domain was 28% less with XMAP215 KD (**Fig. 2.II.3B**) and 35% greater with XMAP215 OE (**Fig. 2.II.3C**).

As XMAP215 is a well-characterized MT polymerase, we wondered whether there might be a change in the number of total growing MTs within the growth cone that may be accounting for the change in the percentage of microtubules reaching filopodia. For this purpose, along with XMAP215 KD or OE, we concomitantly expressed GFP–MACF43, which binds growing MT plus-ends [64], and used automated imaging analysis to quantify the number of GFP–MACF43 comets in high-resolution live images. Despite observing more broadly distributed GFP–MACF43 trajectories within the XMAP215 KD growth cones compared to controls (**Fig. 2.II.4A**), there were no significant differences in the number of growing MTs in XMAP215 KD growth cones (**Fig. 2.II.4B**). Thus, with the levels of XMAP215 protein that are present in our partial KD condition, the number of MTs undergoing polymerization is not negatively affected, although MTs are unable to properly penetrate into filopodia. It is also important to note that this lack of MT penetration is not due to reduction in MT polymerization rate, as it was previously shown that MT polymerization rate was not significantly reduced with partial XMAP215 KD in these growth cones [112].

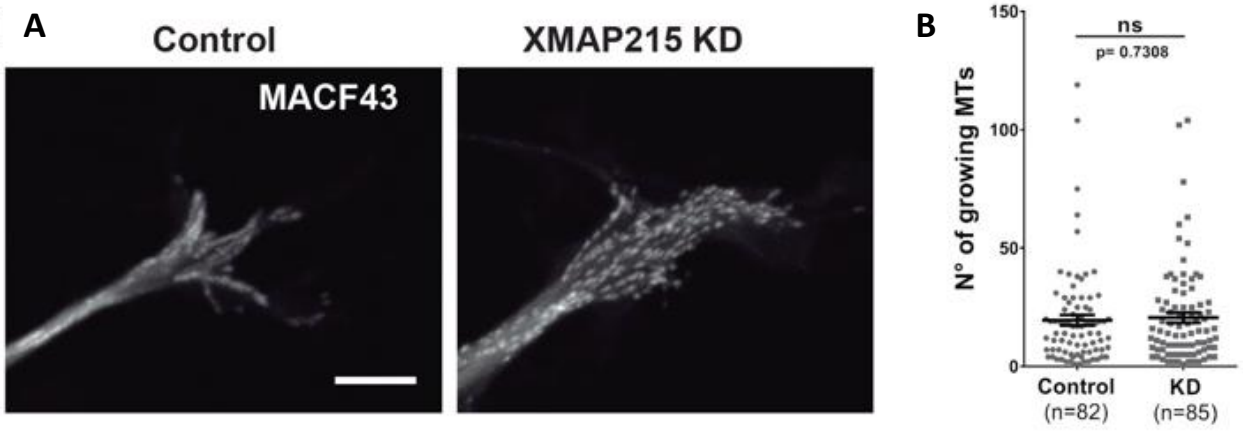

Figure 2.II.4. XMAP215 partial KD does not affect MT polymerization rates in the growth cone. No difference was observed between XMAP215 KD and control when comparing the number of growing MTs. ns, not significant from a Student's t-test analysis. Data presented as mean±s.e.m.

XMAP215 is required for normal MT–F-actin alignment in growth cones

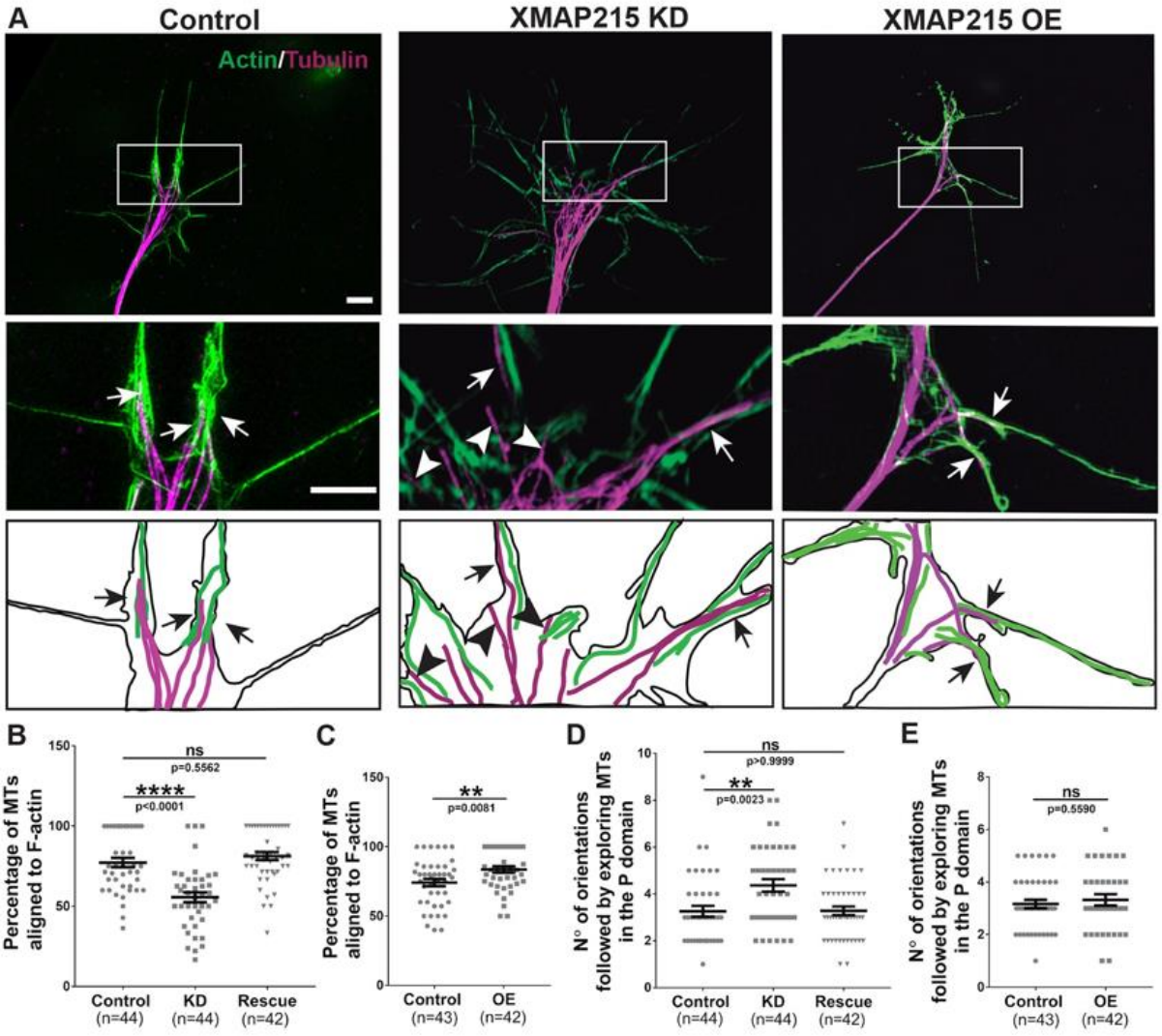

Figure 2.II.5. XMAP215 is required for normal MT–F-actin alignment in growth cones. (A) Top: representative SIM images of growth cones from control, XMAP215 KD and XMAP215 OE neural explants stained for actin and tubulin. Scale bar: 8 µm. Middle insets: magnification of the boxed region of interest in the upper panels. Scale bar: 3 µm. Arrows point to MTs that are aligned with F-actin, while arrowheads point to exploring MTs that are not aligned with F-actin. Bottom insets: 'camera lucida'-type depictions with subtracted background and highlighted MTs and F-actin. (B,C) XMAP215 KD decreases (B) while XMAP215 OE increases (C) the percentage of exploring MTs aligned to F-actin, compared to controls. (D,E). XMAP215 KD increases (D) while XMAP215 OE does not affect (E) the number of orientations followed by exploring MTs in the growth cone peripheral (P) domain. **P<0.01; ****P<0.0001; ns, not significant, from a one-way ANOVA analysis comparing multiple conditions, and from Student's t-test comparing XMAP215 OE to control. Data presented as mean±s.e.m.

MT trajectories and penetration into the peripheral domain depend upon MT extension along F-actin bundles. Thus, we wondered whether XMAP215 might play a role in MT alignment to F-

actin bundles in the growth cone periphery. Upon XMAP215 KD, there was a 28% decrease in the percentage of F-actin-aligned MTs, compared to controls (**Fig. 2.II.5A, B**), while there was a 16% increase in F-actin-aligned MTs in the case of XMAP215 OE (**Fig. 2.II.5C**). It was noted that there were some MT plus-ends that were nowhere close to bundled F-actin in the XMAP215 KD condition (**Fig. 2.II.5A**, arrowheads). These results suggest that XMAP215 promotes MT–F-actin alignment in the growth cone. As trajectories of MTs within the growth cone are normally restricted to following F-actin bundles [7,46], we quantified the number of different MT orientations within the growth cone after XMAP215 KD. We defined the orientations as being different if the direction followed by the tip of a MT forms an angle greater than 30° with other neighboring MTs, and angles were measured with respect to a central line that follows the growth direction of the axon. We observed that XMAP215 KD led to a 34% increase in the number of unique orientations followed by exploring MTs in the peripheral domain in comparison to controls (**Fig. 2.II.5D**), while XMAP215 OE did not generate any changes (**Fig. 2.II.5E**). Taken together, these results suggest that XMAP215 is important for MT spatiotemporal guidance along F-actin tracks within growth cones. Additionally, the MT–F-actin alignment defects were rescued by co-expression of KD-resistant XMAP215–GFP mRNA (**Fig. 2.II.5B, D**), attributing these effects specifically to XMAP215. Furthermore, all of the aforementioned experiments were completed using another antisense oligonucleotide to knock down XMAP215 and obtained similar results (data not shown), suggesting that the observed effects of XMAP215 KD on MT–F-actin alignment was not because of off-target effects of the antisense oligonucleotide.

The N-terminus of XMAP215 is necessary and sufficient to promote MT–F-actin alignment

Several previous studies have determined that the XMAP215 N-terminal domain [TOG1–5, amino acids (aa) 1–1460] is composed of five TOG domains that bind tubulin dimers [34,94,101] and a MT lattice-binding domain that comprises the region between TOG4 and TOG5 as well as

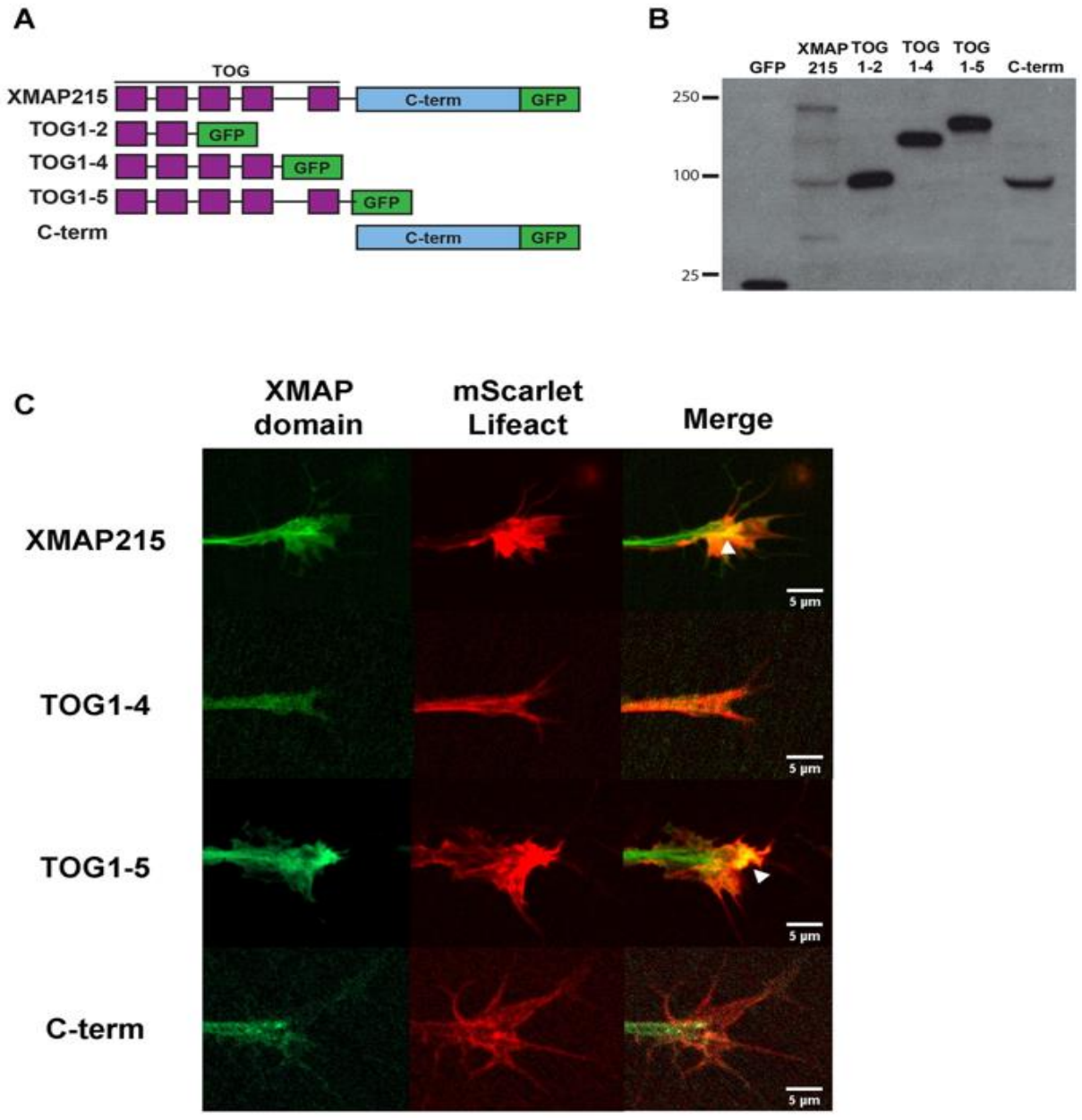

Figure 2.II.6. The N-terminal TOG1–5 domains of XMAP215 are necessary and sufficient to localize to F-actin in the growth cone periphery. (A) Schematic representation of the GFP-tagged XMAP215 domain constructs used, showing full-length XMAP215, XMAP215 domains TOG1–2, TOG1–4, TOG1–5 and C-terminal region (C-term). (B) Western blot showing the expression of the different XMAP215 domain constructs in Xenopus embryo lysates. (C) Representative confocal images showing localization of GFP-tagged XMAP215 mutants (green) and F-actin (red) in the growth cone. White arrowhead in full-length XMAP215 and TOG1–5 merged panels denote XMAP215 and actin fluorescence co-localization. Scale bar: 5 µm. (See Movies 1–4).

part of TOG5 [101]. Additionally, the TOG1–2 region is known for being responsible for the MT polymerase activity [101]. The C-terminal domain (aa 1461–2070) is conserved and known to bind the protein TACC3 [103,129], and is important for XMAP215 localization at centrosomes [104,130,131]. It was also recently shown to be required for MT nucleation and direct binding to gamma-tubulin [120]. To investigate which domain(s) of XMAP215 are responsible for promoting MT–F-actin alignment, I generated a series of XMAP215 deletion constructs (similar to those previously described in Widlund et al., 2011) (**Fig. 2.II.6A**) and expressed them in X. laevis embryos (**Fig. 2.II.6B**). I first compared their localizations in the growth cone in conjunction with F-actin (mScarlet–Lifeact) using time-lapse imaging, and I observed that each XMAP215 deletion mutant displayed unique localizations (**Fig. 2.II.6C**; Movies 1– 4). Both XMAP215 full-length (FL) and the TOG1–5 construct displayed characteristic MT lattice binding, which has previously been observed in these growth cones [112]. However, there was little to no MT plus-end tracking seen with the TOG1–5 construct (Movie 3). While the XMAP215 C-terminal domain did display distinct MT plus-end tracking localization (likely due to C-terminal domain interaction with endogenous TACC3), the localization did not overlap with F-actin in the periphery (Movie 4). Most strikingly, there was a clear co-localization pattern of XMAP215-FL and TOG1–5 with F-actin in the growth cone periphery (**Fig. 2.II.6C**, white arrowheads), while the TOG1–2 and TOG1–4 constructs did not show this co-localization with F-actin (they displayed only diffuse localization throughout the growth cone). This localization data suggests that a region within TOG1–5 is required for XMAP215 co-localization with F-actin in growth cones.

Then (with the help of my lab colleagues' growth cone imaging data), we determined whether expression of each mutant could rescue the MT–F-actin alignment phenotype of the

XMAP215 KD condition (**Fig. 2.II.7A**). Of all the deletions, only the TOG1–5 rescue had a similar growth cone MT phenotype to that of the control and the rescue with XMAP215 full length (**Fig. 2.II.7A**). In addition, expression of TOG1–5 was able to rescue the percentage of

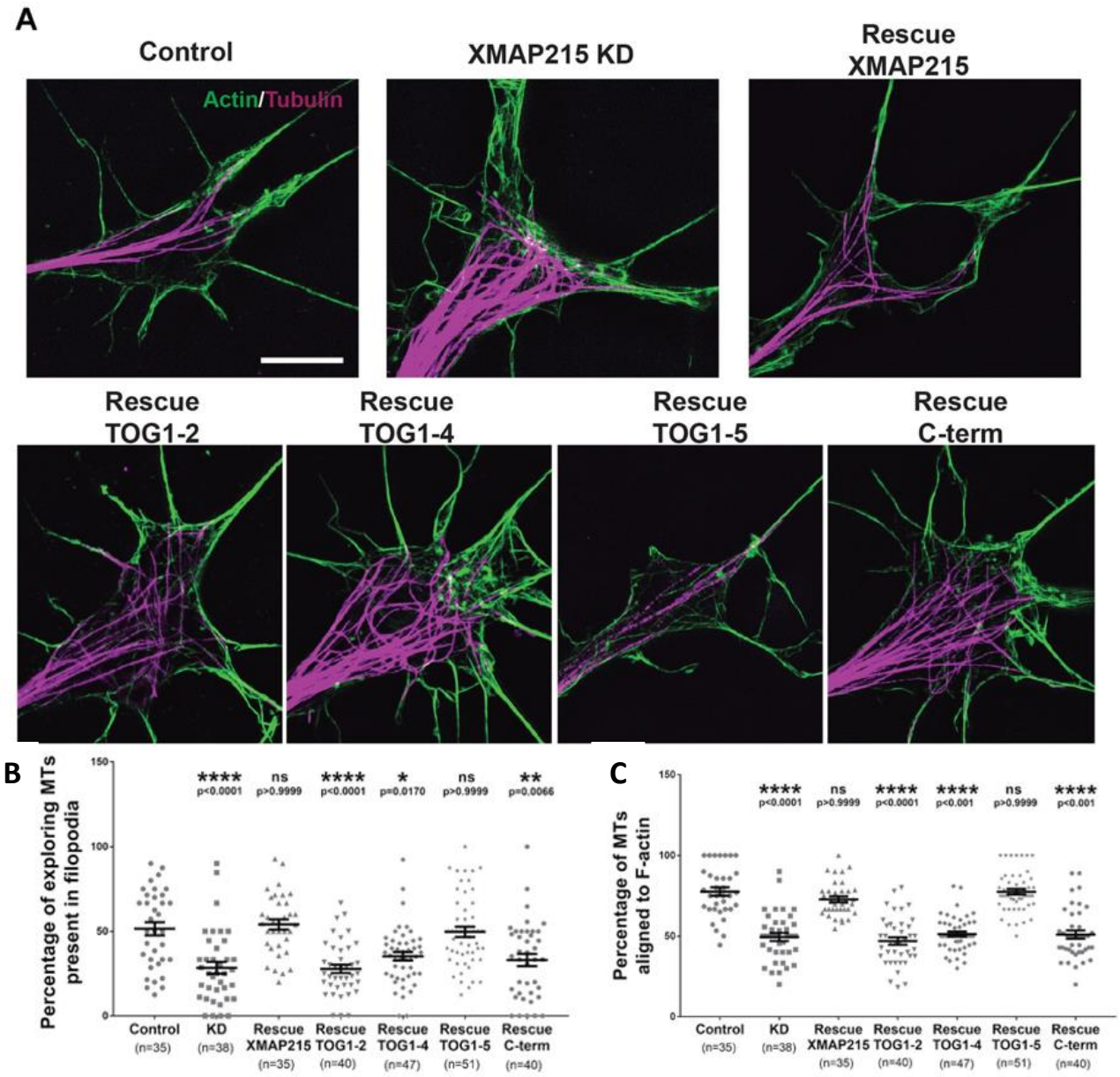

Figure 2.II.7. The N-terminal of XMAP215 is necessary and sufficient to promote MT–F-actin alignment. (A) Representative SIM images of growth cones from control, XMAP215 KD and XMAP215 KD rescue with the XMAP215 domain constructs as indicated. Scale bar: 5 µm. (B–E) Determination of the XMAP215 domain responsible for MT–F-actin alignment. Expression of TOG1–5, but not TOG1–2, TOG1–4 or C-term, rescues the increase in the number of exploring MTs (B), the decrease in the percentage of MTs aligned to F-actin (C), the increase in the number of orientations followed by exploring MTs in the peripheral (P) domain (D), and the decrease in the percentage of exploring MTs present in filopodia (E), induced by XMAP215 KD. *P<0.05; **P<0.01; ***P<0.001; ****P<0.0001; ns, not significant, from a one-way ANOVA analysis. Data presented as mean±s.e.m.

MTs aligned to F-actin (**Fig. 2.II.7C**), and the percentage of MTs present in filopodia (**Fig. 2.II.7B**), to a similar extent to that of XMAP215 full length (**Fig. 2.II.7A-C**). These results are consistent with the localization data and suggest that the region comprising all five TOG domains is both necessary and sufficient for XMAP215 to promote MT–F-actin alignment in the growth cone.

XMAP215 can interact with F-actin directly, but does not affect F-actin bundles

Given previous findings that XMAP215 promotes the ability of MTs to enter filopodia (**Fig. 2.II.3**) and promote MT alignment to F-actin bundles (**Fig. 2.II.5**), I wondered whether XMAP215 might directly bind to F-actin. Thus, I first tested for XMAP215–F-actin binding using an F-actin co-sedimentation assay, and, intriguingly, I observed that XMAP215 is able to

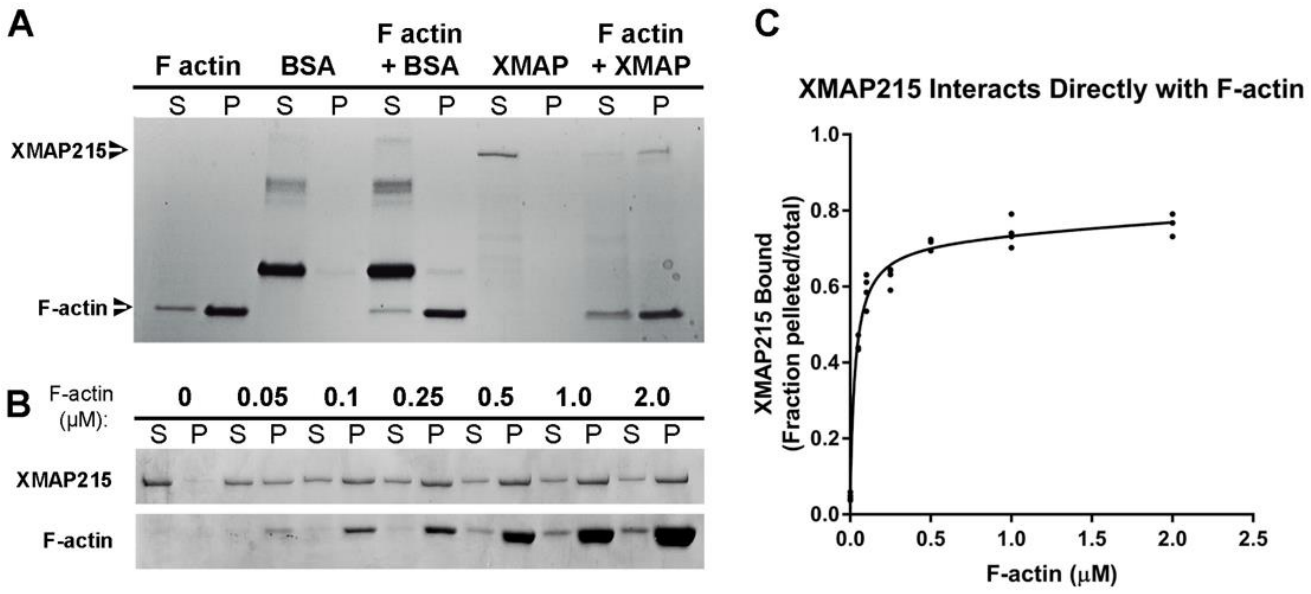

Figure 2.II.8. XMAP215 can directly bind to F-actin but does not affect local F-actin density. (A, B). XMAP215–F-actin co-sedimentation assays. Coomassie Blue- stained gels from binding assays containing a constant F-actin concentration (A) or increasing F-actin concentrations (B), show direct binding of XMAP215 to F-actin. BSA was used as a negative control. S, supernatant; P, pellet. (C) XMAP215–F-actin binding curve obtained by plotting the percentage of XMAP215 present in the pelleted fraction over the total, against the F-actin concentration. Data points from multiple experiments plotted for each concentration. Non- linearly fit binding curve displays a Kd value at a sub-micromolar binding affinity, 0.032±0.0051 μM (mean±s.e.m.). Bmax=0.682±0.0283.

co-sediment with F-actin in vitro (**Fig. 2.II.8A**). While using BSA as a negative control showed little to no sedimentation with F-actin, I saw XMAP215 presence switched from supernatant to pelleted fractions upon addition of F-actin. Next, by adding increasing concentrations of F-actin (**Fig. 2.II.8B**), I was able to obtain a binding curve for XMAP215 against F-actin. XMAP215 was shown to bind F-actin at a low (F-actin) concentration and with a high affinity. Fitting the data to the binding curve gave an XMAP215 Kd value of 0.032 ± 0.0051 μM (mean ± s.e.m.), and XMAP215 maximum binding corresponded to a B_{max} of 0.682 ± 0.0283 when the data was non-linearly fit to a curve (**Fig. 2.II.8C**). These results indicate the novel finding that XMAP215 is able to directly bind F-actin in addition to MTs.

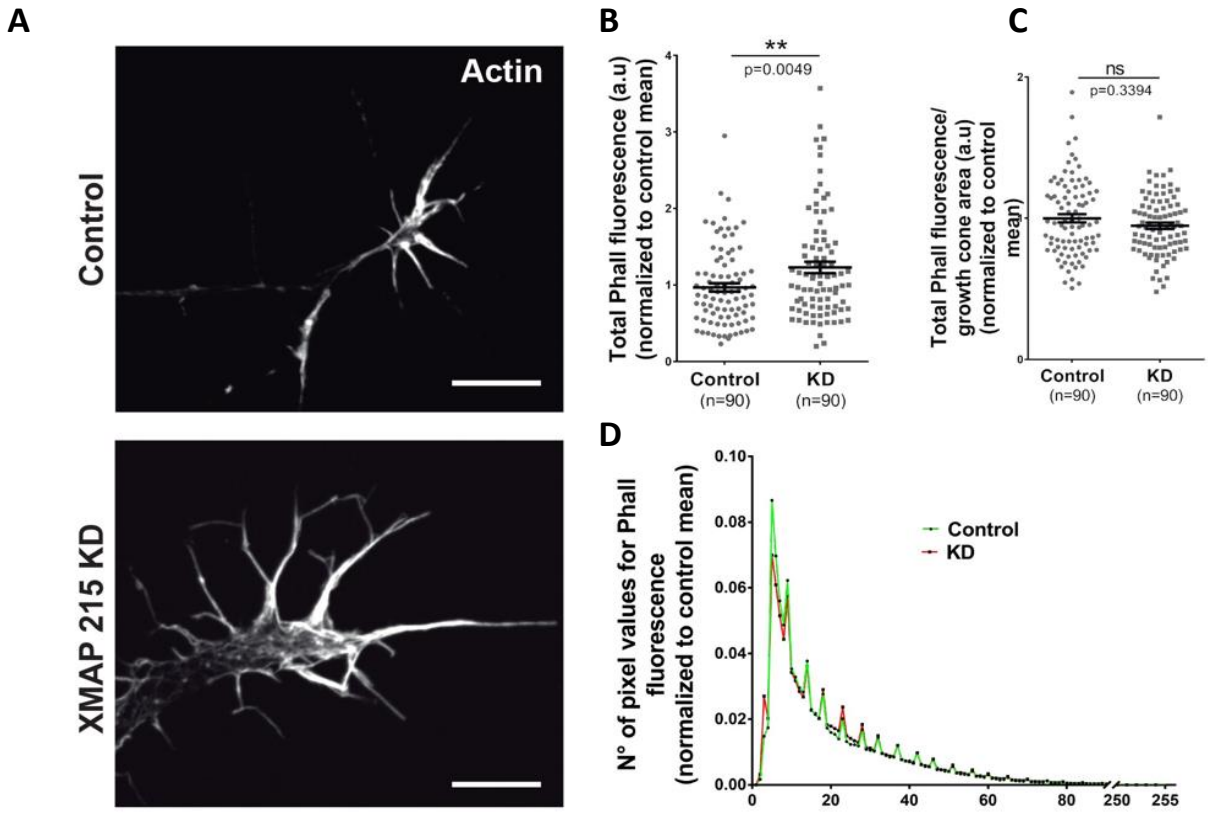

Figure 2.II.9. XMAP215 KD correlates with increased total F-actin levels, although F-actin distribution is not affected. (A) Representative phalloidin-stained images of growth cones from control and XMAP215 KD neural explants. Scale bars: 10 μm. (E–G) Quantification of F-actin amount and distribution. XMAP215 KD increases total phalloidin fluorescence (E), while it does not affect phalloidin fluorescence normalized by growth cone area (F) or the number of pixel values for phalloidin fluorescence (G). a.u., arbitrary units; Phall, phalloidin. **P<0.01; ns, not significant, from Student's t-test comparing XMAP215 KD to control. Data presented as mean±s.e.m.

I next wanted to determine if XMAP215 KD led to specific changes in the amount and distribution of F-actin within the growth cone (**Fig. 2.II.9A**). With the help of lab colleagues' imaging data, we measured phalloidin fluorescence intensity within the growth cone as a read-out for F-actin and observed a 27% increase in overall fluorescence intensity within the growth cone in XMAP215 KD compared to controls (**Fig. 2.II.9B**). However, when F-actin levels were examined after normalizing the total fluorescence intensity by the growth cone area (since XMAP215 KD growth cones are larger than controls), there was no difference observed in the XMAP215 KD compared to controls (**Fig. 2.II.9C**). To investigate this further, the number of pixel values for phalloidin fluorescence was examined (as a means to determine if Phalloidin was accumulating more or less in the different regions of the growth cone). There were no observable differences when comparing XMAP215 KD to controls (**Fig. 2.II.9D**), suggesting that the F-actin distribution within the growth cone was not specifically affected. These results demonstrate that XMAP215 is capable of a direct interaction with F-actin, although the increase in overall F-actin levels is not due to denser F-actin bundles but correlates with the increased size of the growth cone. It remains to be determined how XMAP215 KD leads to this increase.

III. DISCUSSION

In this chapter, I reveal new functions for the MT polymerase XMAP215 in promoting MT–F-actin interaction in both spinal cord explants from X. laevis embryos and in vitro biochemical assays. With the help of my lab colleague and collaborator, we utilized knockdown and overexpression studies to determine that XMAP215 is required for the axon to respond to the repellent guidance cue Ephrin A5 and affects axonal extension by influencing growth cone pausing events. In addition, I show that XMAP215 promotes MT alignment with F-actin bundles

in the growth cone, and XMAP215 is important for determination of growth cone size, filopodia length, and MT morphology and distribution throughout the growth cone. Additionally, I found that XMAP215 is able to bind F-actin in vitro and co-localize with F-actin in the growth cone peripheral domain. XMAP215 and its family members have been some of the most intensively studied and well-characterized MT polymerases over the last decade [94,101,102,118,121,132]. Moreover, they have received recent attention for having additional MT-related functions, including MT nucleation [119,120], mitotic spindle scaling [133,134] and MT destabilization [135,136]. This chapter, focusing on using F-actin co-sedimentation assays and growth cone imaging, adds a new element to the arsenal of XMAP215 functions, as it is demonstrated that XMAP215 also exhibits the potential to directly interact with F-actin. This provides the first strong evidence that XMAP215 may function as a MT–F-actin crosslinker in growth cones, although it is still unclear whether XMAP215 is sufficient to bind both cytoskeletal structures simultaneously, or whether additional protein complexes are required for mediating MT–F-actin interaction in growth cones.

Interestingly, my lab colleague observed that XMAP215 KD leads to changes in growth cone area and filopodial length (**Fig. 2.II.1A**). While it is unclear exactly how XMAP215 KD could lead to such increases, it is likely through an indirect mechanism. As there are complicated feedback mechanisms between MTs and F-actin within growth cones, it is possible that when alignment of MTs with F-actin is reduced, the overall cytoskeletal architecture and mechanical response of the growth cone is disrupted, thus leading to growth cone pausing and a corresponding increase in growth cone area. Early studies showed that the local loss of F-actin bundles on one side of the growth cone drives subsequent remodeling of MT organization, where MTs are no longer present in the F-actin bundle depleted zone, and instead reorient towards the remaining F-actin bundles [41]. Additionally, F-actin in filopodia are critical for appropriate

guidance cue sensing [137], while separately, the absence of F-actin bundles can act as a repulsive signal, inducing growth cone turning [41]. The findings from XMAP215-depleted growth cones replicate a similar scenario in that a decrease in MT–F-actin alignment randomizes the directionality of exploring MTs, indicative of a loss in MT guidance by the F-actin bundles in the growth cone peripheral domain. This loss in MT guidance and resultant MT–F-actin cytoskeletal discoordination could facilitate a loss in growth cone directionality, and prompt the growth cone to pause and await cues that would recalibrate it to its environment. Mechanically, growth cone extension may also demonstrate decreased efficiency if MT–F-actin interactions are reduced around the area of transient focal point contacts, as dynamic MTs are required at sites of adhesion remodeling [138].

Importantly, the results here demonstrate that XMAP215 affects several MT phenotypes such as MT organization, extension into growth cone periphery and filopodia, and MT–F-actin alignments (**Fig. 2.II.2-2.II.5**). When XMAP215 levels were reduced, MT behaviors were severely impacted throughout the growth cone. MT trajectories into the peripheral domain showed increased randomization, while central domain MTs demonstrated an increase in looping. Additionally, there was also increased widening of the MT array throughout the growth cone neck and central domain that occurs with XMAP215 KD. This phenotype is strikingly reminiscent of the growth cone MT bundling defect previously observed upon myosin II inhibition [139]. These studies suggested that MT arrays must be spatially consolidated to form the core of the axon as the growth cone progresses forward, and that actin- and myosin II- dependent compressive forces are required for MT bundling [139,140]. Interestingly, it was previously observed that the reduction of axon outgrowth that occurs with XMAP215 KD could be partially rescued by myosin II inhibition [112]. Thus, it is tempting to speculate that XMAP215 might somehow

interact with myosin II, in addition to F-actin, during the regulation of MT dynamics within growth cones. However, while MT bundling defects caused by partial XMAP215 KD may account for some of the MT phenotypes that we observe, such as growth cone neck widening and changes in growth cone size, it does not explain the changes in peripheral MTs aligning to F-actin in filopodia. In addition, the N-terminal portion of XMAP215, capable of rescuing the MT–F-actin alignment defect, is also the region that is necessary to co-localize with F-actin in the growth cone.

It has been well-established that MTs follow along F-actin bundles in growth cones [10,46], and that when MTs lose the ability to interact with F-actin (for example, by filopodial F-actin bundle removal), this induces lateral excursions by MTs that penetrate the peripheral domain at various angles [47] and promote formation of random MT loops [41]. A similar phenotype is observed when the MT–F-actin linker Spectraplakin is knocked out [50]. Consistently, increasing MT–F-actin interaction can lead to areas that are devoid of MTs in S2 Drosophila cells [141]. Thus, the MT phenotypes that are observed with XMAP215 KD are consistent with previous studies in which MT–F-actin interaction is disrupted. The deletion construct analysis and rescue experiments demonstrate that the XMAP215 N-terminus, comprising the TOG1–5 domains, is both necessary and sufficient for promoting MT–F-actin alignment (**Fig. 2.II.5-2.II.6**). Many previous studies have dissected the specific functions of the various domains of XMAP215 (for example, [101,118,120]), and the N-terminal TOG1–5 domains are known to bind to α/β-tubulin heterodimers and promote MT polymerization [101]. In my experiments, the deletion comprising only the TOG1–4 domains, which lacks the MT lattice-binding domain, was not able to rescue any of the MT–F-actin phenotypes within XMAP215 KD growth cones. In addition, the cytoplasmic localization of GFP-tagged TOG1–4 did not show distinct MT lattice-binding phenotypes or co-

localization with actin in the periphery of the growth cone, unlike TOG1–5 or full-length XMAP215 (**Fig. 2.II.6C**, Movies 1–4). The C-terminal portion, while not showing distinct co-localization to actin in the growth cone, did show MT plus-end tracking (most likely through coiled-coil homodimerization or C-terminal interactors TACC3 and SLAIN1/2) [96,103]. Thus, it seems likely that the N-terminal portion of XMAP215, specifically the area between its TOG4 and TOG5 domains, is important in determining a close MT–F-actin interaction in the growth cone periphery.

In order to determine if XMAP215 can bind directly to F-actin, I performed an F-actin co-sedimentation assay with purified XMAP215 protein. I determined that XMAP215 and F-actin can indeed bind directly, the binding saturates at low F-actin concentrations, and the binding affinity is in the sub-micromolar range in vitro (**Fig. 2.II.8**). Given that it was previously shown that MT plus-end-tracking protein CLASP can likely bind F-actin through its N-terminal Dis1 (TOG) domain [21], it is possible that one or more of the TOG domains of XMAP215 can also bind to F-actin. Thus, with TOG domains of XMAP215 binding to F-actin while the MT lattice-binding domain interacts with MTs, MTs would be able to extend along F-actin into the growth cone periphery. While augmenting XMAP215 levels affected growth cone morphology, MT distributions and MT–F-actin alignment in the growth cone, these effects were not the result of altered F-actin densities or levels in the growth cone (**Fig. 2.II.9**). Additionally, it was previously reported that F-actin retrograde flow rates were not affected after partial XMAP215 KD [112]. Given that the N-terminus of XMAP215 was also sufficient to rescue axonal responsiveness to Ephrin A5, we speculate that there may be phosphorylation sites within the N-terminus that are phosphorylated downstream of guidance signals and modulate the ability of XMAP215 to crosslink MTs and F-actin in a spatially-restricted manner.

While this study is the first to demonstrate that XMAP215 can directly bind F-actin, promote MT–F-actin alignment in growth cones, and mediate axon guidance, it is notable that two well-known XMAP215 interactors have also been implicated in processes that are consistent with this function. The most frequently characterized binding partner of XMAP215, TACC3, was previously described to be necessary for stabilizing XMAP215 on the MT plus-end [98,103,104,129] and for the growth cone response to the guidance cue Slit2 [142]. Furthermore, the Drosophila orthologue of XMAP215, Mini spindles (MSPS), genetically and biochemically interacts with the plus-end-tracking protein CLASP (also known as Orbit, MAST and CHB) [95], which was one of the first MT-associated proteins identified to participate downstream of axon guidance cue signals [17]. In that seminal study, CLASP was shown to specifically bind to MT plus-ends that entered the growth cone periphery and could regulate MT entry into this domain [17]. Additional studies on CLASP function have since demonstrated that changing levels of this MT-associated protein can result in striking changes in actin architecture throughout the growth cone [51,52].

Taken together, the results shown in this chapter demonstrate how XMAP215 can regulate MT polymerization and extension along F-actin bundles into the growth cone periphery, and that these interactions can be modulated downstream of a repulsive guidance cue. Partial KD of XMAP215 leads to decreased MT–F-actin alignment, resulting in an inability to exert proper coordination between MTs and F-actin during growth cone extension, increased pausing and desensitization to guidance cues. This chapter explores and defines a novel function of XMAP215 in MT–F-actin behavioral coordination and axonal guidance, in addition to its classical and recently emerged roles in MT polymerization and nucleation. Future work should seek to address whether there are other participants in this functional coupling and how MT–F-actin interaction can be temporally and spatially regulated. A better understanding of how MT-

associated proteins can dynamically tune their behaviors to regulate MT dynamicity and stability, and separately or additionally facilitate MT–F-actin cytoskeletal coordination downstream of environmental cues, is necessary to fully describe the mechanistic underpinnings of proper neuronal pathfinding.

IV. Materials and Methods

Xenopus embryonic neural tube explants

Eggs collected from female X. laevis frogs were fertilized in vitro, dejellied and cultured following standard methods [143]. Embryos were grown to stage 22–24 [144], and neural tubes were dissected as described [112]. All experiments were approved by the Boston College Institutional Animal Care and Use Committee and performed according to national regulatory standards.

Constructs, RNA and antisense oligonucleotides

Capped mRNAs were transcribed in vitro using SP6 or T7 mMessage mMachine Kit (Ambion). RNA was purified with LiCl precipitation. Constructs used were: XMAP215–GFP (a gift from the Hyman lab; Widlund et al., 2011) sub-cloned into pT7TS; GFP–MACF43 (a gift from the Hoogenraad Lab) and GFP in pCS2+. XMAP215 domain constructs TOG1–2–GFP, TOG1–4–GFP, TOG1–5–GFP, and the C-terminus were obtained by PCR from the XMAP215–GFP plasmid, and sub-cloned into pT7TS for generation of mRNA or into pFB HTA for protein purification. Previously validated morpholino antisense oligonucleotides targeted to the translation start site of X. laevis XMAP215 (5′-TCATCCACTCGCTGTCATCCCCCAT-3′), and another antisense oligo targeted to a splice site (5′-GGCTTTCCAAACCTACCATGAAACA-3′)

validated herein (**Fig. 2.S.1A**), in addition to standard control antisense oligo (5′-cctcttacctcagttacaatttata-3′) (Gene Tools, LLC) were used. The embryos were injected four times in dorsal blastomeres at two-to-four cell stage in 0.1× Marc's Modified Ringer's (MMR) solution containing 5% Ficoll. Total mRNA amounts injected per embryo were: 400 pg of GFP; 700 pg of XMAP215–GFP for rescue experiments and 4000 pg of XMAP215–GFP for overexpression experiments; 300 pg of GFP–MACF43; 2000 pg of TOG1–2, 1000 pg of TOG1–4, 2000 pg of TOG1–5 and 2000 pg of C-terminus (these concentrations are molar equivalents to 4000 pg of XMAP215 and 400 pg of GFP). Antisense oligonucleotides were injected in a concentration of 8 ng/embryo (5′-tcatccactcgctgtcatcccccat-3′) and 20 ng/embryo (5′-ggctttccaaacctaccatgaaaca-3′), in both cases equivalent to a 70% knockdown [112].

Immunocytochemistry

Embryonic explant cultures were fixed with 0.2% glutaraldehyde and labeled as described [40]. Immunostaining was done using rat anti-tyrosinated tubulin [YL1/2] (1:1000, ab6160, Abcam), rabbit anti-de-tyrosinated tubulin (1:1000, AB3201, Millipore), mouse anti-DM1a (1:100, T6199, Sigma-Adrich), mouse anti-GFP (1:200, 3E6, Invitrogen) or rabbit anti-GFP (1:500, AB290, Abcam) antibodies, Alexa Fluor 488–phalloidin, Alexa Fluor 568–phalloidin and Alexa Fluor 633–phalloidin (1:500, Molecular Probes). The secondary antibodies used were goat anti-rat Alexa Fluor 568 (1:500, ab175476, Abcam), goat anti-rabbit Alexa Fluor 488 (1:500, A-11008, Life Technologies), goat anti-mouse Alexa Fluor 488 (1:500, A32723, Life Technologies), and goat anti-rabbit Alexa Fluor 647 F(ab′)2 fragment specific (1:500, 111-605-047, Jackson ImmunoResearch).

Image acquisition

High-resolution images of cultured spinal cord explants were obtained with a CSU-X1M 5000 spinning-disk confocal (Yokogawa) on a Zeiss Axio Observer inverted motorized microscope with a Zeiss Plan-Apochromat 63×/1.40 numerical aperture lens, or with a phase contrast 20× objective (Zeiss). Images were acquired with an ORCA R2 charge-coupled device camera (Hamamatsu) controlled with Zen software. For analyzing the number of growing MTs, time-lapse images were collected every 2 s for 1 min using the 63×/1.40 oil objective. The number of growth cone pauses and duration of the pauses were obtained by analyzing time-lapse images collected every 5 min for 4 h using a phase contrast 20× objective. This objective was also utilized to collect images for quantifying axon length, number of axons per explant and guidance cue assays. Structured illumination super-resolution images were collected on a Zeiss Axio Observer.Z1 for super-resolution microscope with Elyra S.1 system, utilizing an Objective Plan-Apochromat 63×/1.40 oil (DIC). Images were acquired with a PCO-Tech Inc. pco.edge 4.2 sCMOS camera. The images were obtained in a chamber at approximately 28°C and utilizing the immersion oil Immersol 518F 30°. Stacked images were obtained with a z-step of 100 nm per growth cone. Channel alignment and structured illumination processing were applied to the super-resolution images using the Zeiss Black program. The fluorochromes Alexa Fluor 488–phalloidin, Alexa Fluor 633–phalloidin, Alexa Fluor 568 and Alexa Fluor 488 were used.

Image analysis

For the following quantifications, the growth cone was defined as the region contained between the growth cone neck and the tip of filopodia. The number of growth cone growing MTs was analyzed from GFP–MACF43 movies using plusTipTracker, as previously described [145,146].

All the rest of the quantifications were done using Fiji software. To determine the growth cone area, the region starting on the growth cone neck and extending to the tip of the filopodia was manually selected using the drawing/selection tool of Fiji (**Fig. 2.S.1C**). To determine the number of filopodia, all the filopodia extending from the growth cone central domain into the periphery, contained within the growth cone area, were manually quantified (**Fig. 2.S.1C**), and the length of each filopodium was measured using the Simple Neurite Tracer ImageJ plugin. The quantification of number of exploring MTs and MTs present in the filopodia were performed manually. To determine the number of exploring MTs, all of the MTs entering into the peripheral domain (trespassing the F-actin mesh, orange line in Fig. **Fig. 2.S.2B, C**) were quantified; for the number of MTs present in filopodia, only the MTs present in the peripheral domain that were extending into the filopodia (dotted yellow line in **Fig. 2.S.2A, B**) were considered. For the quantification of MT penetration into the peripheral domain, the region of the MT present in the F-actin mesh and extending throughout the peripheral domain was manually selected using the segmented line tool, and the length was measured (**Fig. 2.S.2A,B**).

For the quantification of MT spreading, the distance between MTs was measured in the growth cone neck at the widest region of the growth cone (spreading through the central domain); and for the central domain width, the distance occupied by MTs, starting at the growth cone neck, was measured. The quantifications of fluorescence intensity for tubulin were performed on the manually selected regions of interest using the drawing/selection tool in ImageJ. Intensity outside of the growth cone area was measured with the same area drawn for growth cone and was considered as background.

The percentage of MTs aligned to F-actin was quantified by measuring the distance and angle of separation between the MT and F-actin bundle. MT and F-actin were considered aligned

if closer than 300 nm and separated by an angle not greater than 15°. For MT orientation quantification, a line was drawn following the axon growth (central line) and the central line was intersected by arrows showing the direction followed by each MT. The angle between the central line and the arrows were measured and every 30° was considered as a different orientation. The length of the axons was measured using the Simple Neurite Tracer ImageJ plugin. For the quantification of the number of growth cone pauses and duration of the pauses, a pause was defined as when the center of the growth cone movement at each time point was less than the control mean movement minus the standard deviation, or when the growth cone changed the orientation of the movement by more than 180°, as growth cones pause before turning. For the duration of the pauses, the total number of frames where the growth cone was paused was divided by the number of pauses, and then multiplied by the number of minutes between two consecutive frames. For the guidance cue assay, the number of growth cones on and off Ephrin A5 stripes was manually quantified. Only growth cones with the soma localized off the stripes were quantified. Additionally, a growth cone was considered 'off stripe' when it had not been on an Ephrin A5 stripe at any time. All the quantifications that were manually performed were quantified by two different individuals in double blind experiments.

Protein purification

XMAP215 was purified using a bac-to-bac purification system as previously described [94,147]. The pFB HTA XMAP215 vector was used to create bacmid and amplified baculovirus, which was subsequently used to infect cultures of Hi-5 insect cells (*Trichoplusia ni*) (Thermo Fisher Scientific, B85502) at a density of 2.0×106 cells ml−1. Following 48 h incubation, cells were centrifuged, and lysates were filtered and applied to Nickel NTA affinity columns (Qiagen).

Protein elution was done using a 250 mM imidazole elution buffer (50 mM HEPES pH 7.25, 200 mM NaCl, 250 mM imidazole, 0.1% Triton-X, 1 mM DTT, 0.5 mM EDTA, 5% glycerol, 1 mM PMSF, 1× complete protease inhibitor cocktail). Buffer was exchanged using Amicon ultracentrifugation 100,000 MWCO column (storage buffer: 10 mM K-HEPES pH 7.25, 100 mM KCl, 5.0 mM EGTA, 2.0 mM MgCl2, 0.1 mM CaCl2, 10% glycerol), then snap frozen and stored at −80°C. Purified monomeric actin (Cytoskeleton Inc., APHL99) was diluted to 0.4 mg/ml in a general actin buffer (5 mM Tris pH 8.0, 0.2 mM CaCl2, 0.2 mM ATP, 0.5 mM DTT) and polymerized by the addition of a 10× actin polymerization buffer (500 mM KCl, 20 mM MgCl2, 10 mM ATP) at room temperature.

F-actin co-sedimentation assays

F-actin co-sedimentation assays were performed as described previously (Srivastava and Barber, 2008). Polymerized F-actin or an equivalent amount of F-actin control buffer were incubated with either BSA protein (as a negative control) or purified XMAP215 in injection buffer (10 mM Tris pH 7.0, 150 mM NaCl, 1 mM ATP, 0.1 mM CaCl2, 2.0 mM MgCl2, 0.2 mM DTT and 1.0 mM EGTA) for 30 min at room temperature. Protein was precleared to remove any aggregates. Actin was added to XMAP215 purified protein in excess. Following incubation, samples were centrifuged at 100,000× g for 20 min at 22°C using a Beckman TLA100.4 ultracentrifuge. For F-actin binding curves, a constant concentration of 0.1 μM of XMAP215 was incubated with increasing concentrations of 0, 0.05, 0.1, 0.25, 0.5, 1.0 and 2.0 μM of phalloidin-stabilized F-actin. Samples were run on SDS-PAGE gels and stained with Coomassie Brilliant Blue G-250 before being imaged. ImageJ was used to calculate densitometry of protein bands on SDS-PAGE gels, and plotted using GraphPad Prism. Experiments were repeated 3–4

times before curves were plotted (curves fit by GraphPad Prism non-linear regression assuming a one-site saturation model).

Stripe assay

Stripe assays were performed following the modified version of the stripe assay described previously [123]. The Ephrin A5-Fc solution was prepared by mixing 10 µg ml−1 of the Ephrin A5-Fc, human (R&D Systems, 374-EA) with 2.5 µg ml−1 of anti-human IgG, Fc-specific Cy3-conjugated (Sigma-Adrich, C2571), and the Fc control solution was generated by mixing 10 µg ml−1 Fc (Calbiochem, 401104) with 2.5 µg ml−1 of anti-human IgG, Fc-specific (Sigma-Adrich, I2136). Both solutions were kept for 30 min on a rotator, covered from light. Zig-zag striped silicon matrices attached to glass coverslips were used. The Ephrin A5-Fc solution was applied to the matrices and incubated for 30 min at 37°C. After three washes in 1× PBS, the Fc control solution was applied on the glass coverslips and incubated for 30 min at 37°C. Following that, three washes in 1× PBS were done and the glass coverslips were coated with 20 µg ml−1 laminin. X. laevis spinal cord explants were plated and imaged 24 h later.

Experimental design and statistical analysis

All graphs and statistical analyses were performed using the statistical software Prism 5 (GraphPad Software Inc.). Three to four independent experiments were performed for each condition to ensure reproducibility. Images of 8–10 explants acquired from 2–3 different embryos were obtained for each condition in every independent experiment. All data sets were analyzed for normal distribution using the D'Agostino normality test. When comparing two

conditions, the unpaired Student's t-test was performed, and when comparing multiple conditions, one-way ANOVA was used, by comparing the mean of each column with the mean of the control column under the multiple comparison option. In the cases that the data did not pass the normality test, Mann–Whitney test was used for comparing two conditions, and Kruskal–Wallis test for multiple comparisons. To analyze MT morphology, as it is a categorical variable, a $\chi 2$ test was performed. The α-value was set at 0.05 for all statistical tests, and the P-values are represented as follows: *P<0.05, **P<0.01, ***P<0.001 and ****P<0.0001. Values are expressed as mean±s.e.m

V. Supplemental Data

For associated movie files:
https://jcs.biologists.org/content/joces/suppl/2019/04/26/jcs.224311.DC1/JCS224311supp.pdf

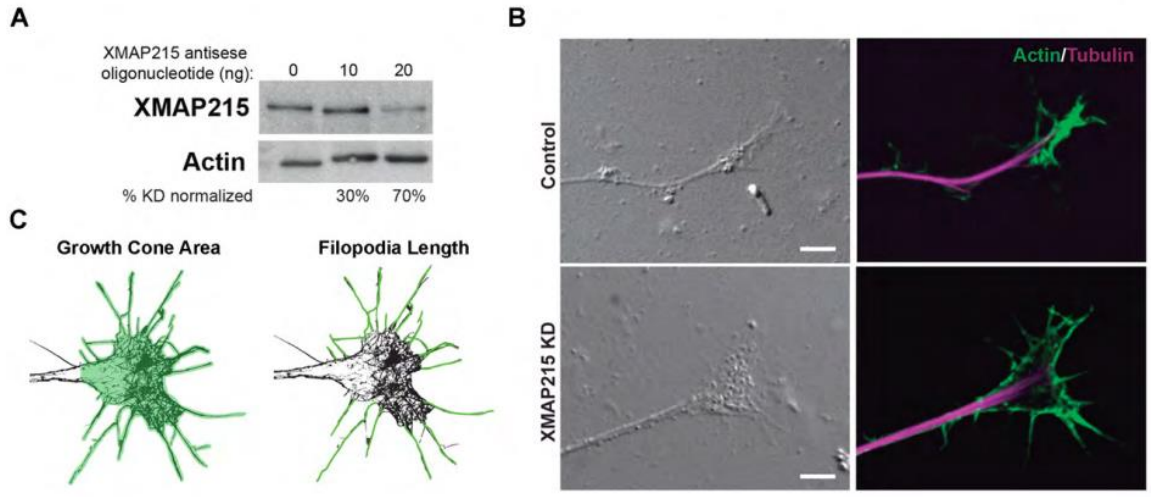

Figure 2.S.1. A) Western blot showing increasing levels of XMAP215 knockdown with increasing levels of antisense oligonucleotide. Actin was used as a loading control. B. DIC images (left) and actin and tubulin merge images (right) of growth cones from control and XMAP215 KD neural explants. Scale bar: 5 µm. C. Diagrams illustrating the measurements taken to analyze either growth cone area (left), or filopodia length (right) following XMAP215 KD, rescue, or OE. Structures analyzed are highlighted in green. Growth cone measurements correspond to data shown in Figure 2.II.1A. Average filopodia length corresponds to data shown in Figure 2.II.1C.

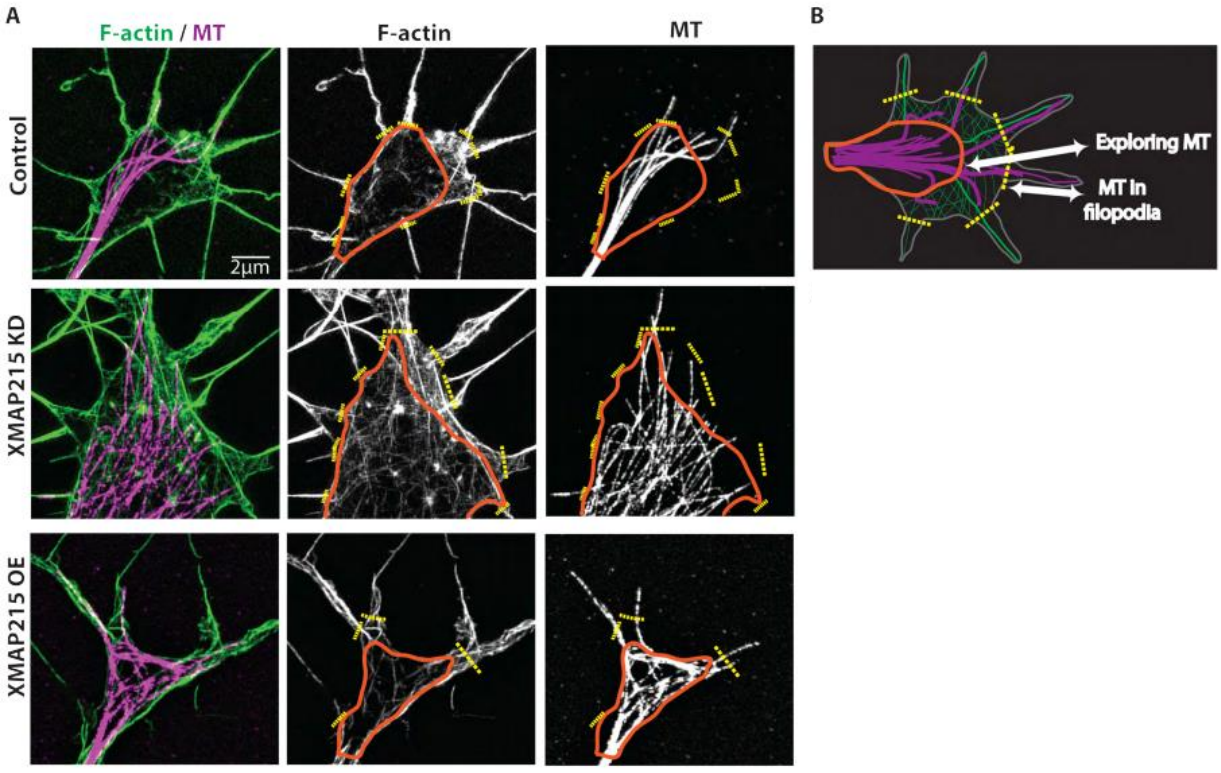

Figure 2.S.2. Example of the measurements taken of MT and actin-stained SIM imaging, corresponding to data displayed in Figure 2.II.3. A. Representative images of control, XMAP215 KD and XMAP215 OE growth cone stained for F-actin, MT and merge. Orange lines delineate the central domain, the beginning of the actin mesh is considered as the limit of the central domain, and the yellow dotted lines denotes the beginning of the filopodia. B. Growth cone cartoon showing that MTs that progress out of the central domain (orange line) are considered "exploring MTs", and the ones progressing beyond the doted yellow lines are considered "MTs present in the filopodia.

Chapter 3. XMAP215 displays a unique lattice based function that links MTs to F-actin in the Growth Cone

(Adapted from Cammarata et al., 2020 – Molecular Biology of the Cell (In Submission))

I. Introduction

The neuronal growth cone is a structure that is found at the end of growing axons, governing proper guidance and pathfinding capabilities for the neuron. In order for neurons to make proper connections in the brain, cytoskeletal networks need to be tightly controlled and regulated. These cytoskeletal networks are largely made up of microtubules and actin filaments (F-actin), which each control unique portions of the growth cone's ability to drive forward and steer [111, 112, 113]. While F-actin provides for the protrusion of new membrane growth and reorganization, microtubules act as scaffolds for guidance cue signaling pathways in the growth cone [1]. In addition, there is constant interplay between these two systems, facilitating correct localization of each other in the proper compartments of the growth cone [115].

Importantly, populations of dynamically-growing microtubules are found to extend into the periphery of the growth cone and into the ends of filopodia (**Figure 3.I.1.**) [46]. In order for microtubules to penetrate out of the compartmentalized central domain of the growth cone and explore the periphery, dynamic microtubules follow F-actin bundles, using them as tracks to be guided into the periphery [7,46]. Here, dynamic microtubules interact with guidance cues and internal signaling pathways, initiating downstream changes in microtubule and F-actin

cytoskeletons [1]. In addition to facilitating microtubule advancement into the periphery, F-actin higher order structures are capable of restricting dynamic microtubules from reaching the periphery when the microtubules are strongly bound to F-actin retrograde flow [7, 10]. This dual facultative and restrictive role of F-actin regulates advancing microtubules in the growth cone, and together, regulate protrusion and steering of the axon.

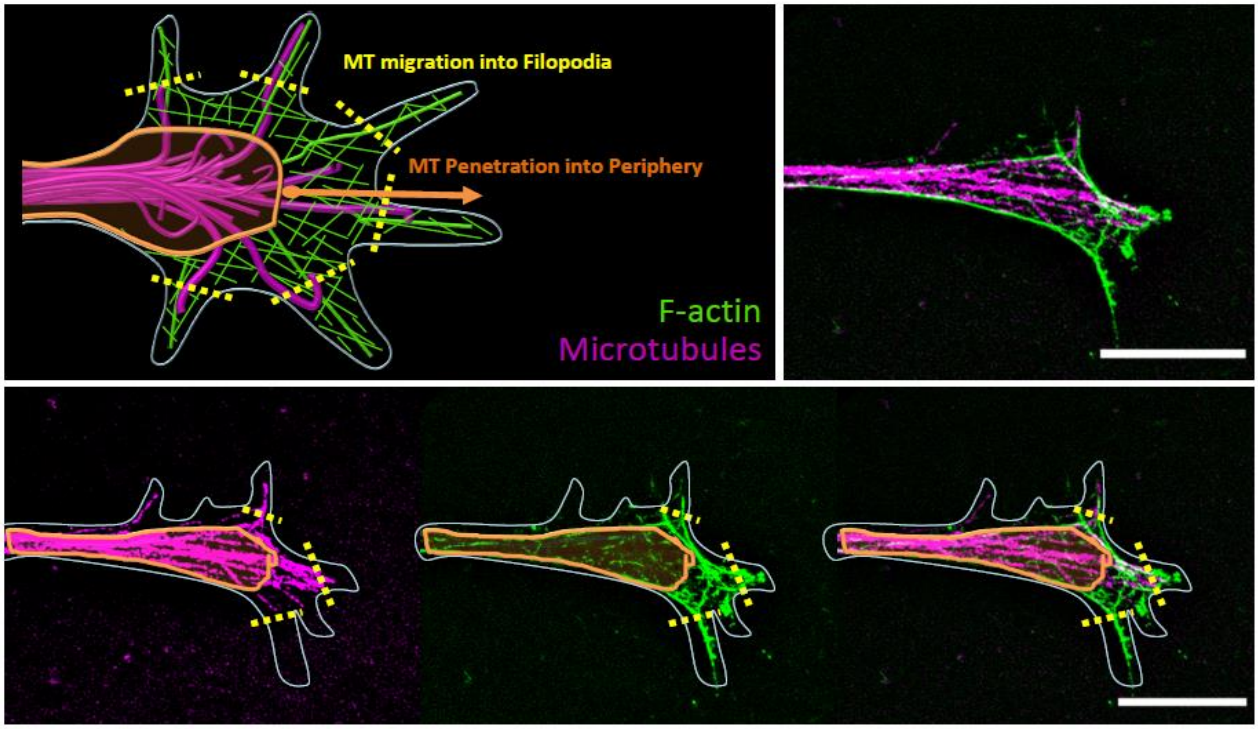

Figure 3.I.1. Depiction of Growth Cone regions and parameters of analysis for MT exploration in Growth Cone. A) Growth cones structure is dominated by MTs in the central domain (magenta) and a rich F-actin periphery (green). Exploring microtubules can break out of the central domain (orange), and be guided by F-actin bundles into filopodial extensions (yellow dotted lines). A, example two colored SIM image of a growth cone is depicted as either merged (top right), or with a diagrammatic overlay highlighting different regions depicted in A. Scale bar = 10 μm.

The ability of microtubules to be guided by F-actin tracks is thought to be initiated by groups of microtubule associated proteins (MAPs) that decorate the microtubule lattice and plus end [19,22,52,53,114–117]. These proteins, depending on their localization to microtubule and actin filaments, as well as their strength of interaction, can alter spatial localization of microtubules in the growth cone [115]. It has been shown that when microtubules are tightly coupled to F-actin in

the growth cone, microtubules are carried with F-actin retrograde flow back towards the central domain [17,49]. This has been shown to be the case when levels of MAPs, like CLASP, are increased in the growth cone, or when certain phosphorylation conditions in the growth cone are met [17,51,52]. Oppositely, certain MAPs, like EB3/Drebrin, allow microtubules to be transiently coupled to F-actin, allowing microtubules to be free to polymerize while simultaneously using bundles of F-actin as routes of guidance [22]. It is thought that through this unique mechanism, proteins linking MTs and F-actin together rapidly bind on and off from either filament, allowing a close guidance based association of MTs for bundles of F-actin, while not being subjected to the strong treadmilling translocation through F-actin retrograde flow.

One such protein that is uniquely positioned for this task is the microtubule polymerase, XMAP215 (part of the Dis1/TOG family). XMAP215 has been analyzed thoroughly for its ability to affect microtubule polymerization [94,101,102,105,118,121,132], while only recently shown to affect microtubule nucleation [119,120]. These unique functions of XMAP215 are attributed to its unusual pentameric TOG (Tumor overexpressed gene) domain array. Individually, these TOG domains contribute to both GTP and GDP-tubulin binding, catalyzing tubulin subunits onto the ends of microtubules [94,101,148]. However, in addition, XMAP215 also contains a highly charged microtubule lattice binding region in between its TOG4 and TOG5 domain, and contains a largely disordered C-terminal domain involved in protein-protein interactions [34,96,101,103,104]. While much is known about the earlier TOG domains, there is less known about the structurally diverse TOG5 domain [34,105]. In addition, up until recently, there was no information regarding XMAP215's ability to interact with the F-actin cytoskeleton in any fashion [149].

I have shown that this important protein is capable of binding to F-actin directly, and can facilitate guidance of microtubule populations into the periphery of the growth cone. However,

the mechanism of XMAP215's interaction with both F-actin and microtubule populations to carry out this function in the growth cone remained a mystery. In this Chapter, I utilize biochemical assays in combination with high and super resolution imaging to determine the role of XMAP215 in linking microtubules to the F-actin cytoskeleton in the growth cone. Here, I establish the TOG5 domain as a necessary region to influence interactions with F-actin directly. In addition, I determined that XMAP215 lattice binding activity and TOG5 mediated F-actin binding domains are essential for influencing microtubule guidance into the growth cone peripheral domain. Finally, I establish that this dual cytoskeletal role is separate from its classical polymerase activity. Thus, my work highlights the important role that XMAP215 plays in directing microtubule extension into targeted regions of the growth cone through F-actin interaction, facilitating protrusion and steering pathways of the axon during growth.

II. Results

The TOG5 domain is uniquely important in allowing direct interaction with F-actin in vitro

While XMAP215 has been previously implicated in coordinating microtubule extension into the growth cone periphery through an F-actin-related mechanism [109], it was still unclear as to what particular region of XMAP215 binds to F-actin however. In order to probe for a distinct F-actin binding domain, I created numerous XMAP215 deletion constructs and purified protein for each (**Figure 3.II.1A**, and **Figure 3.S.1A**). I then utilized F-actin sedimentation assays in order determine whether these protein fragments could directly bind to F-actin [150]. First, I tested larger constructs made up of several TOG domains: TOG1-4, TOG1-4+microtubule lattice-binding domain (TOG1-4++), and TOG1-5. When I incubated ~0.25 μM TOG1-4 protein with increasing

concentrations of F-actin (0 to 2.5 µM F-actin), I saw little increase in sedimenting TOG1-4 protein at >100,000 x g (**Figure 3.II.1B, C**). Given that TOG1-4 protein was not sufficient to promote binding to F-actin, I wondered next whether the highly charged microtubule lattice-binding region [34,101] was playing a key role. However, when I analyzed binding of the TOG1-

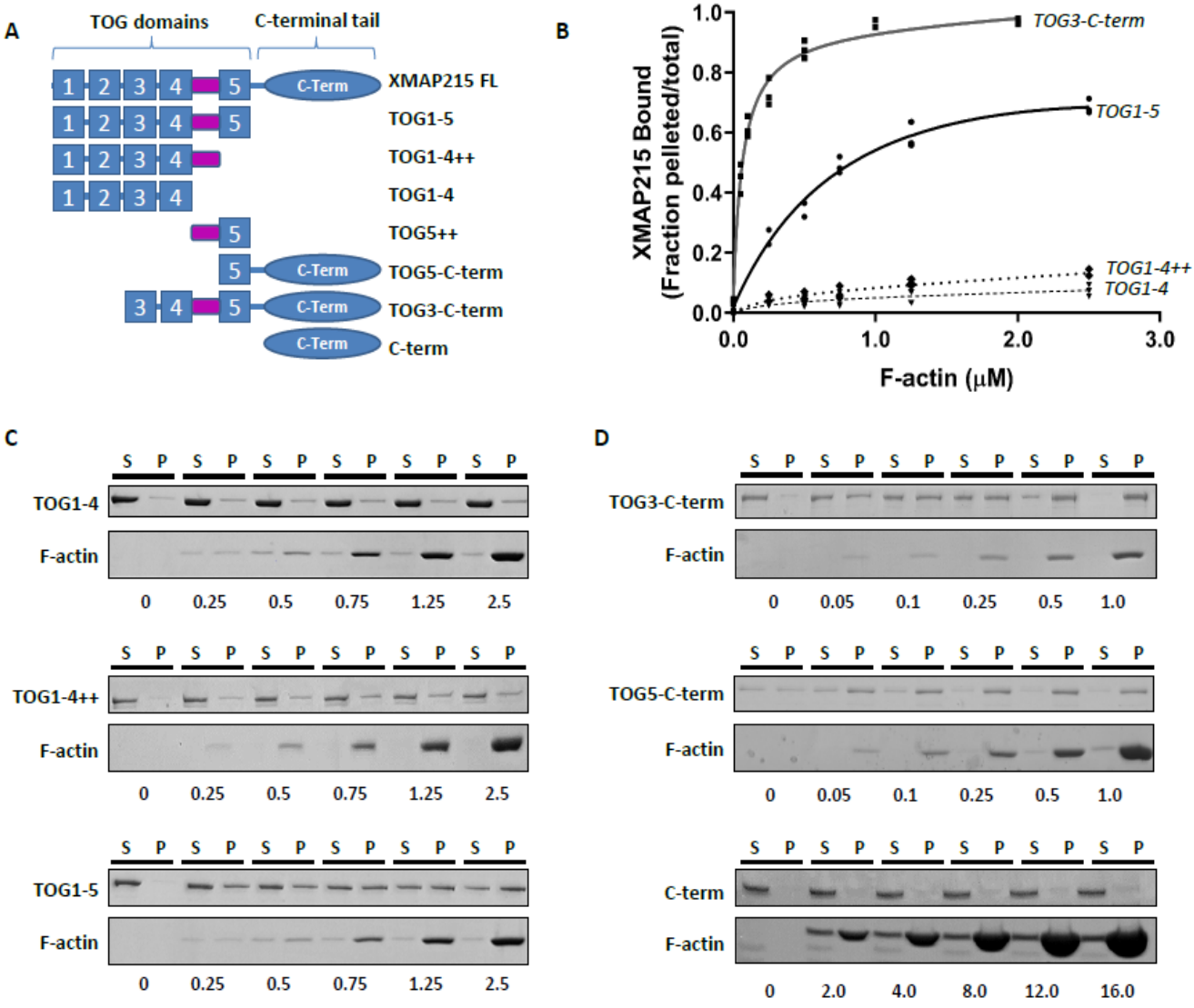

Figure 3.II.1. The TOG5 domain is uniquely important in allowing direct interaction with F-actin in vitro. A) Diagram of XMAP215 deletion proteins purified for use in sedimentation assays. B) F-actin Binding Curves of different TOG and C-term-containing purified proteins interacting with F-actin in sedimentation assays. C) TOG1-4, TOG1-4++, and TOG1-5 proteins incubated with increasing amounts of F-actin protein in F-actin Sedimentation Assays. Approximately 0.250 µM XMAP215 deletion protein, F-actin concentrations ranging from 0-2.5 µM. D) TOG3-C-term, TOG5-C-term, and C-terminal domain proteins (approximately 0.250 µM) incubated with increasing amounts of F-actin protein (0-1.0 µM F-actin). Sedimentation of C-terminal domain utilized high F-actin concentrations.

4++ region, I observed little sedimentation with F-actin, similar to the results with TOG1-4. However, when I purified and examined XMAP215 constructs that included the TOG5 domain, we observed a large increase in apparent binding to F-actin (**Figure 3.II.1C**). Plotting densitometry values on a binding curve showed a saturating curve, with an apparent K_D of ~1.2 μM and ~70% maximal binding (**Figure 3.II.1B**). This showed that specifically adding on the TOG5 domain, a largely uncharacterized domain [105], to the N-terminus of the protein was important for binding to F-actin with a strong affinity.

While I had observed that the TOG5 domain was important for XMAP215 binding to F-actin, I next set out to test whether it was sufficient for binding. I purified a host of proteins containing the TOG5 domain along with other domains to see how they affected binding. Interestingly, the TOG5 domain alone, TOG5+MT lattice (TOG5++), or TOG3-TOG5 domains did not facilitate binding to F-actin (**Figure 3.S.1A**). However, when adding on the C-terminal domain to TOG5, I did observe direct binding to F-actin (**Figure 3.II.1D**, **Figure 3.II.1B**). In addition, proteins containing TOG3-Cterm and TOG5-Cterm showed saturated binding to F-actin, with TOG3-Cterm giving an apparent binding affinity of ~ 0.06 μM with ~85% maximal binding (**Figure 3.II.1B**). TOG5-Cterm was able to sediment with F-actin, although a binding affinity was not accurately measurable due to saturation at very low F-actin concentrations and problems of aggregation at room temperature. I also tested whether the XMAP215 C-terminal domain alone could bind to F-actin, but found that no affinity was measurable even at very high F-actin concentrations of 16.0 μm. This shows while TOG5 alone is not sufficient to bind F-actin, other adjacent domains – either the complete pentameric TOG array, or the C-terminal domain - are likely required to facilitate a proper confirmation for TOG5 binding to F-actin.

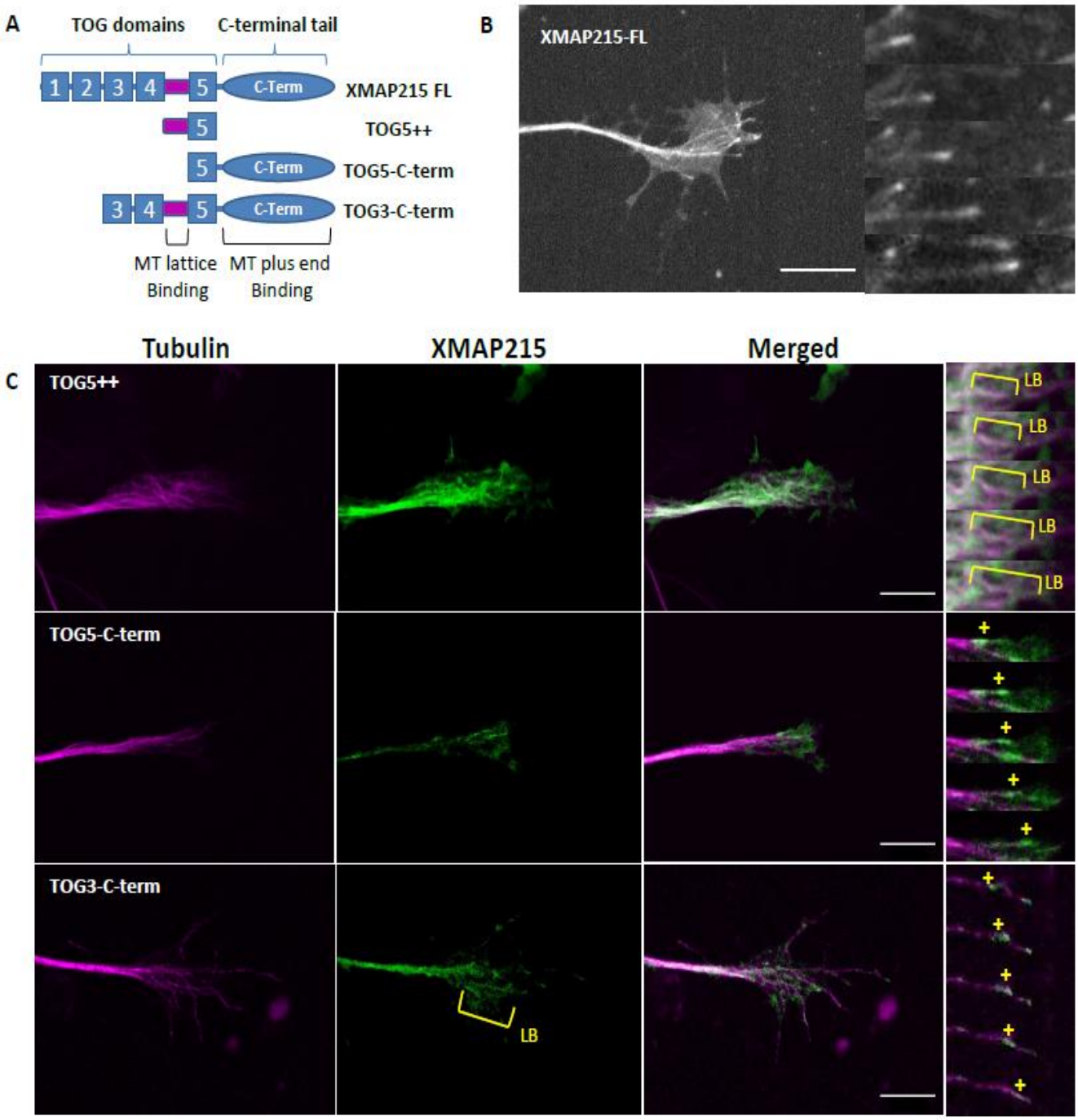

Figure 3.II.2. Localization of XMAP215 to the MT lattice or plus end in growth cones is facilitated by distinct domains. A) Diagram depicting mNeonGreen-labelled XMAP215 deletion proteins and associated domains, comprised of N-terminal TOG domains (1-5), a MT lattice binding region (purple), and a plus-end localizing C-terminal domain (C-term). B) Live cell imaging of XMAP215-FL-GFP overexpressed in embryonic neuronal growth cones. Right inset depicts time-lapse montage of XMAP215 along both the lattice and the plus end of a MT. C) Live cell imaging of XMAP215 deletion constructs shown in A overexpressed in growth cones. Tubulin (magenta), XMAP215 deletion protein (green), and merged image of the two channels are depicted. Inset pictures display successive frames of either plus-end binding (+) or lattice binding (LB). Scale Bar = 10 μM.

Localization of XMAP215 to the microtubule lattice or plus end in growth cones is facilitated by distinct domains

While XMAP215 has been previously implicated in localization to both the plus end and lattice of microtubules in growth cones (**Figure 3.II.2B**) [112], and facilitating microtubule/F-actin interactions [109], no previous study has yet examined whether the plus-end-localized or lattice-bound fraction of XMAP215 facilitates this novel microtubule/F-actin interaction. First, I sought to determine which domains of XMAP215 promote localization to either plus-end or lattice in growth cones. I created several deletion mutants of XMAP215 that contain a previously characterized microtubule lattice binding region [101], as well as a C-terminal domain that is implicated in microtubule plus end binding through protein-protein interactions [96,98,103,104,129] (**Figure 3.II.2A**).

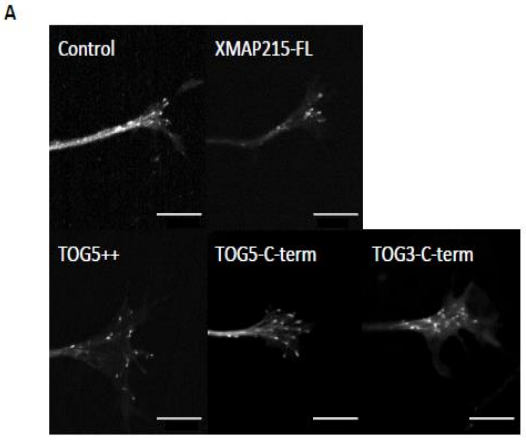

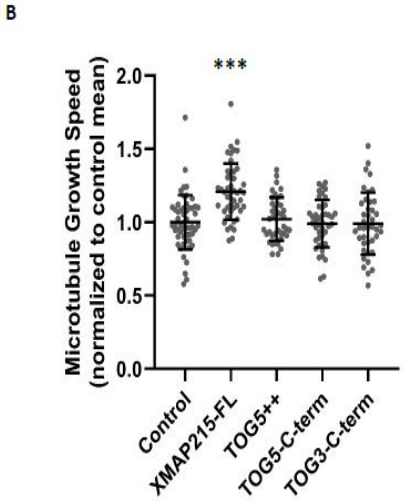

Figure 3.II.3. Removal of TOG1-2 domains of XMAP215 diminish microtubule velocity effects. A) Plus end tracking of MACF43 puncta velocities following overexpression of XMAP215-FL, TOG5++, TOG3-Cterm, and TOG5-Cterm constructs in growth cones. B) Microtubule growth velocity speeds quantified automatically through use of plusTipTracker software. Average comet velocity of growth cones displayed as normalization to control mean velocity (MACF43 only).

Importantly, while full length XMAP215 contains five TOG domains and the C-terminal region, the deletion mutants that I created all lack at least the TOG1-2 domains. Deletion of the GTP-tubulin binding TOG1-2 domains hinders these proteins from acting as microtubule polymerases [101,105], which was confirmed when looking at changes in microtubule growth speeds

after OE of deletion proteins in growth cones (**Figure 3.II.3A, B**). Normally, full length XMAP215 localizes to both the lattice of the microtubule and the plus end of the microtubule [112] (**Figure 3.II.2B**, insert right). While these proteins were not acting as microtubule polymerases, they did still localize correctly to either the microtubule lattice (triple arrows, TOG5++ and TOG3-Cterm), or the microtubule plus end (single arrow, TOG3-Cterm and TOG5-Cterm) (**Figure 3.II.2C** insert right). By establishing differentially localized pools of XMAP215 protein that do not affect microtubule polymerization levels, I could then test whether populations of microtubules were still being affected by XMAP215 in a polymerization-independent manner.

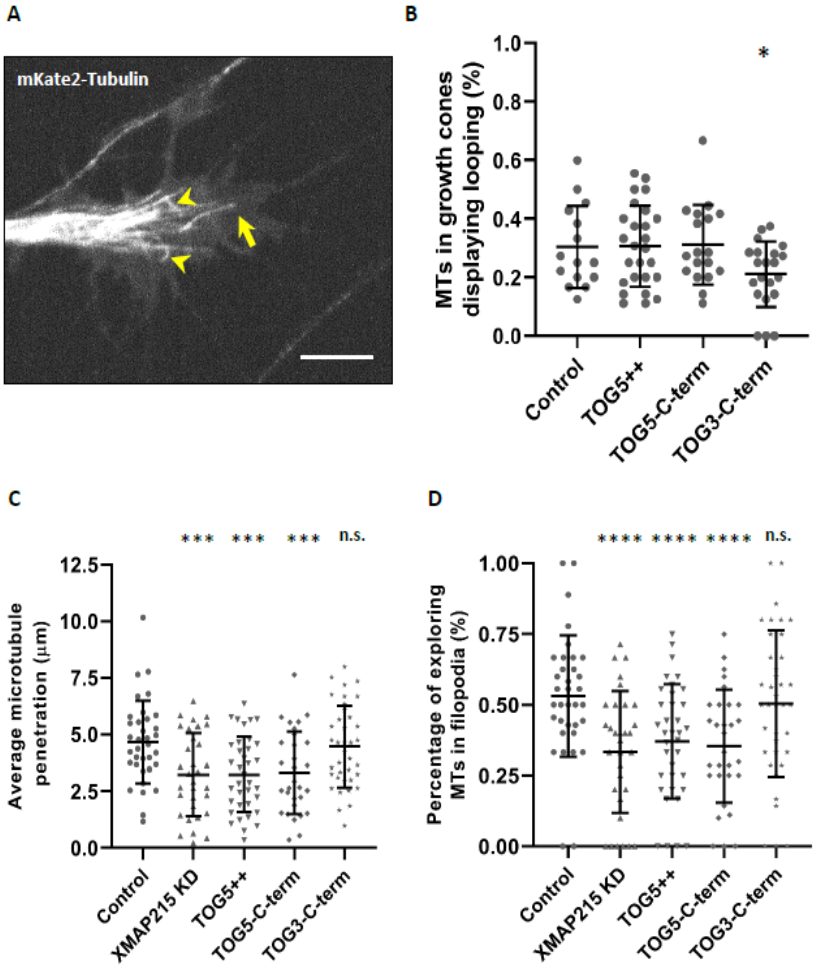

Figure 3.II.4. TOG3-C-term construct is capable of affecting MT looping and extension phenotypes in the growth cone. A) Expression of mKate-tubulin in growth cone. Arrows = straight MTs extending towards periphery. Arrowheads = looping MTs coupled to retrograde flow. B) Percentage of MTs undergoing looping over total MTs. C) Average lengths of MTs extending into the periphery following XMAP215 knockdown (KD), or XMAP215 KD and rescue with indicated deletion construct. D) Percentage of exploring MT populations that extend into filopodia measured following XMAP215 KD, or XMAP215 KD and rescue with indicated deletion construct. * P<0.05, *** P<0.001, **** P<0.0001. Scale Bar = 10 µM.

TOG3-Cterm construct is capable of affecting microtubule looping and extension phenotypes in the growth cone

Indeed, I saw that certain truncation mutations did change characteristics of microtubules in the growth cone. As my previous chapter highlights a novel F-actin interactions through microtubule bound XMAP215 [109], I thought that this might also be affecting microtubule populations here in a similar manner. I then tested microtubules for looping, a phenotype commonly involved in microtubule attachment to F-actin retrograde flow or for inability of microtubules to escape the central domain of the growth cone during normal internal signaling states [14,109,127]. When overexpressed in the growth cone, TOG5++ and TOG5-Cterm did not significantly affect microtubule looping in the central domain over control levels (1.01% and 2.47 % difference, P = 0.951 and 0.877, respectively). However, OE of TOG3-Cterm significantly decreased the microtubule looping that was occurring in growth cones over control (30.35% reduction, P = 0.035) (**Figure 3.II.4A**). This potentially indicated that microtubules could not escape the central domain of the growth cone without interaction with guide F-actin bundles, and so I then looked at how microtubules were penetrating into the peripheral domain. Here, I partially knocked down XMAP215 levels to around 70%, which leaves enough wild-type XMAP215 protein present in growth cones to allow for normal rates of microtubule polymerization (previously validated in [109,112]). When XMAP215 levels are partially knocked down, there is a significant reduction in microtubule penetration distances (30.72 % reduction, P value = 0.002), and microtubules present in filopodia (37.18% reduction, P value = 0.0004) (**Figure 3.II.4C, D**).

Adding back deletion mutant mRNA showed that only TOG3-Cterm was capable of rescuing microtubule phenotypes back to control levels (MT penetration P value = 0.629, MT

percentage in filopodia P value = 0.634). It is notable that while TOG5++ was not able to bind directly to F-actin (**Figure 3.S.1A**), TOG5-Cterm and TOG3-Cterm were capable (**Figure 3.II.1D**, **Figure 3.S.1B**). Thus, only constructs capable of binding to F-actin, and containing the lattice-binding domain, were able to rescue microtubule extension phenotypes. Importantly, I also established that XMAP215 is capable of facilitating microtubule extension into the periphery of growth cones without its main polymerase function.

Microtubule lattice-bound XMAP215 is capable of rescuing knockdown-induced microtubule/F-actin misalignments in growth cones

Given that F-actin commonly facilitates exploratory microtubule extension into the periphery of growth cones [7,46], where they can act as guidance cue sensors [1], I wanted to examine how XMAP215 was affecting microtubule and F-actin alignments in the growth cone. Thus, I analyzed microtubule and F-actin bundles in the growth cone using super resolution Structured Illumination Microscopy, after expression of XMAP215 deletion constructs. I partially knocked down XMAP215 as before, and then rescued with either TOG5++, TOG5-Cterm, or TOG3-Cterm OE. I found that XMAP215 constructs (shown in red), that contain lattice-binding regions, localize along microtubules in the growth cone (**Figure 3.II.6A**, center panel). Plus-end localizing constructs like TOG5-Cterm were difficult to establish tracking to the ends of the microtubule, which may have been due to fixation artifacts of samples, or background interference.

In order to assess if microtubules were using F-actin as tracks, I analyzed microtubules that were exploring along these F-actin bundles. Microtubules that were exploring at an angle >30.0º off from the F-actin bundle, or if they were greater than 300 nm away from the F-actin bundle

were considered misaligned (arrows), following previously explained criteria [109]. Diagrams of microtubules and F-actin are given in "camera lucida" type images to more easily depict aligned and misaligned filaments (**Figure 3.II.6A**, right panel). When I examined how these constructs could rescue microtubule alignments to F-actin, I saw similar results to the microtubule penetration phenotypes shown earlier. While XMAP215 KD produced a 22.45% reduction in microtubules aligned to F-actin bundles (P = <0.0001), neither TOG5++ nor TOG5-Cterm

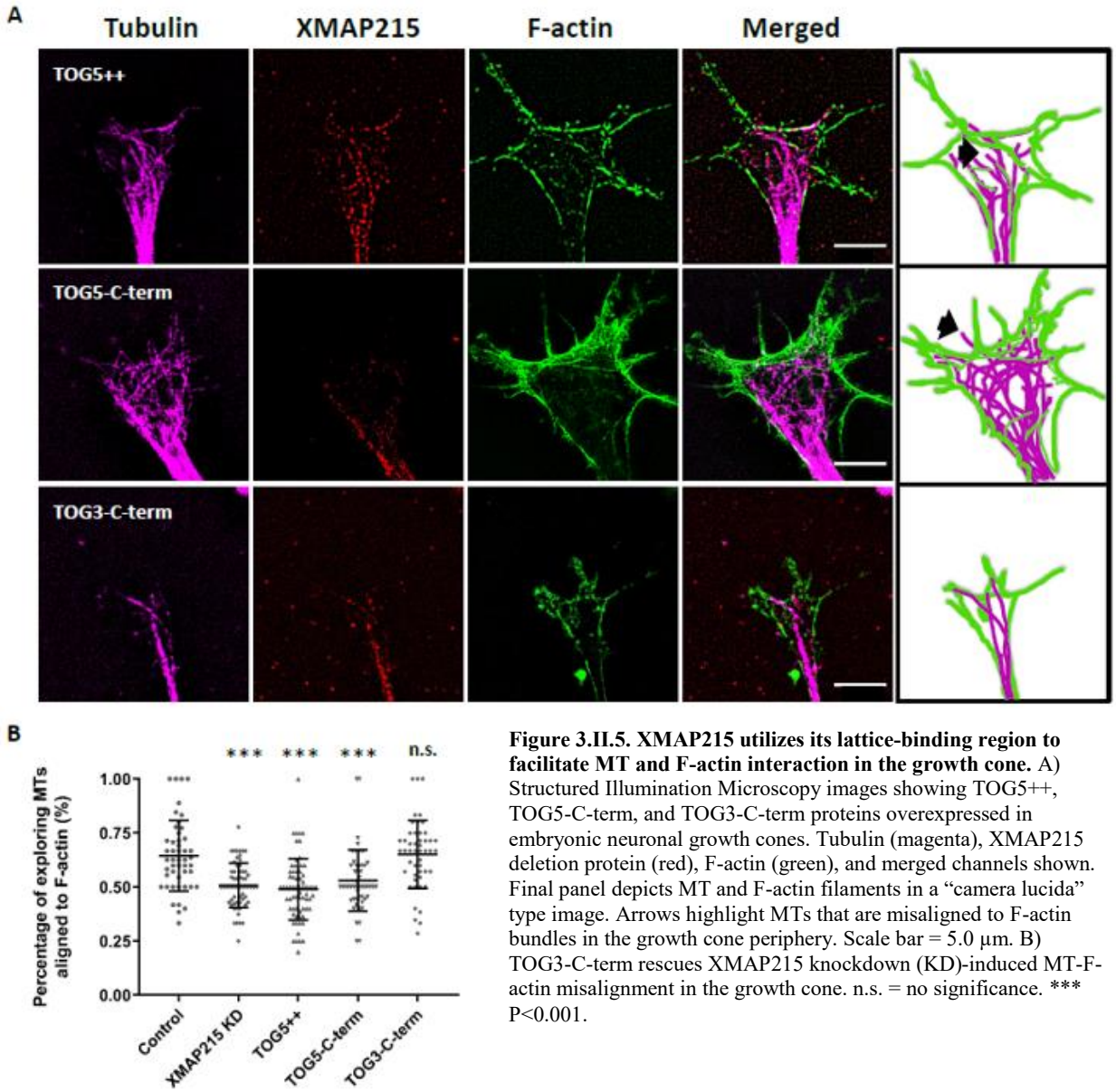

Figure 3.II.5. XMAP215 utilizes its lattice-binding region to facilitate MT and F-actin interaction in the growth cone. A) Structured Illumination Microscopy images showing TOG5++, TOG5-C-term, and TOG3-C-term proteins overexpressed in embryonic neuronal growth cones. Tubulin (magenta), XMAP215 deletion protein (red), F-actin (green), and merged channels shown. Final panel depicts MT and F-actin filaments in a "camera lucida" type image. Arrows highlight MTs that are misaligned to F-actin bundles in the growth cone periphery. Scale bar = 5.0 μm. B) TOG3-C-term rescues XMAP215 knockdown (KD)-induced MT-F-actin misalignment in the growth cone. n.s. = no significance. *** P<0.001.

constructs could rescue levels of microtubule/F-actin alignment back to control levels. However, OE of TOG3-Cterm was capable of rescuing XMAP215-KD induced misalignment completely back to control levels (1.16%, P value = 0.850) (**Figure 3.II.6B)**. Thus, together with its ability to promote microtubule extension into the periphery, and into filopodia, XMAP215 displays a microtubule dependent guidance mechanism for microtubules dependent on F-actin interaction and microtubule lattice binding.

III. Discussion

In this Chapter, I expand upon the recent discovery of XMAP215 functioning as a novel microtubule/F-actin co-interactor. Using biochemical assays, super resolution imaging, and structure-function analysis, I mechanistically explore XMAP215's role in facilitating microtubule exploration in key regions of the neural growth cone through F-actin related mechanism. In order for microtubules to reach the periphery of the growth cone and affect axonal outgrowth and steering mechanisms [42], microtubules require the ability to polymerize, as well as a way to be guided through dense F-actin mesh [10,41]. In this chapter, I explored XMAP215's ability to interact with F-actin in a direct fashion using biochemical assays. In addition, I showed that XMAP215 requires a microtubule lattice binding localization to carry out

Construct	Direct F-actin Binding	MT Lattice Binding	MT Plus end Binding	Rescues Filament Alignment
TOG5++		+		
TOG5-C-term	+		+	
TOG3-C-term	+	+	+	+
TOG1-5*	+	+*		+*

Figure 3.III.1. Table summarizing F-actin binding, MT localization, and rescuing of MT/F-actin filament alignments abilities of XMAP215 deletion constructs. Asterisk (*) denotes data concluded from (Slater and Cammarata et al., 2019).

its extension of microtubules into the peripheral domain of the growth cone. Finally, I show that the ability of XMAP215 to link microtubules to F-actin bundles in the growth cone requires both an F-actin binding domain, and microtubule lattice localization, all capable of acting independently from its classical polymerase function (**Figure 3.III.1)**.

XMAP215 has been studied quite extensively over the last few decades as a microtubule polymerase [94,101,102,105,118,121] and depolymerase [94,135,151]. Only recently, however, have new functions been attributed to it, such as acting as a microtubule nucleation factor [119,120], as well as acting as a potential microtubule and F-actin crosslinking protein [109]. In order to establish a more precise view of XMAP215 acting as a cross-linking protein, I had to establish the domain capable of binding to F-actin. Previous studies hinted at a region of XMAP215 between the TOG4 and the TOG5 domain that was important in facilitating microtubule/F-actin interactions in growth cones [109]. Probing this region for F-actin binding activity, I purified numerous deletion constructs (**Figure 3.II.1A, Figure 3.S.1C**), containing the microtubule lattice binding region, as well as the TOG5 domain.

Both of these proposed regions were good candidates for F-actin binding. The microtubule lattice-binding domain is a highly positively charged region consisting of stretches of serine and lysine [94,101,152], attributes that make it likely to interact with the outer surfaces of tubulin carboxy-terminal tails and potentially to actin filaments [153,154]. However, If XMAP215 is a cross linking protein, domains of tubulin binding and F-actin binding would likely be separate from one another to facilitate binding to both filaments. When differentiating between the TOG1-4 construct, and the TOG1-4++ construct in F-actin binding, there seemed to be little change shown by my biochemical assays (**Figure 3.II.1**). In addition to the previously characterized microtubule-lattice binding domain in XMAP215, there was also the potential for one specific

TOG domain to facilitate interaction with F-actin. The TOG5 domain is the most widely varied domain in sequence to other TOG domains [34,101,102,105]. In addition, the TOG5 domain, over all other TOG domains, has higher sequence homology to that of the TOG-like domain of another +TIP protein, CLASP [34]. The TOGL1 domain of CLASP has been implicated in direct F-actin interaction [21] and interaction to F-actin in neurons [51,53], indicating that the TOG5 domain of XMAP215 may possess a similar capability here. Interestingly, interactions of either the TOG5 domain alone, or the TOG5 domain with the microtubule lattice-binding region (TOG5++), showed no indication of F-actin binding in our sedimentation assays (**Figure 3.S.1A**). Only with the addition of the complete pentameric TOG array (TOG1-5) or the adjacent C-terminal domain (TOG5-Cterm) did I see successful binding to F-actin (**Figure 3.II.1**). In each case, the presence of the TOG5 domain was required for F-actin binding. Thus, my data indicates that TOG5 domain is acting as an F-actin binding domain, although proper conformation is likely required by other adjacent domains to facilitate the interaction.

Not only did I determine that the TOG5 domain was necessary for F-actin interaction, but the XMAP215 C-terminal domain was important as well. The C-terminal domain of XMAP215 has been studied for its ability to interact with the coiled-coil domains of other proteins such as TACC3 [103,104,129], SLAIN1/2 [96,97], and for its involvement in microtubule nucleation [120]. While I saw apparent binding affinity of the TOG1-5 domains to F-actin of around 1.2 μM, addition of the C-terminal domain to TOG5 produced an over ten-fold stronger affinity of around 0.06 μM for F-actin. Comparing this to the binding affinity of the full length XMAP215 (K_d = ~0.03 μM) [109], the C-terminal domain rescued levels of F-actin binding to that of WT protein levels (**Figure 3.II.1B**). The C-terminal domain on its own, however, had no effect in binding to F-actin (**Figure 3.II.1D**). One recent study indicates the potential of a cryptic TOG6 domain within the

C-terminal domain [155], highlighting the possibility of C-terminal domain co-involvement with this TOG5 oriented function. In addition, little information regarding C-terminal conformational changes upon binding to F-actin or microtubules exist. As the C-terminal domain is largely made up of alpha helices and unordered regions [103,155], structural flexibility may either hinder or facilitate adjacent TOG5 binding to F-actin based on protein-protein interactions or phosphorylation states. Thus, the C-terminal domain may play a role in facilitating the correct conformation of the TOG5 domain in order to ensure correct F-actin binding, although more information regarding this important domain is required. In addition, how other MAP/F-actin binding proteins can influences F-actin interaction through this domain needs to be studied further.

In addition to determining the necessary domain for F-actin interaction, through my biochemical assays and super-resolution imaging of the growth cone, I establish a potential F-actin/microtubule crosslinking function as separate from its role as a polymerase. First, I show that XMAP215 is capable of distinctly binding to either the microtubule lattice (through its microtubule lattice binding domain), or to the plus end of the microtubule (through its C-terminal domain) in growth cones (**Figure 3.II.2A**). Interactions with the lattice and the plus end are still possible without these two initial TOG domains [34], as long as their respective interaction domains are present. Without the use of its TOG1-2 domains, required for catalyzing the addition of GTP-tubulin subunits [94], XMAP215 deletion mutant OE shows no effect on microtubule growth speeds in the growth cone (**Figure 3.II.3**). These TOG1-2 deletion mutants confirmed what was seen previously in other cell types [105] and in vitro [101]. More importantly, while not affecting growth speeds, we show that XMAP215 is capable of influencing microtubule populations in the growth cone. Overexpression of the TOG3-Cterm construct in the growth cone

leads to a significant reduction in microtubule looping (**Figure 3.II.3A, B**). While Microtubules are inhibited in their ability to transition outside the central domain by F-actin arcs and lamellaepodia [7,41], microtubules are thought to interact transiently along F-actin bundles for extension into the periphery [10,46]. When microtubules cannot effectively use these F-actin guidance mechanisms, some populations are stuck inside of the central domain [41], while others penetrate into the peripheral domain in a disorganized fashion [47]. Utilizing a similar knockdown and rescue experimentation system as in previous studies [109], I show that the TOG3-Cterm construct is capable of rescuing both KD induced microtubule penetration (**Figure 3.II.4C**) as well as reductions in populations of microtubules capable of reaching filopodia (**Figure 3.II.4D**). Thus, I believe that XMAP215, specifically its combination of microtubule lattice and F-actin binding domains, facilitates transient microtubule interactions along bundles of F-actin in the growth cone.

To test that possibility further, I took super-resolution images of F-actin and microtubules alignments in the growth cone. Microtubules capable of being guided along F-actin bundles would follow similar trajectories and would grow closely together [54]. While some microtubule associated proteins may cause a strong interaction between microtubule and F-actin [17,50], others are thought to allow a transient microtubule/F-actin interaction, not restricted by F-actin retrograde flow to the same extent [22,115]. When microtubule and F-actin interaction is affected in the growth cone, microtubules can display varied trajectories in the periphery [41,47], as well as showing areas devoid of microtubules [141]. When I analyzed exploratory microtubules in the growth cone, I saw that the TOG3-Cterm construct could again affect microtubule populations (**Figure 3.II.5**). Addition of TOG3-Cterm mRNA to partial XMAP215 KD rescued alignments of microtubules to F-actin in the growth cone back to control levels (**Figure 3.II.6B**).

Importantly, only deletion constructs that contained a microtubule lattice-binding domain, and were capable of directly interacting with F-actin, could rescue all microtubule related phenotypes. Thus, XMAP215 is capable of facilitating microtubule extension and guidance most likely along F-actin bundles in the periphery.

Taken together, my data suggests a unique microtubule guidance mechanism directed through XMAP215/F-actin interaction. In this Chapter, we have shown that pools of lattice bound XMAP215 are capable of rescuing microtubule guidance defects. In addition, I have shown that the TOG5 domain is critically important for binding directly to F-actin, while the C-terminal domain assists in this functional binding. Through transient interactions with F-actin, microtubules can escape the central domain of growth cone and explore the periphery [10,22]. In this way, XMAP215 can spatially regulate populations of exploring microtubules, controlling downstream signaling events through these guidance cue "sensors" in the periphery.

Indeed, in the previous chapter, it was shown that XMAP215 could affect microtubule and F-actin interactions downstream of Ephrin repellent signaling cascades in the growth cone [109]. Furthermore, while not affecting F-actin retrograde flow rates [112], this unique F-actin related XMAP215 function was shown to affect growth cone pausing, highlighting its role in changing the internal signaling state through microtubule spatial alterations [109]. Importantly, I show here that this function of XMAP215 is separate from its microtubule polymerase function, solidifying XMAP215's diverse and important role in linking microtubule and F-actin cytoskeletons together. While capable of binding to microtubule and F-actin directly, the ability of XMAP215 in cross-linking F-actin and microtubule simultaneously needs to be validated still. In addition, since XMAP215 is part of large +TIP complexes and signaling networks, it would be beneficial

to understand the extend of other protein's involvement in this microtubule/F-actin related function of XMAP215.

IV. Materials and Methods

Xenopus embryonic neural tube explants

Eggs collected from female *X. laevis* frogs were fertilized *in vitro*, dejellied, and cultured following standard methods [156]. Embryos were grown to stage 22-24 [144], and neural tubes were dissected as described [146]. All experiments approved by the Boston College Institutional Animal Care and Use Committee and performed according to national regulatory standards.

Constructs, RNA, and Antisense oligonucleotides

Constructs used in Xenopus embryonic growth cone imaging: pT7TS XMAP215-FL-GFP (a gift from the Hyman lab [101]), pT7TSr TOG3-Cterm-mNG, pT7TSr TOG5-Cterm-mNG, pCS2+ TOG5+lattice-mNG (TOG5++). Constructs were subcloned (PCR of full-length XMAP215-GFP vector) into either pT7 or pCS2+ vectors for mRNA transcriptions and subsequent microinjection into Xenopus embryos. Constructs used in in vitro protein purification and biochemistry experiments: pFB XMAP215, pFB TOG1-4, pGEX GST TOG1-4+lattice, pFB TOG1-5, pStr TOG3-Cterm (gift from Petry lab), pStr TOG5-Cterm (gift from Petry lab), pGEX GST TOG5, pGEX GST TOG3-5, pGEX GST TOG4-5, and pFB XMAP215 C-terminal only. Constructs subcloned (PCR of full-length XMAP215-GFP vector) into either pFastbac, pStr, or pGEX GST vectors for protein purification and in vitro experiments. For constructs to be in vitro transcribed into mRNA, template DNA transcribed using SP6 or T7 mMessage Machine Kit

(Ambion). Previously validated antisense oligo targeted to a splice site (5' ggctttccaaacctaccatgaaaca 3') were used in these experiments for XMAP215 KD experiments (Lowery 2013, Slater and Cammarata 2019), in addition to using a standard control antisense oligo (5' cctcttacctcagttacaatttata 3') (GeneTools, LLC, Philomath OR, USA). All embryos were injected 4 times in dorsal blastomeres at two to four cell stage in 0.1X MMR/ 5% Ficoll at concentrations listed: 750 pg of XMAP215-FL-GFP and equimolar concentrations of either TOG5+lattice, TOG3-Cterm, or TOG5-Cterm. Antisense oligonucleotides injected at 20 ng/embryo, equivalent to 70% KD [112,149].

Protein purification

XMAP215-FL and other constructs in pFastBac vectors were purified using a bac-to-bac purification system as previously described [94,147,149]. Constructs contained in the pFB vector were used to create bacmid and amplified Baculovirus using cultures of SF9 insect cells. P2 Baculovirus containing proteins of interest were transfected into Hi-5 insect cells for protein expression (*Trichoplusia ni*) (ThermoFisher Scientific) at a density of 2.0 x 10^6 cells/ml. Filtered lysate purified using Nickel or Cobalt column chromatography. Protein eluted with a 250 mM imidazole elution buffer (50 mM HEPES pH 7.25, 200 mM NaCl, 250 mM imidazole, 0.1% Triton-X, 1 mM DTT, 0.5 mM EDTA, 5% glycerol, 1 mM PMSF, 1X complete protease inhibitor cocktail). Constructs containing pStr or pGEX GST transformed into pRare containing Rosetta2 bacteria, grown in Amp/Chloramp broth, induced using 0.1-0.4 mM IPTG at 16 hours (20.0C), and purified using either Nickel/Cobalt, Streptavidin, or Glutathione agarose. Constructs with GST tags were cleaved off beads using Prescission Protease (GE Healthcare) overnight at 4.0C. Subsequent lysate passed over fresh equilibrated glutathione agarose for

further clarification. Protein buffers exchanged using Amicon ultracentrifugation 10,000 or 100,000 MWCO column (Storage Buffer: 10 mM K-HEPES pH 7.25, 100 mM KCl, 5.0 mM EGTA, 2.0 mM MgCl2, 0.1 mM CaCl2, 10% glycerol) and snap frozen/stored at -80.0°C. Purified monomeric actin (Cytoskeleton Inc) diluted to 0.4 mg/ml in a general actin buffer (5 mM Tris pH 8.0, 0.2 mM CaCl2, 0.2 mM ATP, 0.5 mM DTT) and polymerized through the addition of a 10X actin polymerization buffer (500 mM KCl, 20 mM MgCl2, 10 mM ATP) at RT.

F-actin co-sedimentation assays

F-actin co-sedimentation assays performed as previously described [157]. Polymerized F-actin incubated with purified XMAP215 (or deletion construct) protein in injection buffer (10 mM Tris pH 7.0, 150 mM NaCl, 1 mM ATP, 0.1 mM CaCl2, 2.0 mM MgCl2, 0.2 mM DTT, and 1.0 mM EGTA) for 15 min at RT. All protein precleared before incubation with F-actin to remove aggregates. For non binding-curve experiments, F-actin was added to XMAP215 purified proteins in excess. For binding curve experiments, XMAP215 (or deletion protein) concentration was kept constant, with increasing concentrations of F-actin. Proteins that did not show binding at lower concentrations of F-actin were incubated with much higher concentrations to determine if any binding possible (XMAP215 C-term). Following incubation, samples were centrifuged at 100,000 x g for 20 min at 20 °C using a Beckman TLA100.4 ultracentrifuge. Phalloidin used to stabilize F-actin in these experiments (with no apparent effect to F-actin binding). Samples were run on SDS-PAGE gels and stained with Coomassie Brilliant Blue G-250 before imaging. Densitometry of protein bands on SDS-PAGE gels analyzed using ImageJ, and plotted using GraphPad Prism. All experiments plotted using data from 3-4 repeat

experiments (curves fit by GraphPad Prism non-linear regression assuming a one-site saturation model).

Immunocytochemistry

Embryonic explant cultures were fixed with 0.2% glutaraldehyde and labeled as described [40]. Growth cones were stained using rat anti-tyrosinated tubulin (1:800, ab6160, Abcam), mouse anti-mNeonGreen (1:400, 32F6, Chromotek,) and Phalloidin^{488} (1:400, Molecular Probes). Secondary antibodies used were goat anti-rat AlexaFluor^{633} (1:500, Life Technologies), and goat anti-mouse AlexaFluor556 (1:500, Life Technologies). All antibodies used were pre-absorbed to reduce any potential cross-reactions. Blocking and all antibody diluent solutions made with 5% goat serum.

Image Acquisition

Live cell imaging and Structured Illumination imaging setup previously described in Slater and Cammarata, 2019. Live cell imaging of cultured spinal cord explants were obtained with a CSU-X1M 5000 spinning-disk confocal (Yokogawa, Tokyo, Japan) on a Zeiss Axio Observer inverted motorized microscope using a Zeiss 63× Plan Apo 1.4 numerical aperture lens and oil based objective (Zeiss, Thornwood, NY). Images acquired with an ORCA R2 charge-coupled device camera (Hamamatsu, Hamamatsu, Japan) controlled by Zen software. Time-lapse images were collected every two seconds for 1 min. For fixed samples using Structured Illumination, images were collected on a Zeiss Axio Observer.Z1 microscope with Elyra S.1 system, utilizing an Objective Plan-Apochromat 63x/1.40 Oil objective. Images were acquired

with a PCO-Tech Inc. pco.edge 4.2 sCMOS camera. Images were processed in Zen Black to allow Channel alignment and Structured Illumination processing.

Image Analysis

The following descriptions provide the basis for analysis of microtubules within the growth cone. All methodology for image analysis of growth cones has been thoroughly described according to Slater and Cammarata, 2019 [149]. The growth cone was defined as the region contained between the growth cone neck and the tip of filopodia for the following imaging analysis. To quantify the amount of microtubule penetration into the peripheral domain, microtubules were measured from the start of their emergence into the area devoid of F-actin mesh to the ends of filopodia. Average penetration of all exploring microtubules were taken per growth cone. Measurements were manually taken using the segmented line tool in ImageJ. Quantification of number of exploring microtubules and microtubules present in the filopodia were all performed manually in ImageJ. The percentage of microtubules that are aligned to F-actin bundles were quantified by measuring both the distance between microtubule and F-actin bundle, and the angle of microtubule and F-actin filament. Microtubule and F-actin were considered aligned by the criteria that each filament is within 300 nm from each other and separated by a trajectory angle no greater than 15 degrees.

Experimental design and Statistical Analysis

All graphs and statistical analyses were performed using GraphPad Prism 8. Images of growth cones acquired from multiple varied explants per condition. At least three independent experiments were performed for each condition to ensure reproducibility. Student T-test was

performed when statistical comparisons between two conditions were being made. One-way ANOVA was used to determine that means between multiple conditions were statistically different beforehand. All data sets were analyzed using the D'agostino normality test to determine normal distribution. The alpha value was set at 0.05 for all statistical tests. The P values are represented by: *P<0.05, **P<0.01, ***P<0.001 and ****P<0.0001. Values are expressed as mean ± standard deviation.

V. Supplemental Data

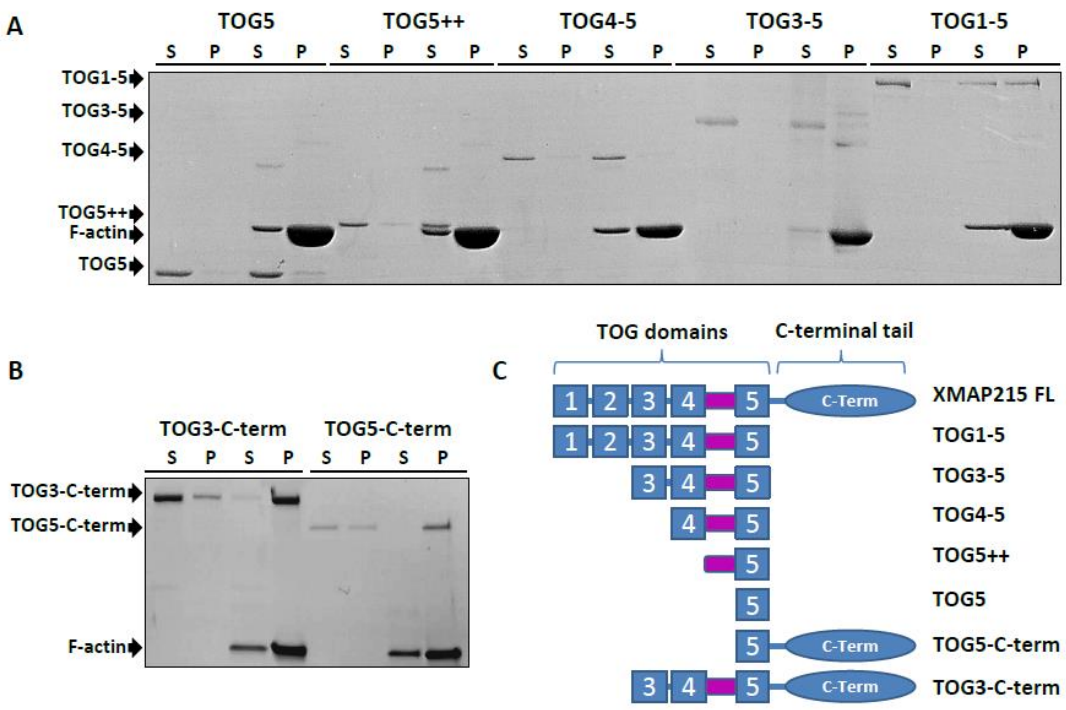

Figure III.S.1. TOG5 requires other domains to stabilize its binding to F-actin directly. A) Purified TOG domain proteins utilized in F-actin Sedimentation Assays to determine direct interaction. Purified TOG5, TOG5+lattice (TOG5++), TOG4-5, TOG3-5, and TOG1-5 proteins incubated with either 6.0 µM (TOG5 and TOG5+lattice), or 2.0 µM F-actin (all others) to determine protein binding to F-actin. TOG1-5 shown as a positive control that induced pelleting when incubated with F-actin. B) TOG3-Cterm and TOG5-Cterm proteins shown in F-actin sedimentation assays incubated either with or without F-actin (2.0 µM).

Chapter 4. Conclusion

I. Contributions to the Literature

This work establishes several important contributions towards the cell biology, molecular biology, and neurodevelopmental fields. Importantly, in this thesis I establish a novel function of the plus end tracking protein, XMAP215, known for its role in MT polymerization [94]. While this protein has been studied for the last three decades [93], no evidence has been shown for how XMAP215 plays a part in coordinating not just microtubules, but also the F-actin cytoskeleton as well. Especially important in the neuronal cell biology community, while many +TIP proteins have been described previously[33], increasing attention is being paid on how microtubule and F-actin cytoskeletons are in coordination with each other [115], and how this coordination can regulate axon guidance and outgrowth mechanisms (**Chapter 1**).

Early on, I show that XMAP215 possesses a unique ability to regulate axon outgrowth and axon guidance through a distinct F-actin related function (**Chapter 2**). This F-actin related function of XMAP215 was hinted at in previous literature [112], although never fully realized until now. In the neuronal cell biology community, a vast amount of research is being carried out on the signaling mechanisms that can control axon outgrowth and guidance, uncovering how axons can make their numerous connections early on in the brain [1,19,115,140]. XMAP215, like other +TIP proteins, is in a perfect position to regulate signaling of the cytoskeletal systems and cell motility, acting as a signaling intermediary downstream of environmental cues and kinase pathways [1]. In the second chapter of this thesis work, I present data that highlights XMAP215's

role in regulating axon outgrowth and guidance mechanisms through time-lapse imaging of growing axons and Ephrin repellent stripe assays.

Importantly, I then go on to further narrow down this function towards the N-terminal TOG1-5 of XMAP215, highlighting the TOG1-5 involvement in F-actin colocalization, and rescue of MT and F-actin alignment defects. Interestingly, this data pointed me towards the importance of the region between the TOG4 and TOG5 domain for F-actin and MT interaction, however, how XMAP215 was interacting with the microtubule, and just as importantly, F-actin, still had to be revealed (questions elucidated further in Chapter 3). Finally, after pointing towards a new MT/F-actin mechanism for XMAP215 that could govern the fate of MT guidance in the growth cone (and total axon outgrowth), I then set out to determine if this F-actin interaction could be a direct mechanism. Utilizing purified proteins and biochemical assays, I showed that indeed, XMAP215 does bind directly to F-actin (an ability never been shown before). While there are several +TIPs that can interact with F-actin in the cell [33,115], there are very few that interact with F-actin directly [115], or have the functional diversity that XMAP215 seems to have [105,109,112,119,120,158].

After establishing that XMAP215 is capable of binding directly to F-actin, I go on to demonstrate mechanistically the important domains that are required for this interaction, as well as how XMAP215 is interacting with the microtubule while utilizing this F-actin function (**Chapter 3**). In this chapter, I discovered that the TOG5 domain was necessary for binding directly to F-actin in vitro, while the C-terminal domain of XMAP215 influenced this interaction (possibly through changing conformation or folding in a way to make the TOG5 domain accessible). Furthermore, I showed here that XMAP215 (TOG3-Cterm) is capable of rescuing MT alignment to F-actin in neuronal growth cones, a construct that interacts with the

microtubule lattice, while the TOG5-Cterm deletion construct did not rescue, as it only bound to the MT plus end. In this fashion, XMAP215 may have an internal switch that changes its localization from lattice bound to plus-end-oriented, similar to +TIPs, CLASP and APC[18,52,53]. In addition, WT XMAP215 localizes to both plus end and MT lattice localizations in the cell normally [109,112]. While not shown in this thesis work, I did notice that differences in phosphorylation of XMAP215 possessed different strengths in binding to F-actin in vitro (data not shown). It is quite possible that further elucidation of this mechanism will reveal phosphorylation to be a key component in switching between a lattice-based, and a plus end based mechanism, splitting XMAP215's polymerization role, and its F-actin/MT linking role. Therefore, in this thesis work, I offer a critical component of determining the overall mechanism of XMAP215, in the context of MT/F-actin interaction, in which the next steps will likely be establishing how XMAP215 binds to F-actin structurally, and how phosphorylation, or other proteins, affect this capability.

Finally, it is quite important that I have established that the novel function that XMAP215 possesses is not related to its MT polymerase function (**Chapter 3**). From the beginning, I made sure that the constructs used in this work did not affect MT polymerization at all by deleting the TOG1-2 domains responsible for GTP-tubulin binding [94,101,105]. However, even after deletion of these domains (and confirmation they did not increase growth velocities in growth cones), rescue of MT and F-actin alignment phenotypes with these constructs still occurred. Thus, our work establishes an important combinatorial role for XMAP215 consisting of two main functions, its polymerase activity [94], and its role as a microtubule and F-actin cytoskeletal linking protein[109]. As this novel XMAP215 mechanism is separate from its plus-end oriented function, and since we see XMAP215 localized on the MT lattice in more cell types

than just neuronal growth cones [34,105,112], it will be quite interesting to speculate on the reach this mechanism plays in other cell contexts, and cellular functions.

II. Future Directions

Determining the ability of XMAP215 to directly crosslink MTs to F-actin

One of the main areas of research that is still being looked into regarding XMAP215 is its ability to crosslink MTs and F-actin together. Utilizing a technique that has been employed for a few decades in the cytoskeletal field, I have set up a dynamic MT reconstitution assay system in our laboratory [159]. While I have used this technique in previous work looking at MT/+TIP interaction for TACC3 (data not shown), an in vitro reconstitution system will be helpful in looking into the MT/F-actin interaction with purified XMAP215. It can then be determined, definitively, if XMAP215 is sufficiently acting as a direct MT/F-actin crosslinking protein or not. As there are very large +TIP complex networks in the growth cone, XMAP215 may utilize an intermediate protein to facilitate its MT/F-actin binding capability [32,36].

It will also be worthwhile to determine how phosphorylation is playing a role in localizing XMAP215 to the microtubule. Similarly to CLASP and APC, phosphorylation affects these +TIP proteins in localizing either along the microtubule lattice, or at the plus end of the microtubule [18,51–53]. In addition, as stated previously in this thesis, the required F-actin binding domain of XMAP215, TOG5, shows high sequence similarity towards the TOGL1 domain of CLASP (30-50% in certain stretches of CDS), the proposed F-actin binding domain for that MT associated protein [21,51]. In this case, there is some basis for further exploration of TOG domains as a new class of F-actin binding domain. Also, previously acquired data shows that purified

XMAP215-FL protein with differential phosphorylation results in an altered strength of binding to actin filaments in vitro (data not shown). Therefore, differential phosphorylation states affect overall localization to the MT as well as F-actin binding activity in certain TOG domains, which may point to the TOG domain as a domain family that possesses dual MT and F-actin filament binding based on structural conformation or discrete signaling states in the cell. Thus, in addition to the common neuronal culture and microscopy assays, utilizing phospho-mutant XMAP215 protein in our in vitro reconstitution assays would be extremely beneficial to determine effects on localization and signaling. In addition, it would be quite interesting to compare the XMAP215 TOG and the CLASP TOGL domains to each other, and analyze the functions of each domain through a chimeric construct approach in growth cones in the future. By utilizing purified XMAP215 proteins along with the techniques described in this thesis, as well as utilizing an in vitro MT/F-actin reconstitution method, further uncovering of the overall mechanism of XMAP215/MT/F-actin interaction is quite possible.

XMAP215's role in affecting the Actin cytoskeleton

A secondary mechanism +TIPs may employ in growth cones is their ability to stimulate actin nucleation [160–162], a function that may be especially relevant in the far reaches of the growth cone filopodia and periphery. While significant strides have been made in unraveling how certain +TIPs may act on both F-actin and microtubule cytoskeletons [32,35,115], and the ramifications that these interactions lend to growth cone behaviors, several chief broad questions remain unanswered. In addition, although we know many details about certain +TIPs and how they can affect microtubule/actin dynamics, much of this research was not conducted in neurons. There is evidence that +TIPs can serve growth cone-specific functions, rather than behaving consistently

across different cell types [112,163]. Thus, it is both valuable and necessary to continue studying the functions of +TIPs both in and outside of the neural context.

Specifically with XMAP215, I have seen interesting morphological effects in the growth cone that cannot be necessarily explained by a transient interaction with F-actin bundles. There are changes in growth cone area and total F-actin levels following XMAP215 manipulation, which likely indicates changes to the internal signaling state of the growth cone, in which the growth cone cannot interpret guidance cues correctly [164] . Although, what this actually means in the context of affecting F-actin related protein levels in the cell is unknown. It is interesting to point towards the EB1/Drebrin complex, which there is preliminary evidence of its ability to inhibit the F-actin severing protein, cofilin [69,76]. Although partial XMAP215 KD has shown no effect on F-actin treadmilling rates[112], XMAP215 may affect other F-actin related protein. Future studies of +TIPs, like XMAP215, which have been examined chiefly for their roles in affecting microtubules, may reveal that they function in unique roles to affect F-actin in the growth cone.

Expanding the Library of +TIPs controlling MT/F-actin interaction

It is also important to note that the known library of +TIPs is still expanding. The more recently identified small kinetochore-associated protein, SKAP [165], was also shown to bind to EB1 and IQGAP in order to mediate microtubule steering and protrusion in HEK cells [166]. However, it remains to be seen whether this association with IQGAP may also indicate a role in microtubule-F-actin crosslinking events. In addition to SKAP, mitotic interactor and substrate of Plk-1 protein, MISP, has been recently demonstrated to interact with EB1 as well as to colocalize with the actin cytoskeleton and focal adhesion proteins [167]. Although its ability to act as a +TIP on microtubule plus-ends has not been confirmed, it would be interesting to see the potential role

it could play in mediating microtubule and F-actin interactions. As identification of +TIPs increases, we must examine their interactions with F-actin and focal adhesion proteins, with signaling cascades, and with one another, in order to fully understand their roles in guidance behaviors.

While the ability of XMAP215 to affect the F-actin cytoskeleton has now been shown through this work, we still do not know all of the proteins that are involved in this specific function. As +TIP proteins are usually associated as large complexes[32], there is likely many other proteins that can facilitate this F-actin function, regardless of XMAP215 being capable of interacting with F-actin directly. It has been known for a long time that XMAP215 interacts with the TACC family of proteins[103,104,129], as well as EB1/SLAIN1/2 complexes[96,97,121], and genetically interacts with CLASP[95]. Each of these proteins either shows some level of F-actin interaction, or indirectly acts with a protein that can interact with F-actin. In this case, looking into the whole network of +TIP proteins that are involved in this function through pull-down experiments and mass spectrometry would be beneficial to fully determine the mechanism taking place.

III. Closing Remarks

The growth cone requires collaborative and dynamic coordination of the F-actin and microtubule cytoskeletons in order to properly navigate the extracellular cues presented to it within the developing embryo. Coupling and uncoupling mechanisms between the two cytoskeletons can alter localization of microtubules, thus promoting their retraction or protrusion [35,115]. Similarly, closely linked microtubules and F-actin can be exposed to the same local signaling cascades, allowing them to undergo coordinated remodeling [18,53]. +TIPs are

increasingly demonstrated to act in this capacity, as they can serve as both modulators of plus-end dynamicity and microtubule-F-actin cross linkers [115], which can be dynamically regulated by phosphorylation events downstream of guidance cue signaling pathways. Extracellular signaling cues can therefore be translated through actin/microtubule binding into growth cone outgrowth and turning events [35].

In my thesis work presented here, research into the microtubule polymerase, XMAP215 (ch-TOG), has revealed a previously unknown mechanism that allows for microtubule and actin collaboration in the growth cone. While I have determined through super resolution imaging and biochemical techniques that XMAP215 is capable of affecting the F-actin cytoskeleton through a microtubule lattice based platform, it is still unknown the extent that this mechanism is employed throughout the cell (and other cell types besides neurons). In addition, how XMAP215 phosphorylation (similar to mechanisms of CLASP and APC) affects the ability of XMAP215 to localize to the MT and function as an F-actin interacting +TIP will undoubtedly be necessary to explore.

Over the last several years, there have been significant advances in the types of techniques used to study the cell biological interactions within growth cones. Techniques like live brain imaging [168] allow researchers to follow growth cones in living tissue. Also, recent biochemical assays employing the protein TIPact, a minimalist molecule containing microtubule and actin binding domains, could potentially be used to uncover more information on how these two cytoskeletons interact [169]. Furthermore, the use of super resolution microscopy techniques has also increased, allowing for image resolution that extends beyond the diffraction limit of light and confocal microscopes. Specifically, recent experiments on photoactivatable complimentary fluorescent (PACF) proteins have shown precise super resolution images of EB1 tracking along

the microtubule plus-ends [170]. Employing new techniques in our work may vastly benefit our understanding of the inner workings of actin-microtubule interactions.

As XMAP215 is a ubiquitous molecule found in most cell types, including being heavily upregulated in embryonic and cancerous cells, it would be interesting to speculate about it's potential as a therapeutic target for certain cancer cell types. In addition, there is a diverse selection of mutations in microtubule-associated proteins that affect mental disorders and neuro-related diseases [171]. XMAP215 has shown itself to be a functionally diverse molecule, being directly involved in cell division, as well as acting as a microtubule polymerase, microtubule nucleator, and now a microtubule/F-actin interacting protein. Since we have shown a novel role that is functionally separate from its characteristic MT polymerase ability, it may be worthwhile to look into how different signaling mechanisms may affect its ability to select between microtubule polymerization and MT/F-actin interaction, as its ability to interact with F-actin is linked to a MT-lattice based localization, as opposed to a plus end mediated function. In conclusion, the work that is presented here in this thesis moves forward the field of cell biology, providing a pathway for studying XMAP215 further and uncovering unique mechanisms that play a part in cytoskeletal remodeling and neuronal signaling pathways. While I have presented data that point towards a novel and uncharacterized function of XMAP215, there is still much more to be discovered in the future.

Chapter 5. Appendix

Appendix Chapter 1. The microtubule plus-end-tracking protein TACC3 promotes persistent axon outgrowth and mediates responses to axon guidance signals during development

*My role in facilitating the completion of this chapter was the following: Axon outgrowth and KHS drug experiments in Figure 1, MT Dynamics data involved in Figure 3, subcloning of constructs and general reagent preparation. However, the full manuscript is included in its entirety, adapted from: (Erdogan et. al., 2017 - Neural Development)

Introduction

Plus-end tracking proteins (+TIPs) selectively bind to the dynamic plus-ends of microtubules (MTs), which extend into the distal part of the axon and growth cone [1]. This enables + TIPs to come into close contact with the cell cortex, where guidance cue receptors reside. These receptors transduce asymmetrically-distributed guidance signals down to intracellular effectors, which then regulate MT dynamics in a spatially-restricted manner that likely plays a key role in growth cone turning events [19,115]. Thus, +TIPs deserve attention for their potential function in regulating MT dynamics during axon guidance. One of the first + TIPs to be discovered for its role in axon guidance was CLASP [17]. Genetic studies in Drosophila demonstrated that CLASP is a downstream target of Abelson tyrosine kinase (Abl) in the Slit/Robo guidance pathway during central nervous system midline crossing [17]. Moreover, the + TIP and MT polymerase, *msps* (fly ortholog of XMAP215/ch- TOG) interacts with CLASP antagonistically during this guidance

decision in an Abl-dependent manner [95]. In addition to its role in Drosophila, XMAP215 has been implicated in promoting axon outgrowth in vertebrates [112]. We have recently shown that the XMAP215-interactor, TACC3, is also a + TIP that regulates MT dynamics in vertebrate growth cones and is essential for normal axonal outgrowth [98]. However, how TACC3 specifically affects axon outgrowth and whether TACC3 plays a role during axon guidance remain to be explored.

In this study, we examine the role of TACC3 in axon outgrowth and pathfinding in vivo within the developing nervous system of Xenopus laevis which is a great model for studying cytoskeletal dynamics during axon outgrowth and guidance [172,173]. Using time-lapse live imaging, we demonstrate that TACC3 is required for persistent axon outgrowth in Xenopus laevis, and that both the N- and C- terminal conserved domains of TACC3 are necessary for enhanced axon outgrowth. Moreover, TACC3-overexpressing growth cones can mitigate the reductive impacts of the MT-depolymerizing agent, Nocodazole, on MT dynamics parameters. We also show that TACC3 and XMAP215 can display a synergistic effect and promote axon outgrowth ex vivo. Finally, examination of whole mount Xenopus spinal cords shows defects in axon guidance in motor neurons when TACC3 levels are depleted, and manipulation of TACC3 levels impact the growth cone response to the repellent guidance cue Slit2 in cultured Xenopus spinal neurons. Together, these investigations provide new insights into the mechanism by which TACC3 functions either alone or in combination with other + TIPs, such as XMAP215, to regulate MT dynamics during axon outgrowth and guidance.

Results

TACC3 promotes persistent axon outgrowth by preventing spontaneous axon retractions

We previously showed that normal axonal outgrowth requires TACC3 [98]. To gain further insight into the mechanism by which TACC3 promotes axon outgrowth, we examined the effect of TACC3 knockdown (KD) and overexpression (OE) on dynamic axon outgrowth parameters. Time-lapse imaging demonstrated that TACC3 KD significantly reduced axon outgrowth velocity by 25% relative to control conditions (TACC3 KD, 0.74 ± 0.03, n = 46, versus control, 1.04 ± 0.03 n = 57, ***p < 0.0001, **Figure A.I.1A**). In addition to the reduced outgrowth velocity, TACC3 reduction dramatically increased axon retraction rates by 5-fold in comparison to control axons (TACC3 KD, 5.27 ± 1.22, n = 107, versus control, 1.06 ± 0.35, n = 99, **p = 0.0015, **Figure A.I.1B**). Conversely, when TACC3 levels were elevated, the frequency of axon

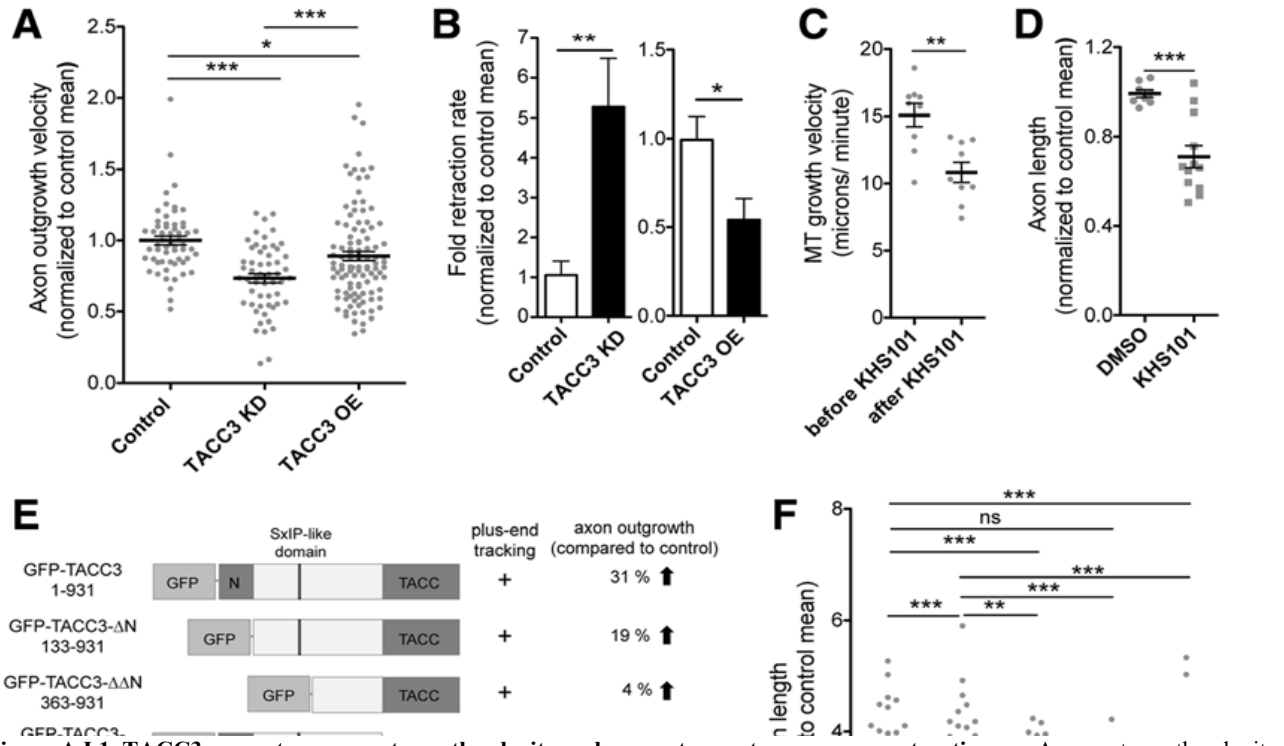

Figure A.I.1. TACC3 promotes axon outgrowth velocity and prevents spontaneous axon retractions. a, Axon outgrowth velocity is significantly decreased in TACC3-depleted axons by 27% (n = 56) and in TACC3 OE, to a lesser extent, by 11% (n = 106) compared to control (GFP only) conditions (n = 58). b, Retraction rate increased 5 fold in TACC3 KD (n = 107) and decreased 0.6 fold in TACC3 OE (n = 155) in comparison to their corresponding non injected (n = 95) and GFP injected (n = 180) controls respectively. c, d, MT growth velocity (DMSO, n = 9, KHS-101, n = 9) (c) and axon outgrowth length (DMSO, n = 8, KHS-101, n = 12) (d) are significantly reduced by 28 and 26% respectively after acute depletion of TACC3 by the inhibitor KHS101. e, Schematic representation of GFP-tagged TACC3 full-length and deletion constructs, along with plus-end tracking ability (denoted by "+") and impact on axon outgrowth length. f, Quantification of axon outgrowth length in cultured neural explants of GFP injected control (n = 997), full-length GFP-TACC3 (1-931aa) (n = 787), GFP-TACC3-ΔN (133–931) (n = 613), GFP-TACC3- ΔΔN (363–931) (n = 563) and GFP-ΔTACC domain (1-635aa) (n = 764). *p < 0.05, **p < 0.01, ***p < 0.001. ns not significant. n = axon/growth cone number.

retraction rates was reduced significantly by 45% compared to controls (TACC3 OE, 0.54 ± 0.12, n = 155, versus control, 0.99 ± 0.12, n = 180, *p = 0.01, Fig. 1b). Although TACC3 OE led to increased axonal length (**Figure A.I.1F**), TACC3 OE actually reduced axon outgrowth velocity by 14% (0.89 ± 0.32, n = 103, versus control, 1.04 ± 0.033, n = 57, *p < 0.0268, Fig. 1a), suggesting that the increased axonal length may result from reduced axon retraction rather than a change in outgrowth velocity.

To further explore the TACC3 KD phenotype, we examined axon outgrowth of cultured neurons in which TACC3 was acutely inhibited by the TACC3 specific inhibitor, KHS-101 [174]. Consistent with the effect seen in TACC3 KD, KHS-101-induced acute inhibition of TACC3 significantly reduced MT growth velocity by 28% (15.09 ± 0.86 μm/min (before drug treatment); 10.84 ± 0.75 μm/min (after drug), **p < 0.0019, **Figure A.I.1C**). Moreover, acute inhibition led to an immediate retraction of axon length by 26% compared to vehicle treated controls (KHS-101, 0.71 ± 0.05, n = 12, versus DMSO, 0.96 ± 0.03, n = 9, ***p = 0.0007, **Figure A.I.1C**). In order to determine which domains of TACC3 are involved in axon outgrowth, we tested various truncation mutants of TACC3. We found that, while full- length TACC3 and ΔN (lacking conserved N-terminal domain) significantly increased axon outgrowth by 30% (1.30 ± 0.03, n = 787, ***p < 0.0001) and 18% (1.18 ± 0.31, n = 613, ***p < 0.0001) respectively, expression of ΔTACC (lacking the conserved TACC domain, which has been shown to be required for centrosome localization and interaction with the MT polymerase, XMAP215) caused a significant reduction by 12% in axon length (0.87 ± 0.021, n = 764, ***p = 0.0002) in comparison to wild-type neurons (0.99 ± 0.02, n = 997) (**Figure A.I.1F**). On the other hand, the larger N-term deletion (lacking both the conserved N-terminus and the putative SxIP-like motif that is known to mediate EB1 interaction for other + TIPs) showed no significant difference

(1.04 ± 0.028, n = 563, p = 0.2012). Additionally, none of the deletion constructs that promoted axon outgrowth were as effective as full-length TACC3 OE (**Figure A.I.1F**). Together, our findings suggest that TACC3 is required for proper axon outgrowth by opposing axonal retracting forces. Additionally, full-length TACC3 is more efficient in promoting axon outgrowth than its truncation mutants, while expression of a version lacking the TACC domain results in a mild dominant negative effect.

TACC3 antagonizes nocodazole-induced MT depolymerization but does not affect MT lattice stability

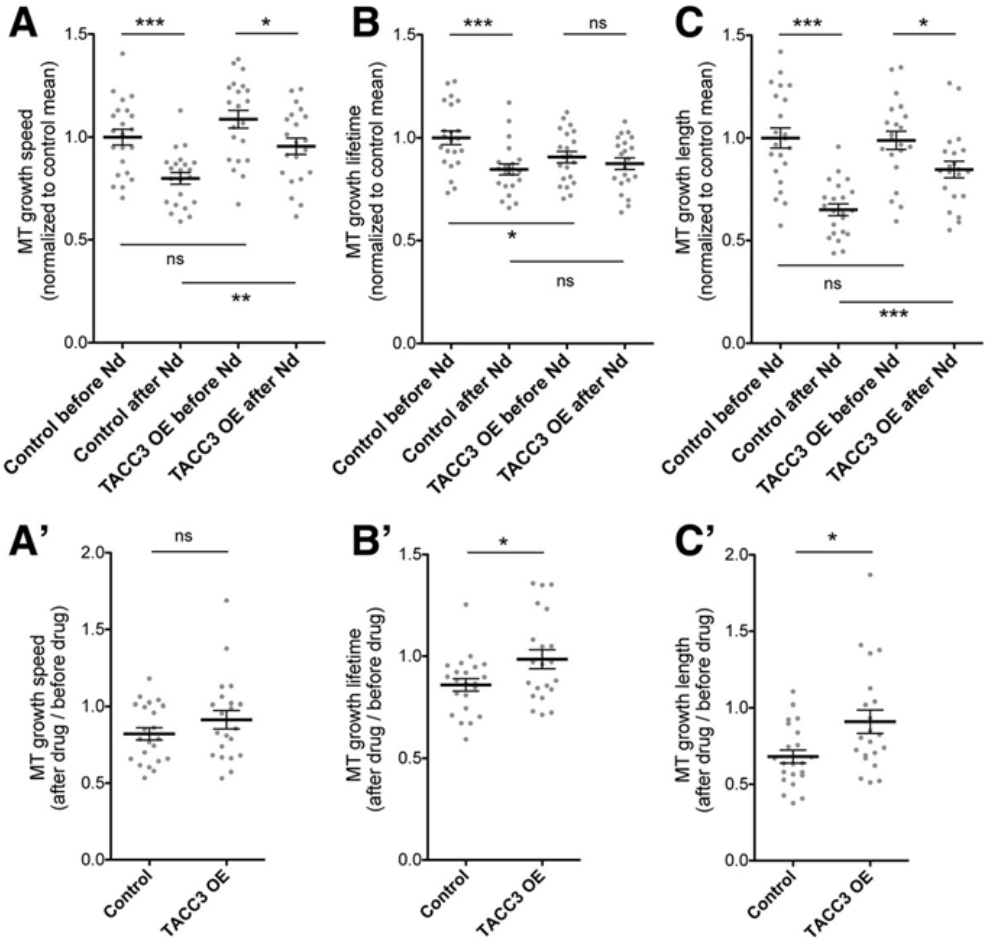

Figure A.I.2. TACC3 antagonizes Nocodazole-induced MT depolymerization but does not affect MT stability. a-c, Quantification of the MT dynamics shows significant reduction in MT growth speed (a), MT lifetime (b) and MT growth length (c) in control (n = 22) and TACC3 OE (n = 21) growth cones in response to 50 pM Nocodazole before and 5 min after drug treatment. However, the effect of Nocodazole on TACC3 OE growth cones is dampened compared to controls. a'-c', Although not significant, reduction in MT growth speed (a') is more prominent in control growth cones compared to TACC3 OE growth cones while the reduction in both lifetime (b') and length (c') in control growth cones are significantly higher than the TACC3 OE growth cones

Previously, we determined that TACC3 promotes efficient MT polymerization by enhancing MT growth velocity within growth cones [98]. However, the mechanism by which TACC3 affects MT polymerization remains to be elucidated. Thus, we sought to gain further insight by assessing the impact of low doses of the MT depolymerizing drug, nocodazole, after TACC3 manipulation. We observed that a low dose of nocodazole led to reduction in several parameters of MT dynamics, and that TACC3 OE could mitigate these effects. While control growth cones exhibited a marked 20% decrease in MT growth speed after treatment with 50 pM nocodazole (before, 1.00 ± 0.04, n = 22, after treatment, 0.79 ± 0.03, n = 22, ***p = 0.0001), TACC3 OE growth cones showed reduction by only 12% (before, 1.08 ± 0.04, n = 21, after nocodazole, 0.95 ± 0.03, n = 21, *p = 0.0316, **Figure A.I.2A**). Similar trends were observed with MT growth lifetime, in which control growth cones showed a 15% reduction (before, 1.00 ± 0.03 s, n = 22, after nocodazole, 0.84 ± 0.03 s, n = 22,***p = 0.0008) versus only a 3% reduction with TACC3 OE (before, 0.91 ± 0.03, n = 21, after nocodazole, 0.87 ± 0.03, n = 21, p = 0.4305, **Figure A.I.2B**), and for MT growth length, there was a 35% reduction in controls (before, 1.00 ± 0.05, n = 22, after nocodazole, 0.65 ± 0.03, n = 22, ***p < 0.0001) versus 14% in TACC3 OE (before, 1.00 ± 0.04, n = 21, after nocodazole, 0.85 ± 0.04, n = 21, *p = 0.02, **Figure A.I.2C**). These results suggest that TACC3 can mitigate the nocodazole-induced reduction in MT growth dynamics parameters. This mitigation can be more clearly visualized when the nocodazole-induced change is represented as the ratio of after treatment/before treatment. Although the relative reduction in MT growth speed when TACC3 is overexpressed is only slightly less compared to controls and is not quite statistically significant (0.91 ± 0.06 n = 21 versus control 0.82 ± 0.04 n = 22, ns p = 0.2, **Figure A.I.2A'**), for other MT growth parameters, TACC3 OE significantly dampens the nocodazole- induced reduction in lifetime (0.99 ± 0.047 n = 21 versus

control 0.86 ± 0.03 n = 22, *p = 0.03, **Figure A.I.2B'**) and length (0.91 ± 0.08 n = 21 versus control 0.68 ± 0.04 n = 22, *p = 0.01, **Figure A.I.2C'**) compared to controls.

In addition to MT polymerization, MT stabilization is considered an important parameter for axon outgrowth and growth cone turning events [40]. Hence, we measured the fluorescence intensities of tyrosinated and detyrosinated tubulin in the growth cone, and assessed dynamic and stable MT lattice profiles in TACC3-manipulated growth cones. We found that the ratio of tyrosinated tubulin versus de-tyrosinated tubulin did not statistically differ in TACC3 KD (0.87 ± 0.07, n = 37, p = 0.2394) nor in TACC3 OE (1.01 ± 0.11, n = 129, p =0.9673) growth cones, with respect to control growth cones (1.00 ± 0.09, n = 143, **Figure A.I.3A-C**). This suggests that TACC3 may not specifically regulate MT lattice stability in growth cones.

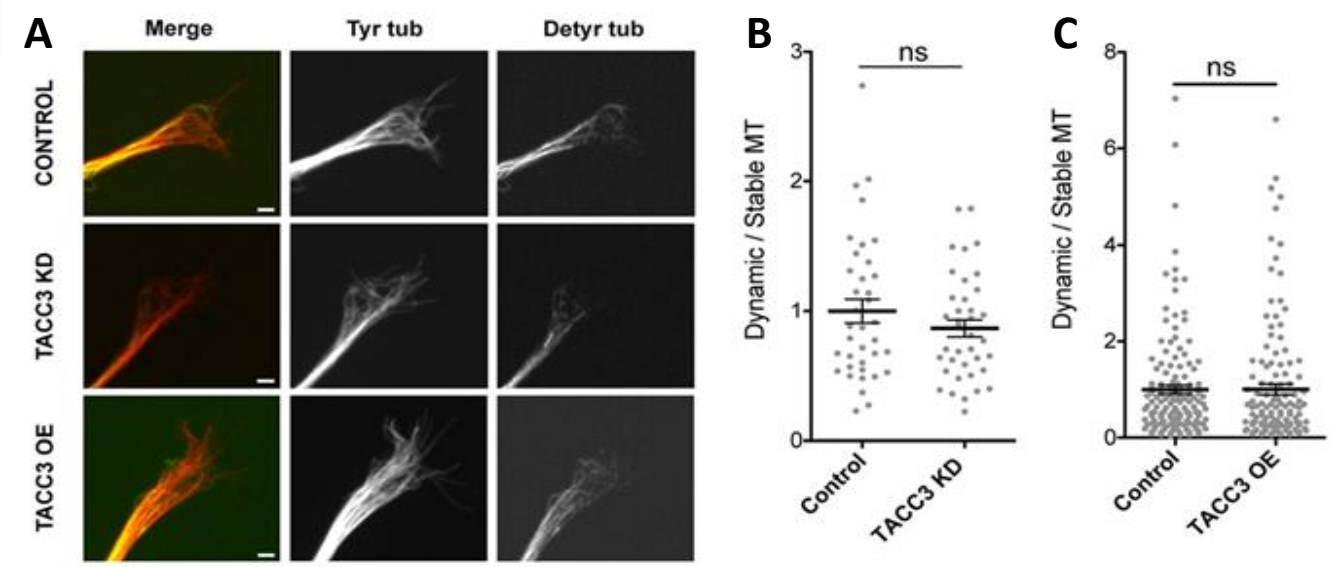

Figure A.I.3. Microtubule stability is not affected by modulation of TACC3 levels in the growth cone. Representative growth cone images of control, TACC3 KD and TACC3 OE, immunostained for tyrosinated tubulin (red) and detyrosinated tubulin (green) to label dynamic versus stable MTs, respectively. e-f, Quantification of the fluorescence intensity of imaging data in G, with TACC3 KD (n = 38) (e) and TACC3 OE (n = 129) (f) growth cones showing no significant changes in dynamic/stable MTs compared to corresponding control growth cones (n = 37 and n =143, respectively). *p < 0.05, **p < 0.01, ***p < 0.001. ns not significant. n = growth cone number. Scale bar, 2 μm.

TACC3 and XMAP215 interact to promote axon outgrowth. We previously found that the TACC3 interactor and MT polymerase, XMAP215, also promotes axon outgrowth [112], and that TACC3 and XMAP215 co-localize at the extreme plus-end of MTs in growth cones in a codependent manner [98]. However, the consequences of their interaction on axon development have not been elucidated. Therefore, we sought to test whether TACC3 and XMAP215 might cooperate synergistically to promote axon outgrowth by partially elevating or reducing TACC3 and XMAP215 levels alone and in combination with each other. While a very mild TACC3 KD (approximately 20–30% less) led to 10% reduction in axon out- growth (204.7 ± 4.8 μm, n = 487, p = 0.3528) and partial XMAP215 KD led to 13% reduction (185.6 ± 6.4 μm, n = 312, *p =

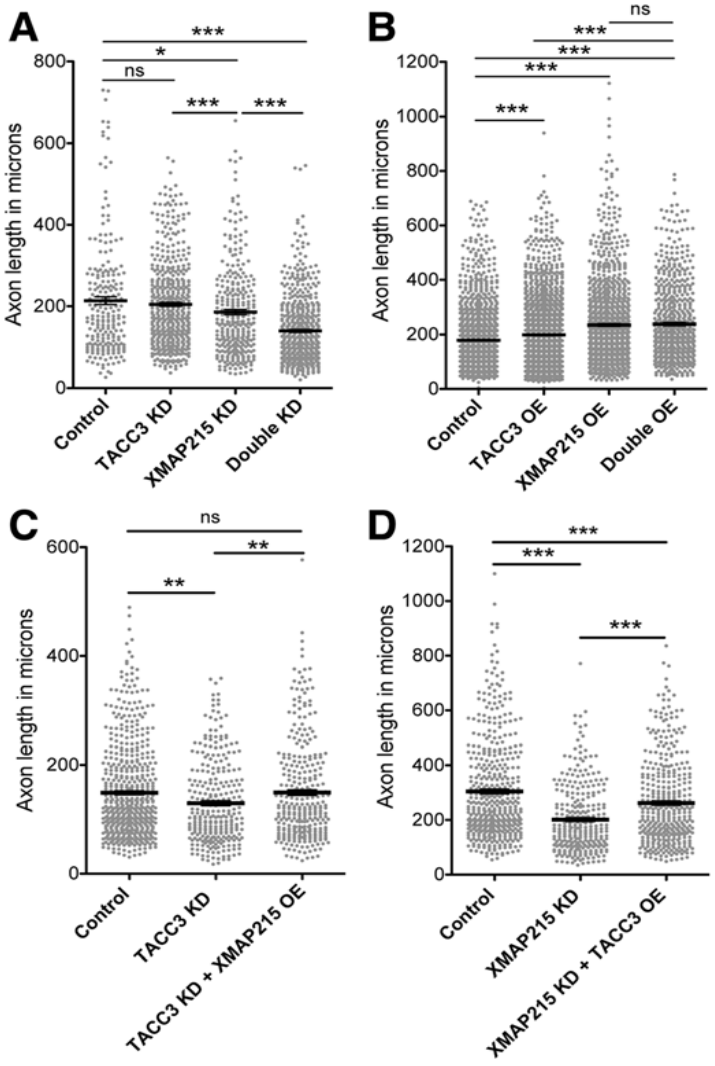

Figure A.1.4. TACC3 and XMAP215 interacts to promote axon outgrowth. a, b, Combinatorial reduction or elevation of TACC3 and XMAP215 levels reveals synergistic in axon outgrowth. Knocking down both TACC3 and XMAP215 (n = 312) showed significant reduction in axon length in comparison to control (n = 219), TACC3 KD (n = 487) and XMAP21 KD alone (n = 312) (a). Overexpression of both (n = 654) showed significant increase in axon length in comparison to control (n = 1288) and TACC3 OE (n = 1585), while double overexpression had no additive effect in comparison to XMAP215 OE (n = 1227) (b). c, d, Reduced axon outgrowth in TACC3 KD (n = 289) (c) or XMAP215 KD (n = 299) (d) neurons is rescued by the overexpression of XMAP215 (n = 313) or TACC3 (n = 397), respectively. *p < 0.05, **p < 0.01, ***p < 0.001. ns not significant. n = axon number

0.0116), partial knockdown of both reduced axon length significantly by 34% (140.6 ± 3.5 μm, n = 552, ***p < 0.0001) compared to control axons (213.6 ± 9.6 μm, n = 219, **Figure A.I.4A**). Conversely, overexpression of both (double OE) increased axon length by 32.7% (237.7 ± 5.4 μm, n = 654, ***p < 0.0001) while TACC3 OE alone increased by 11% (198.9 ± 3.2, n = 1585, ***p < 0.0001) and XMAP215 OE increased by 30.9% (234.5 ± 4.3 μm, n = 1227, ***p < 0.0001) in comparison to controls (179.1 ± 3.2 μm, n = 1288, **Figure A.I.4B**). Interestingly, while double OE significantly increased axon length in comparison to TACC3 OE alone (***p < 0.0001), it did not show a difference when compared to XMAP215 alone (p = 0.6421) suggesting that there may be an upper threshold that is reached with XMAP215 OE by itself.

We next asked whether overexpression of one + TIP might rescue the reduced axon length in the absence of the other. We observed that overexpressing XMAP215 in the stronger TACC3 KD background brought axon outgrowth length to control levels (TACC3 KD + XMAP215 OE, 149.4 ± 5.2 μm, n = 313, **p = 0.005, versus control, 148.8 ± 3.6 μm, n = 558, p = 0.9331) by increasing the length 15% in comparison to TACC3 KD (129.7 ± 4.477 μm, n = 289, **p = 0.0015, **Figure A.I.3C**). On the other hand, overexpression of TACC3 in the XMAP215 KD background increased axon outgrowth length by 30% (XMAP215 KD + TACC3 OE, 262.2 ± 7.8 μm, n = 397, ***p < 0.0001) in comparison to XMAP215 KD (201.3 ± 7.2 μm, n = 299); however, the rescue was not complete when compared to control axons (Control, 304.9 ± 8.5 μm, n = 463, ***p = 0.003, **Figure A.I.4D**). These findings suggest that TACC3 and XMAP215 cooperate during axon outgrowth, with XMAP215 showing more additive effects on TACC3-mediated axon outgrowth.

TACC3 affects axon guidance in vivo and ex vivo

The direction that the growth cone acquires during outgrowth is a result of local modulation of MT dynamics in response to guidance signals [9,39,40,54]. Thus, we wondered whether TACC3 regulation of MT dynamics could play a role during axon guidance. We first examined motor neuron axon outgrowth from the spinal cord in embryos at an early developmental stage (st 28), and we discovered that reduction of TACC3 caused significantly impaired outgrowth and severely disrupted morphology in all embryos examined (**Figure A.I.5A-C**).

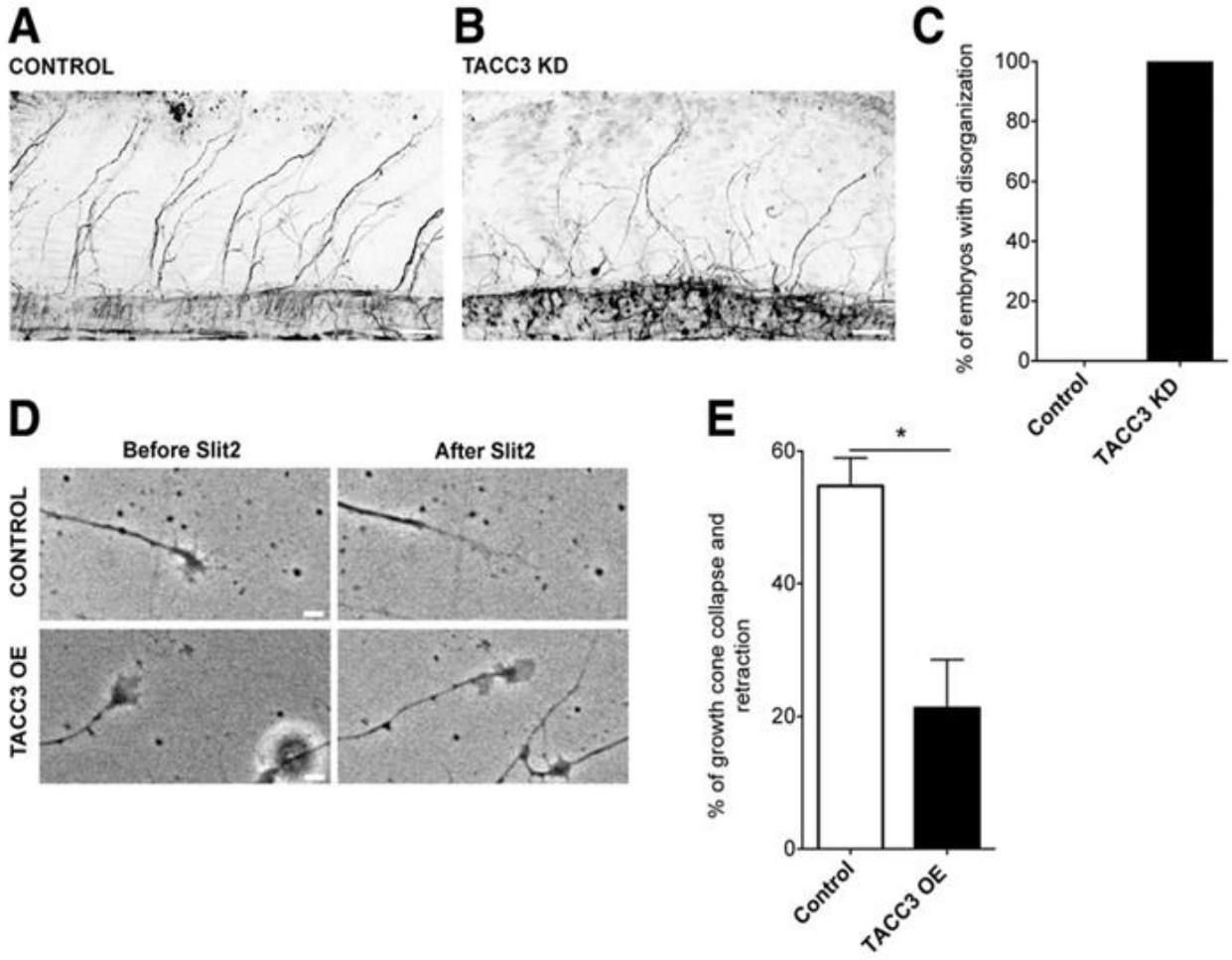

Figure A.I.5. TACC3 affects axon guidance in vivo and ex vivo. a, b, confocal images of laterally-viewed whole-mount Xenopus spinal cord fluorescently labeled for acetylated tubulin, showing peripheral axon outgrowth in control (a) and TACC3 KD (b) embryos at 2 dpf. c, Quantitation of the embryos with motor neuron guidance defects (n = 5 embryos). d, Representative neural tube growth cone images of control and TACC3 OE, before and after addition of 400 ng/ml Slit2. e, Quantification of the percentage of the growth cone collapse events in control (n = 48) and TACC3 OE (n = 82) growth cones show significant reduction in growth cone collapse in TACC3 overexpressing growth cones.

To gain greater insight into whether TACC3 manipulation causes this disorganization under specific guidance signals, we examined growth cone behavior in response to the guidance molecule, Slit2, applied in culture media. Slit2 is a repellent guidance cue which has been previously studied with other + TIPs, such as CLASP [17], and the response of growth cones of different neuron types isolated from *Xenopus* embryos at different stages has been previously documented [175–177]. We monitored the changes in growth cone behavior for 10 min prior and for 30 min after addition of Slit2. Growth cones that showed persistent growth were analyzed for their behavior after Slit2 addition. Growth cones that had reduced lamellaepodial area were considered as collapsed. We found that TACC3 OE growth cones had significantly fewer growth cone collapse and axon retraction events (TACC3 OE, 21.28 ± 7.24 n = 76 versus control, 54.72 ± 4.26 n = 44, *p = 0.0164) in response to Slit2, when compared to wild type growth cones (**Figure A.I.5D-E**). This suggests that overexpressing TACC3 can counteract Slit2-induced growth cone collapse.

Discussion

Dynamic spatial and temporal regulation of MTs within the growth cone is considered to be of key importance during axon outgrowth, guidance decisions and regeneration events [9,14,16,39,40]. Accordingly, MT plus-end tracking proteins (+TIPs) likely play a critical role during axon guidance, as + TIPs dominate the dynamic portion of MTs that reaches the growth cone periphery, where guidance cue receptors reside [19]. However, few + TIPs have been examined within the context of the embryonic growth cone. We previously characterized a MT plus-end tracking function for TACC3, and showed that it can promote MT polymerization and is required

for proper axonal development [98]. Here, we sought to uncover new insights into the mechanism underlying axonal regulation by TACC3.

First, we found that the shorter axons that result from reduced levels of TACC3 were due to slower axon outgrowth velocity along with significantly increased retraction rate. Moreover, TACC3 overexpression leads to longer axons, not because of fast axon outgrowth velocity (the outgrowth rate was actually slower than in controls), but because of reduced axon retraction rate. This suggests that TACC3-mediated MT dynamics may be required for opposing the normally occurring retractive forces within axons. Another possible explanation is that the reduced axon outgrowth velocity and reduced axonal retraction rates after TACC3 OE could be due to stronger anchorage to the underlying substrate and adhesion turnover. While there are some + TIPs that have been implicated to mediate MT focal adhesion interactions [91], TACC3 has not yet been explored in focal adhesion (or point contacts, in the case of growth cones) regulation. However, since TACC3 has been identified as an interactor of CLASP [178], and given that CLASP is known to function during focal adhesion turnover [179], future studies should examine whether TACC3 also plays a role at focal adhesions/point contacts.

+TIPs modulate MT dynamic instability in various ways; for example, XMAP215 promotes MT growth by catalyzing addition of tubulin dimers [94], while CLASP and APC rescue MT from catastrophe by increasing MT stability [180–182]. Here, we showed that TACC3 OE could dampen Nocodazole-induced reduction in MT growth speed, length and lifetime. However, this was not achieved by increased MT lattice stability, as immunofluorescence analysis of dynamic versus stable MTs revealed that TACC3 has no apparent impact on MT stability within the growth cone. It is unclear how TACC3 is able to mitigate the reduction in MT growth speed, length and life-time because of Nocodazole application. One possibility could be that TACC3 overexpression,

which enhances XMAP215 localization at MT plus ends [98], may simply promote more efficient and processive MT polymerization by XMAP215 to counteract the Nocodazole-induced effects.

Individual + TIPs comprise a network of proteins at MT plus-ends which can co-localize and function together to modulate MT dynamics. We have previously shown such cooperation between TACC3 and XMAP215 in growth cones, as we demonstrated that TACC3 and XMAP215 co-localize at MT plus-ends in codependent manner [98]. Here, we found that TACC3 and XMAP215 interact to promote axon outgrowth (**Figure A.I.4**). Partially knocking down both TACC3 and XMAP215 resulted in further reduction in axon outgrowth length, which suggests a synergistic interaction between the two proteins. However, overexpression of both + TIPs did not show further increase in axon length in comparison to XMAP215 OE alone. This might be due to an upper threshold that is reached with overexpression of XMAP215 alone. Conversely, rescue studies show that XMAP215 can fully restore TACC3 KD-mediated reduced axon length to control levels, whereas TACC3 OE fails to show the same impact over XMAP215 KD. As XMAP215 is a processive MT polymerase, reduction in XMAP215 levels may exert more dramatic effect than the reduction in the levels of TACC3, which may play more of an accessory role. Considering that one study suggests that every TACC3 molecule is thought to interact with two molecules of XMAP215 [103], reduced levels of XMAP215 could be a limiting factor. Even though TACC3 OE functions to increase available XMAP215 at MT plus-ends, the reduction in overall XMAP215 levels may result in poor axon outgrowth. While knock down approaches provide supporting evidence regarding the combinatorial role of TACC3 and XMAP215 during axon outgrowth, future studies should utilize mutations that disrupt their interaction [103] in order to understand the dependence of these two proteins on one another during axon outgrowth.

In addition to their role in axon outgrowth, several + TIPs have been implicated in participating in growth cone steering decisions in response to extracellular cues. The first of which is orbit/MAST, the fly orthologue of mammalian CLASP, that has been identified to cooperate with Abelson kinase (Abl) downstream of Slit/Robo guidance pathway [17]. In a parallel genetic and proteomic screen in fruit flies, minispindles (msps), a fly orthologue of Xenopus XMAP215, was identified to function antagonistically against CLASP and Abl during embryonic central nervous system development [95], while another genetic interaction study in flies identified dtacc as an antagonist of CLASP [130,178], reminiscent of the interaction between CLASP and TACC partner, msps. Combining these previous works with our findings on the role of TACC3 in axon outgrowth led us to ask whether TACC3 functions during axon guidance.

As demonstrated in **Figure A.I.5**, our initial observations revealed that reduction in TACC3 levels impairs the normal organization of axons exiting the spinal cord in embryos at st 28. Stimulation of cultured Xenopus retinal neurons at stage 32 or beyond with bath applied Slit2 has been shown to cause growth cone collapse [176]. Additionally, spinal neurons derived from st 28 Xenopus embryos have previously shown to be repelled by Slit2 [175]. Here, we found that Slit2-induced neural tube growth cone collapse events can be reduced by 60% in TACC3 overexpressing growth cones in comparison to control, suggesting an opposing role for TACC3 in Slit2-induced growth cone collapse. Based on its role in MT polymerization [98], its codependent localization at MT plus ends with XMAP215 [98,103], and their interaction during axon outgrowth (**Figure A.I.4**), we propose that TACC3 OE will excessively occupy MT plus-ends, subsequently driving increased recruitment of XMAP215, prompting enhanced MT polymerization in all directions. This global increase in MT polymerization would disturb local

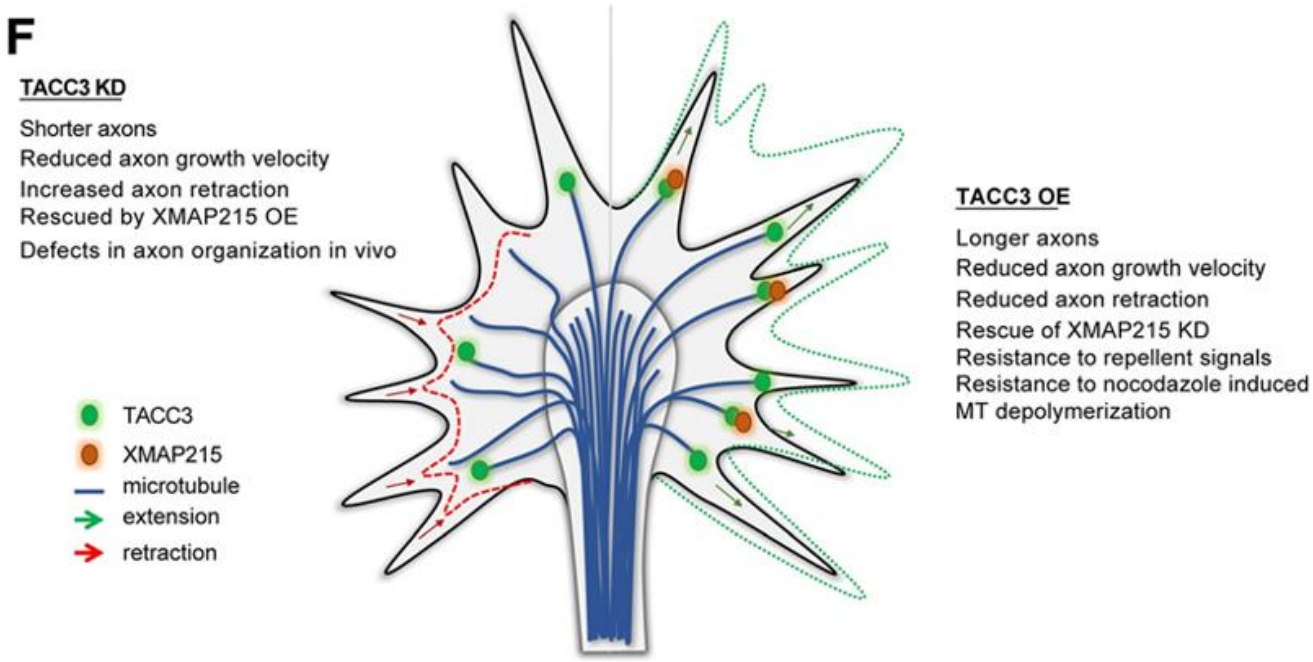

Figure A.I.6. Cartoon model for the role of TACC3 at MT plus ends during axon outgrowth and guidance. Microtubule (blue) plus-ends decorated by TACC3 (green) promotes axon outgrowth, reduces axon retraction, dampens Nocodazole-induced reduction in MT dynamics parameters, rescues XMAP215 KD induced axon length reduction and opposes repellent guidance signals effect.

MT modulation, which is the underlying mechanism for growth cone steering events and it would result in an aberrant, non-obedient growth cone advance (**Figure A.I.6**).

It remains to be determined whether these effects are specific to Slit2 or if TACC3 could exert similar opposing effects in response to other repellent signals, and/or if TACC3 mediates attractive signals as well. Finally, other TACC members, namely, TACC1 and TACC2, have recently been characterized as + TIPs that can promote MT polymerization in Xenopus embryonic cells [183,184]. Although their expression and MT regulatory function show cell type-specificity, it would be intriguing to study whether other members of the TACC family also play a role in axon outgrowth and guidance decisions.

Overall, the work here characterizes the mechanism by which TACC3 regulates MT dynamics within the embryonic neuronal growth cone and promotes axon outgrowth. Using time-lapse

imaging of Xenopus laevis embryonic axons as they grow in culture, we demonstrated that TACC3 promotes persistent axon outgrowth not by accelerating axon growth velocity but by reducing spontaneous axon retraction events. Moreover, we demonstrate that overexpressing TACC3 can mitigate the reduction in MT dynamics parameters that occur after Nocodazole application, suggesting that TACC3 may be promoting MT dynamics by dampening MT depolymerization. Finally, our data suggests that the + TIP TACC3 mediates axon guidance, as reduction in TACC3 levels results in defects in the normal organization of spinal neuron axons within the spinal cord. Moreover, bath application of the Slit2 repellent guidance molecule into cultured neural tube neurons shows that TACC3 OE reduces the Slit2 induced growth cone collapse events, suggesting that TACC3 may involve in generation of response to guidance signals during neuronal development.

Methods

Xenopus embryonic explants

Egg collection and culturing of Xenopus embryonic explants (from embryos of either sex) were performed as described [98,146]. All experiments were approved by the Boston College Institutional Animal Care and Use Committee and were performed according to national regulatory standards.

Constructs and RNA

Capped mRNA constructs were transcribed and purified as previously described [98,112]. Constructs used were GFP-TACC3 (TACC3 pET30a was gift from the Richter lab, University of

Massachusetts Medical School, Worcester, MA), GFP-TACC3-ΔN, GFP-TACC3-ΔΔN, GFP-TACC3-ΔTACC (see Fig. 1e for amino acid residues for full length and each deletion construct, based on GenBank accession number NP-001081964.1) (all TACC3 constructs were subcloned into pSC2+ vector), GFP-MACF43 (a gift from Hoogenraad Lab) in pCS2+, XMAP215-GFP (a gift from the Hyman lab, Max Planck Institute of Molecular Cell Biology and Genetics, Dresden, Germany [101]) subcloned into pT7TS. Embryos either at the 2 cell or 4 cell stage received injections 4 times total in 0.1× MMR containing 5% Ficoll with the following total mRNA amount per embryo; 100 pg of GFP-MACF43 as a control for TACC3 or XMAP215 overexpression, 2000 pg of GFP-TACC3 full-length and deletion constructs (deletion constructs are expressed in wildtype embryos), 3000 pg of XMAP215-GFP. For double overexpression studies, 1000 pg of TACC3 and XMAP215 were injected in total.

Morpholinos

Morpholinos (MOs) were previously described and validated [98,112]. In knockdown (KD) experiments, TACC3 and control MOs were injected at 80 ng/embryo. For TACC3 and XMAP215 double KD analysis, 20.0 ng/embryo for TACC3 and control MOs and 2.0 ng/embryo for XMAP215 MO were injected. In rescue experiments, MO (amounts used as in KD, which is 80 ng/embryo) was injected with mRNA (same amount as in OE, which is 2000 pg/embryo for GFP-TACC3 and 3000 pg/embryo for XMAP215-GFP) in the same injection solution. The efficacy of MOs has been previously assessed by Western blot of 35–36 stage embryos, as described [98,112].

Whole-mount immunohistochemistry

Two-day-old embryos were fixed, as described [112]. Primary antibody (diluted in blocking buffer made up by 1% DMSO, 1% Triton, 1% BSA, in PBS) to acetylated tubulin (1:1000, monoclonal, clone 6-11B-1, Sigma, St. Louis, MO, USA) and goat anti-mouse Alexa-Fluor 568 conjugate secondary antibody (1:1000, polyclonal, A- 1100, Life Technologies) were used. For imaging, the spinal cord was exposed by peeling off skin, and somites were kept intact. Embryos were transferred in a drop of benzoate:benzyl alcohol (BB:BA) to the imaging chamber (made by placing Gene Frame, sticky on both sides, onto a microscope slide). After the tissue was cleared, it was covered with a 1.5× coverslip. Image acquisition and quantitation of fixed and labeled explants were described previously [112]. TACC3 KD-induced change is scored based on the percentage of embryos with disorganized axons in each condition.

Immunocytochemistry

Embryonic explant cultures were fixed and labelled [40] with primary antibodies (1:1000 diluted in blocking buffer made up by 1% non-fat dry milk in calcium and magnesium free PBS) to tyrosinated tubulin (rat monoclonal, ab6160, Abcam) and detyrosinated tubulin (rabbit poly-clonal, AB3201, Millipore), and with the secondary antibodies goat anti-rat Alexa Fluor 568 (1:1000, ab175476, Abcam) and goat anti-rabbit Alexa Fluor 488 (1:1000, A-11008, Life Technologies), respectively.

Growth cone response assay

Recombinant mouse Slit2 protein (R&D Systems) (400 ng/ml) was administered to cultured neural tube explants derived from stage 28 Xenopus embryos in 400 µl culture media supplemented with 1% Penicillin/Streptomycin and 0.1% BSA. A perfusion chamber was set up to exchange media with Slit2-containing culture media. Time-lapse images of growth cones were acquired for 10 min with 30 s intervals before and immediately after Slit2 addition for 30 min with 30 s intervals, using a Zeiss Axio Observer inverted motorized microscope with a Zeiss 20×/0.8 Plan Apo phase objective. Frame to frame axon growth was tracked manually and retraction or growth cone collapse events were recorded over a movie. Ratio of the number of retracting frames over total frames for each axon was scored. Images given in the figures show the image of growth cone right before adding Slit2 and the image of the growth cone at collapse.

Nocodazole application

Nocodazole to final concentration of 50 pM was administered in 400 µl culture media. Concentration of Nocodazole was determined after series of titrations and 50 pM was found to be the optimum to keep the MTs intact in order to perform MT dynamics analyses. Time-lapse images of growth cones were acquired for 1 min with 2 s intervals before and 5 min after Nocodazole administration, using a Yokogawa CSU-X1M 5000 spinning disk confocal on a Zeiss inverted motorized microscope with a Zeiss 63× Plan Apo 1.4 NA and a Hamamatsu ORCA R2 CCD camera. MT dynamics were assessed, as described [98].

PlusTipTracker software analysis

MT dynamics were analyzed from GFP-MACF43 movies using plusTipTracker [145,146]. Imaging conditions and tracking parameters were previously validated and same parameters were used: maximum gap length is 8 frames; minimum track length is 3 frames; search radius range 5–12 pixels; maximum forward angle, 50°, maximum backward angle, 10°; maximum shrinkage factor, 0.8; fluctuation radius, 2.5 pixels; time interval, 2 s. MT growth lifetime is the measure of persistent outgrowth till MT undergoes catastrophe. MT growth length is the total growth over a movie and MT growth velocity is the average of each MT growth event. MT dynamics parameters were compiled from multiple individual experiments, and to avoid day-to-day fluctuations, the final complied data were normalized to the mean of the control data for each experiment.

Image acquisition and analysis

For axon outgrowth imaging, phase contrast images of axons were collected on a Zeiss Axio Observer inverted motorized microscope with a Zeiss 20×/0.5 Plan Apo phase objective and analyzed using ImageJ [98]. Time-lapse images for axon outgrowth velocity was collected for 4 h with 20 min intervals and images were analyzed using plusTipTracker QFSM plugin and velocity was measured as the average of instantaneous velocity per axon as described [112]. Axon retraction events were analyzed from the same data set used to assess axon growth velocity. Frame to frame axon growth was tracked manually and retraction events were recorded over a movie. Ratio of the number of retracting frames over total frames for each axon was scored. Axon outgrowth and MT dynamics data were normalized to controls, to account for day-to-day fluctuations in room temperature. Image acquisition and quantitation of fluorescence intensity of fixed and labeled explants were described previously [98]. Experiments were performed multiple

times to ensure reproducibility. Graphs were made in GraphPad Prism. Statistical differences were determined using unpaired two tailed t-tests when comparing two conditions and one-way analysis of variance with Tukey's post-hoc analysis when multiple conditions were compared.

Appendix Chapter 2. Abelson-induced phosphorylation of TACC3 modulates its interaction with microtubules and affects its impact on axon outgrowth and guidance

*My role in facilitating the completion of this chapter was the following: Growth cone imaging in Figure 1, subcloning, and SDM of TACC3 phospho mutants. However, the full manuscript is included in its entirety adapted from: (Erdogan et. al., 2020 - Cytoskeleton)

Introduction

Regulation of cytoskeletal dynamics within the growth cone is essential for growth cone motility and navigation as the axon travels to its target (reviewed in Lowery and Van Vactor, 2009). Guidance molecules that the growth cone encounters during its trip can act as repellent or attractant depending on the time, location and the signal composition of the environment that the growth cone passes. Integration and interpretation of these signals relies on signaling cascades that are initiated downstream of guidance cue receptors which will ultimately converge upon cytoskeletal elements for their rearrangements and control of growth cone motility.

Guidance signals are not homogeneously presented to the growth cone in vivo. While the growth cone might be exposed to repellent signals on one side, it can be exposed to attractant signals on the other side, which necessitates the asymmetric reorganization of the underlying cytoskeleton. In order to manage this asymmetric regulation, signals received by guidance cue receptors must be processed locally and immediately downstream of the site where the signal is received without necessarily leading to a global response. For example, repulsive guidance cues can cause a global growth cone collapse when they are bath-applied, whereas their local application causes

collapse on the side that the protein is received, which results in growth cone steering away from the source of the signal [16]. The interaction between guidance cue receptors and downstream targets is required for the growth cone's directional movement. Microtubule plus-end tracking proteins (+TIPs), due to their localization close to the growth cone periphery, are potential targets for guidance signals. Their interaction with microtubules at the plus-ends is important for regulating microtubule growth dynamics and coordination of signal exchange between the growth cone periphery and the central domain, which is critical to the growth cone's directional movement.

The interaction between +TIPs and microtubules can be modulated by guidance signals and their downstream intracellular signaling events. Phosphorylation of +TIPs is one such event that has been shown to modulate +TIP affinity for microtubules. For example, the affinity of CLASP for microtubules has been shown to be regulated differentially in the growth cone depending on its phosphorylation status by GSK3 kinase. Increased microtubule lattice binding activity of CLASP, as a result of GSK3 inhibition, results in axon growth inhibition through inhibition of microtubule advance into the growth cone periphery. On the other hand, plus-end binding of CLASP, as a result of GSK3 activity, promotes axon outgrowth via stabilization of microtubules [53]. In addition to GSK3, CLASP has also been identified as a direct target of Abelson (Abl) tyrosine kinase [17,51]. Further examination of the interaction between CLASP and Abl in Xenopus spinal neurons identified CLASP as a target for Abl phosphorylation and showed that phosphorylation can affect CLASP localization in neuronal growth cones [51].

Similar to CLASP, several +TIPs have been implicated to be involved in regulation of microtubule dynamics during directional movement of cells and growth cones [19]. However, only a few of them have been studied and implicated as a target for guidance cue-initiated

intracellular signals [19]. We have previously characterized a microtubule plus-end tracking function for TACC3 in neuronal growth cones and showed that TACC3 overexpression enhances microtubule growth dynamics and promotes axon outgrowth [98]. Additionally, we have proposed a function for TACC3 during axon guidance. Reducing levels of TACC3 resulted in disorganized axon elongation of neural tube neurons in Xenopus laevis embryos and its overexpression mitigated growth cone collapse induced by bath-applied Slit2 in cultured neural tube explants [142]. To further investigate the mechanism by which TACC3 overexpression exerts this opposing role against Slit2 activity, we became interested in looking at potential phosphorylation events that might target TACC3. Our previous studies highlighted a possible genetic interaction network between TACC3, its microtubule polymerase interactor XMAP215, and Abelson tyrosine kinase (Abl) [95]. Thus, we become interested in testing whether TACC3 could be a target for Abl phosphorylation downstream of Slit2 and whether its phosphorylation status would alter the interaction of TACC3 with microtubules as well as its impact on axon outgrowth and guidance.

Results

Abelson kinase induces phosphorylation of TACC3

To investigate whether Abelson tyrosine kinase (Abl) induces phosphorylation of TACC3, we co-expressed GFP-TACC3 and Abl in HEK293 cells. Tyrosine phosphorylation of TACC3, following GFP immunoprecipitation of GFP-TACC3, was observed with 4G10, an antibody that specifically labels phosphorylated tyrosine residues (**Figure A.II.1A**, lane 4). Phosphorylation of TACC3 was only observed when it was co-expressed with Abl (**Figure A.II.1A**, lane 3 vs lane 4). Additionally, this phosphorylation specifically happened with the tyrosine kinase Abl, since Fyn, which is another tyrosine kinase, did not induce TACC3 tyrosine phosphorylation (**Figure**

A.II.1A, lane 6). Although we did not determine whether the induced tyrosine phosphorylation was a result of direct interaction between Abl and TACC3, our data show that Abl expression can induce phosphorylation of tyrosine residues on TACC3.

To study the role of TACC3 phosphorylation, we next wanted to identify the tyrosine residues that are targeted by Abl. Mass-spec analysis of full-length TACC3 identified 4 tyrosine residues: two (Y759, Y762) in the conserved TACC domain, the domain that is responsible for

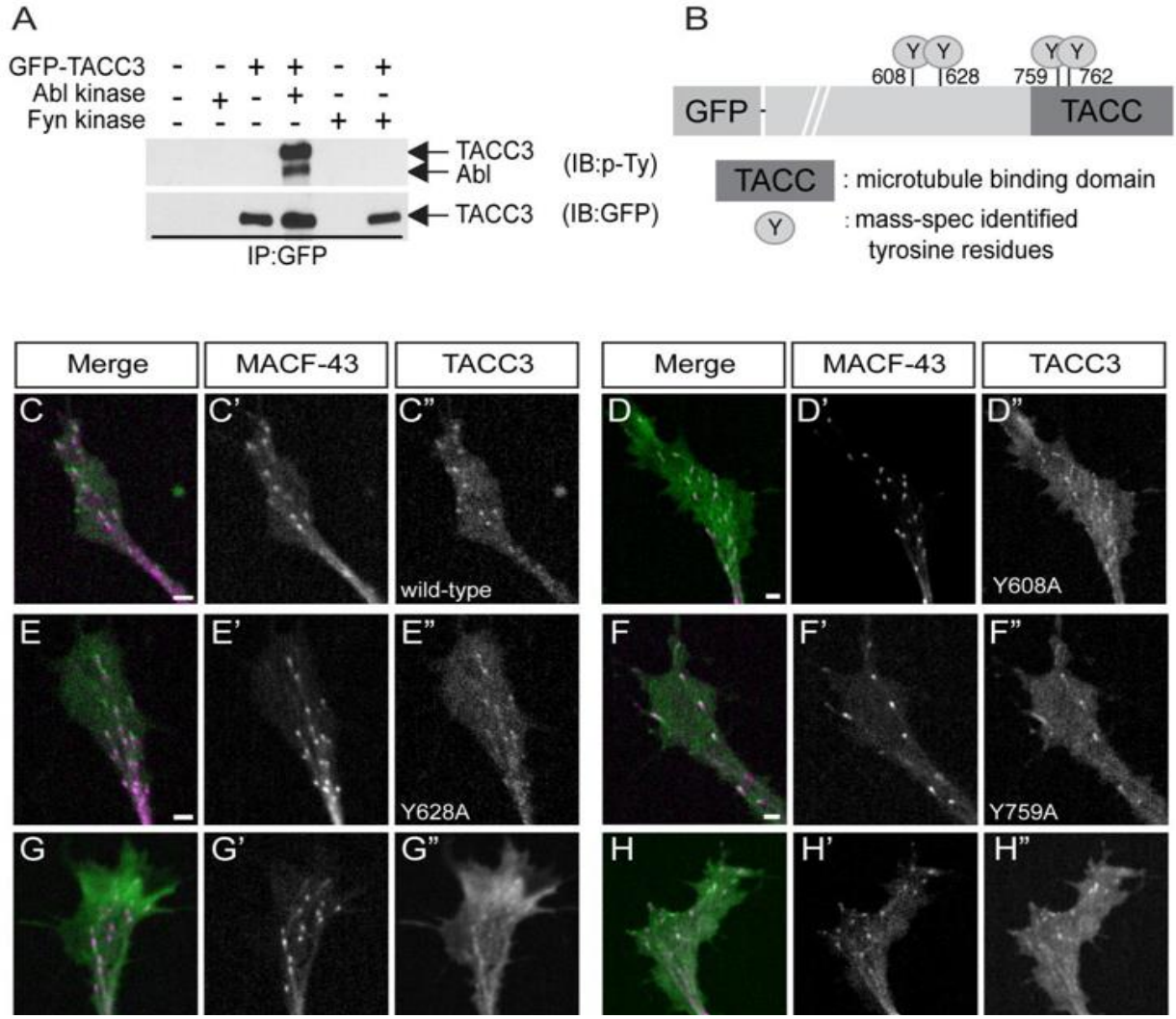

Figure A.II.1. Abelson kinase induces phosphorylation of TACC3 Abelson kinase induces phosphorylation of TACC3. (A) Western blot performed with phospho-tyrosine specific antibody showing Abelson-induced tyrosine phosphorylation of full-length TACC3 (lane 4). Phosphorylation signal is not present when TACC3 is expressed alone (lane 2) or with another tyrosine kinase Fyn (lane 6). (B) Cartoon showing mass-spec-identified tyrosine residues of TACC3 targeted by Abl phosphorylation. (C-H) Confocal images of growth cones expressing MACF-43 (magenta) and TACC3 (green) with phospho-null mutations at identified residues, showing localization of TACC3 phospho-null mutants to microtubule plus-ends. Scale bar, 2 μm.

microtubule plus-end binding, and two (Y608, Y628) outside of the TACC domain (**Figure A.II.1B**). These phosphorylation events only occurred when Abl was co-expressed with TACC3. To assess the importance of these tyrosine residues, we generated single and combinatorial phospho-null mutants of TACC3 by substituting tyrosine with alanine or phenylalanine. However, neither single nor combinatorial phospho-null mutations caused a reduction in tyrosine phosphorylation levels, determined by Western blot analysis (Supplementary Figure 1A-D). Moreover, all of the single and combinatorial mutants were still able to track microtubule plus-ends (**Figure A.II.1C-H**, Supplemental Movies 1-6). This initial examination suggests that other tyrosine residues might also be phosphorylated in TACC3 and thus contribute to the overall phospho-tyrosine signal detected by Western blot.

Tyrosine phospho-null mutations impair the localization of the TACC domain at microtubule plus-ends in growth cones and mesenchymal cells

Since none of the TACC3 phospho-null mutants based on mass-spec-identified tyrosine residues showed a reduction in phosphorylation signal, and they were all still able to localize to microtubules, we decided to examine other tyrosine residues within TACC3. The full-length TACC3 possesses a total of 11 tyrosine residues throughout the entire protein. Six of these tyrosine residues (Y725, Y759, Y762, Y832, Y846, Y857) are in the TACC domain (aa715-aa931), one (Y130) is in the N-terminal domain (aa1-aa133), and four (Y320, Y428, Y608, Y628) are in the middle domain (aa134-aa634) (**Figure A.II.2A**).

The C-terminal TACC domain of the TACC3 protein shows high sequence similarity among vertebrates as well as among other TACC family members [185]. Moreover, the TACC domain is the portion of the TACC3 protein that is responsible for its microtubule plus-end tracking

behavior [98] and also for interacting with the microtubule polymerase XMAP215 [103]. Therefore, we decided to specifically investigate the importance of tyrosine residues within the TACC

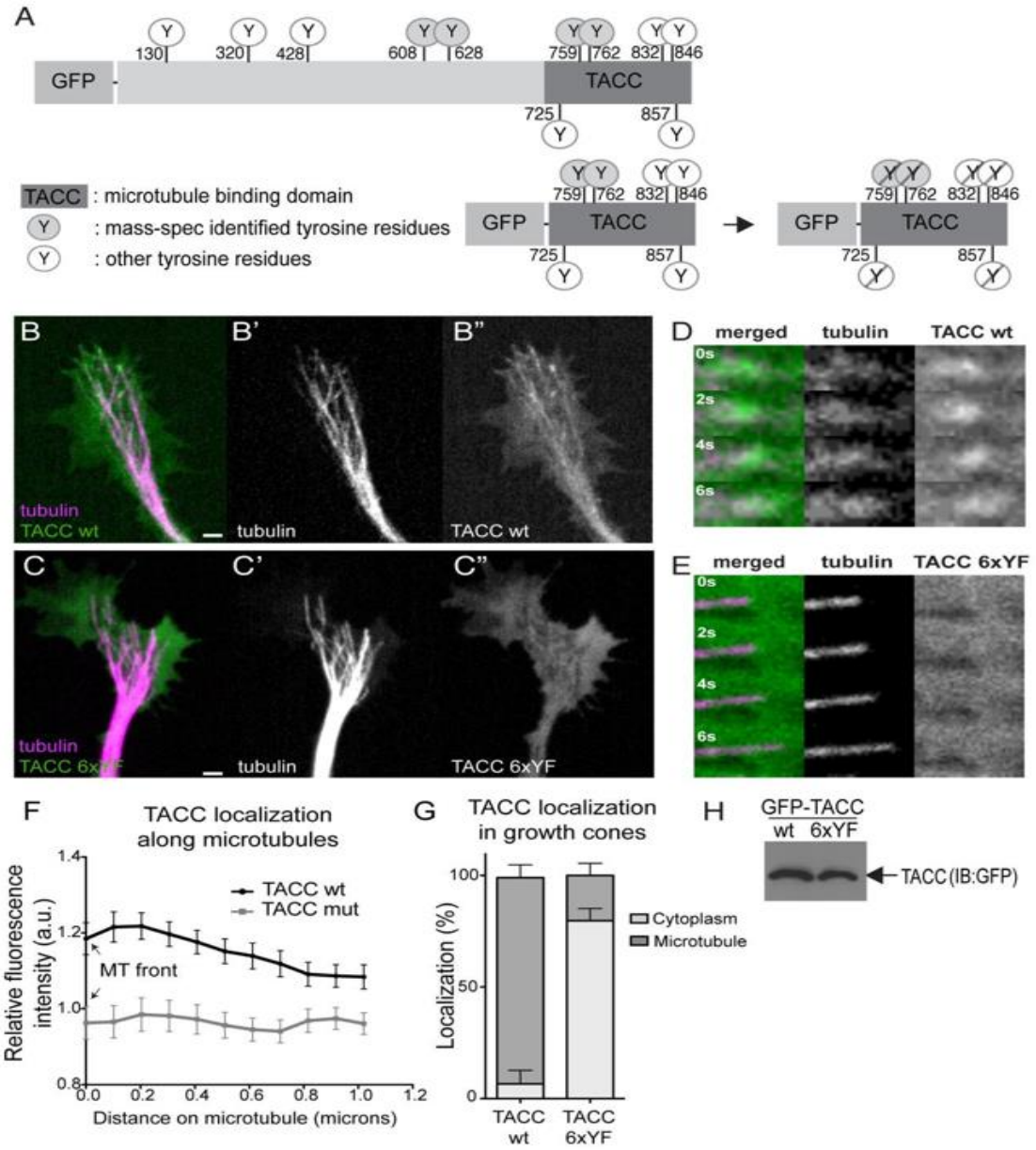

Figure A.II.2. Tyrosine phosphorylation of TACC3 affects its localization in the growth cone. (B-C) Confocal images of neuronal growth cones, obtained from time-lapse recordings expressing tubulin (magenta) (B', C') and TACC (green) wild type (B") or tyrosine phospho-null mutant (C"). (D-E) Magnified montages of time-lapse sequences of single microtubule. TACC wild type (green) localizes to microtubule (magenta) plus-ends (D) while TACC tyrosine phospho-null mutant (green) is absent from microtubule (magenta) plus-ends and remains mostly cytoplasmic (E). (F) Fluorescent intensity profile (y-axis) along microtubules (x-axis) determined by line- scan analysis showing green fluorescent intensity (TACC wt or TACC p-null mutant) relative to background. Line is drawn starting from the beginning of the microtubule plus-end. (G) Plot showing the quantification of microtubule plus-end versus cytoplasmic localization of TACC constructs within the growth cones as percentage of total growth cones examined. On average, TACC wild-type shows microtubule plus-end binding in 92.5% of the growth cones examined while TACC tyrosine p-null mutant showed plus-end localization in 20% of the growth cones and remained mostly cytoplasmic in 80% of the growth cones examined. (H) Western blot performed with GFP antibody showing the expression of GFP-TACC wild type and GFP-TACC phospho-null mutant. Scale bar, 2 µm.

domain to determine whether they might be contributing to the Abl-induced phosphorylation we observed earlier. To investigate this, we mutated all six of the tyrosine residues within the TACC domain to phenylalanine (**Figure A.II.2A**) and tested these mutants for their phosphorylation status.

Surprisingly, despite lacking a phosphorylatable tyrosine with the TACC sequence, GFP-TACC phospho-null (p-null) mutants showed similar phospho-tyrosine signals compared to the wild-type TACC domain, as verified with Western blot (Supplementary Figure 2A-B). Since there are no tyrosines left in the TACC domain, the only other source that might contribute to the observed Western blot signal is GFP. Therefore, we performed a Western blot for the GFP tag alone with a phospho-tyrosine specific antibody, and we found that GFP was indeed being phosphorylated specifically in the presence of Abl kinase (Supplementary Figure 2C-D). Thus, GFP itself was probably contributing to the overall signal that we obtained with the GFP-tagged TACC constructs previously. However, while Abl-induced phosphorylation of GFP muddled the Western blot results, we still had previously determined that tyrosine residues of TACC3 were indeed being phosphorylated as a result of Abl signaling, and we decided to pursue whether tyrosine phosphorylation directly affected the ability of the TACC domain to bind microtubules.

When we examined whether TACC protein with tyrosine phospho-null mutations (TACC 6xYF) could still localize to microtubules, we found that both full-length TACC3 (data not shown) and TACC domain-only phospho-null mutants showed changes in their microtubule localization (**Figure A.II.2B-C**, Supplemental Movie 7-8). In both neuronal growth cones (and mesenchymal cells, data not shown) isolated from Xenopus embryos, TACC phospho-null mutants showed less localization along microtubules, determined by line-scan averages of fluorescent intensities obtained from microtubule plus-ends (**Figure A.II.2D-F**). TACC phospho-null mutant remained

cytoplasmic in 80% of the growth cones and showed microtubule localization in 20% of the growth cones examined, while wild-type TACC localized at microtubule plus-ends in 93% of growth cones examined (**Figure A.II.2G**). We also confirmed protein expression levels by Western blot and showed that the GFP-TACC mutant expression was comparable to GFP-TACC (**Figure A.II.2H**). These data suggest that retaining phosphorylatable tyrosines within the TACC domain is important for TACC localization along microtubules.

TACC tyrosine phospho-null mutant-expressing axons grow less persistently, thereby resulting in shorter axons compared to TACC wild-type-expressing axons

We have previously shown that TACC3 binding to microtubules is critical for promoting axon outgrowth [98]. To test whether phosphorylation of the TACC domain is important in regulating axon outgrowth parameters, we measured the length of axons in cultured Xenopus laevis neural tube explants expressing either TACC wild type (wt) protein or TACC phospho-null mutant protein. While expression of TACC wt led to formation of longer axons, expression of the TACC phospho-null mutant (0.86 ± 0.04 N=155) was unable to promote increased axon outgrowth, and instead, showed a 17% reduction in axon length compared to controls (1.00 ± 0.03 N=277) and a 34% reduction compared to TACC wt (1.15± 0.06 N=199) (**Figure A.II.3A**).

To further assess the difference in axon length between the neurons expressing TACC wt and the phospho-null mutant, we measured axon outgrowth velocities. Interestingly, despite the fact that phospho-null mutant-expressing axons are not as long as TACC wt-expressing axons, we found only minor (insignificant) differences in outgrowth velocity. The average normalized axon forward movement velocity was 8% faster in TACC phospho-null mutant conditions (1.10± 0.03 N=172, **p=0.0082) compared to controls (1.00 ± 0.02 N=198) and only 4% slower, compared

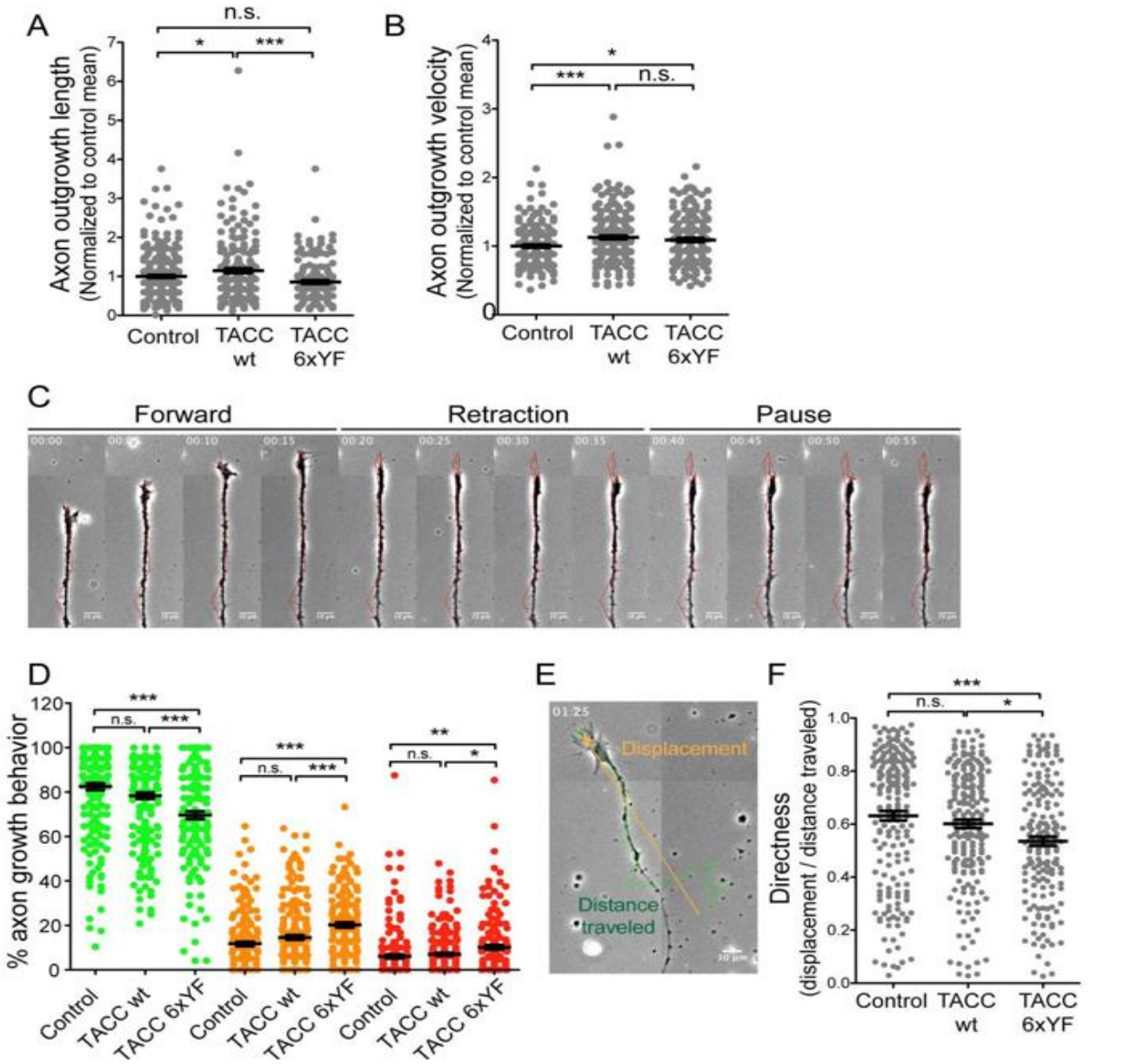

Figure A.II.3. TACC tyrosine phospho-null mutant expressing axons grow less persistently thereby grow shorter axons compared to TACC wt axons. (A) Quantification of axon length in cultured neural tube explants shows TACC phospho-null mutant expressing neurons grow axons shorter by 16.8% compared to control and 34% compared to TACC wt, while TACC wt expressing explants grow axons longer by 12.8% compared to control. (B) Measurement of axon forward movement velocity showing TACC wt increases axon forward movement velocity by 10% compared to control while TACC phospho-null mutant increases by 8%. (C) Representative phase contrast image montage of an axon depicting phases of forward movement, retraction and pause. (D) Plot showing the percentage of forward movement (green), pause (orange) and retraction (red) of axon growth. TACC phospho-null mutant expressing axons spend 18% less time moving forward compared to control and 12% compared to TACC wt (green dots). TACC phospho-null mutant axons (20.20 ± 1.150 N=168) spent 42% more time pausing compared to control and 27% compared to TACC wt (orange dots). They also tend to retract more frequently; 39% compared to control and 30% compared to TACC wt. (E) Representative image of an axon growth track depicting displacement and distance traveled between t=0 and t=1h 25min (F) Plot showing the directness of axon growth. TACC phospho-null mutant axons grow 12% less directly compared to TACC wt) and 17% compared to control axons. TACC wt axons also grow 5% less directly compared to control but it was not significant. The asterisk (*) indicates statistical significance with $\alpha < 0.05$ * $P < 0.05$, ** $P < 0.01$, **** $P < 0.0001$, ns: not significant, from an ANOVA analysis comparing multiple conditions with Tukey's post hoc analysis. Values given are mean of normalized data pooled from independent experiments.

to TACC wt (1.13 ± 0.03 N=217, not significant p=0.3). Average outgrowth velocity in TACC wt-expressing axons, on the other hand was 10% faster compared to control axons (**Figure A.II.3B**). Our data suggests that TACC phospho-null mutant-expressing axons grow at similar rates to the TACC wt-expressing axons, suggesting that the reduced axon length in the phospho-null condition could be due to another parameter of axon growth other than outgrowth velocity.

To further investigate this, we also tracked other growth behaviors of axons and recorded the number of frames that they moved forward, paused and/or retracted over the course of 4 hour long time-lapse imaging (**Figure A.II.3C**, Supplemental Movie 9-10, intervals were every 5 minutes). We found that TACC phospho-null mutant-expressing axons (69.61 ± 1.77 N=168) spent 18% less time moving forward compared to controls (82.30 ± 1.5 N=183, ***p<0.0001) and 12% less compared to TACC wt (78.20 ± 1.43 N=218, ***p<0.0001) (**Figure A.II.3D**, green dots). Additionally, TACC phospho-null mutant axons (20.20 ± 1.150 N=168) spent 42% more time pausing compared to controls (11.67 ± 1.00 N=183, ***p<0.0001) and 27% more compared to TACC wt 14.67 ± 0.97 N=218, ***p=0.0003) (**Figure A.II.3D**, orange dots). They also tended to retract more frequently: 39% compared to controls (6.125 ± 0.89 N=183, **p=0.0043) and 30% compared to TACC wt (7.098 ± 0.67 N=218, *p=0.0132) (**Figure A.II.3D**, red dots, Supplemental Movie 11).

In addition to pause and frequency rates, we also examined the directness of axon outgrowth. The still images of neural tube explants that were used to measure axon length show the final displacement of an axon. However, axons do not necessarily follow a linear trajectory as they grow. In fact, they often spend time wandering, which is part of their exploratory behavior. Therefore, the directness of outgrowth can be determined by dividing the displacement distance by the total distance traveled (**Figure A.II.3E**). We found that TACC phospho-null mutant

expressing- axons (0.5353 ± 0.02 N=179) grow 12% less directly compared to TACC wt-expressing axons (0.6012 ± 0.02 N=195) and 17% less compared to control axons (0.6313 ± 0.02 N=192, **Figure A.II.3F**). These data suggest that while axon outgrowth speed is not affected by TACC tyrosine phospho- null mutations, growth persistency, which is determined by pause and retraction frequency, as well as growth directionality, both seem to be impaired in TACC phospho-null mutant expressing axons. Thus, this could explain the shorter axon length that we observed in TACC phospho-null mutant-expressing neural tube explants.

TACC tyrosine phospho-null mutant-expressing growth cones display increased numbers of filopodia that contain microtubules

Axons of neurons expressing the TACC phospho-null mutant tend to stop and retract more frequently compared to those expressing wild-type TACC. Additionally, we observe that their growth is less directed compared to TACC wt and controls. An inverse correlation between growth cone advance rate and growth cone size has been reported previously [186]. Therefore, we became interested in examining the growth cone size, along with other morphological features, to see whether increased pause and retraction rates in TACC phospho- null mutant-expressing growth cones might also occur alongside changes in growth cone morphology.

We initially examined the growth cone area, filopodia length, and filopodia number in cultured neural tube explants that are fixed and stained for microtubules (tubulin) and actin (phalloidin), followed by high resolution Structured Illumination Microscopy (SIM) imaging. Somewhat surprisingly, we found no significant difference in any of the morphological features examined (**Figure A.II.4A-C**). The average growth cone area of TACC phospho-null mutant-expressing growth cones (406.5 ± 37.17 μm, N=88, p=0.6) was 13% smaller than control (432.6 ± 39.62

μm, N=77) and 6% larger than TACC wt (382.5 ± 30.17 μm, N=94, p=0.6) (**Figure A.II.4A**). The average filopodia number did not differ across conditions either (p=0.4). TACC phospho-null mutant growth cones had an average of 6.9 ± 0.41 N=93 filopodia, which was 10% less than control growth cones (7.6 ± 0.45 N=89) while TACC wt had 9% fewer filopodia than control (7.0 ± 0.38 N=101) (**Figure A.II.4B**). The average filopodia length in TACC phospho-null mutant growth cones was 17.03 ± 0.84μm, N=113, while it was 16.07 ± 0.77 μm, N=119 in control growth cones, and 15.96 ± 0.51 μm, N=126 in TACC wt expressing growth cones (**Figure A.II.4C**).

However, while average filopodia number was similar among conditions, the number of filopodia that contained microtubules was found to be significantly higher in the TACC phospho-null mutant-expressing growth cones. Almost 30% of the filopodia had microtubules in the TACC phospho-null mutant growth cones (29.13 ± 2.932 percent of total filopodia examined, N=82), which is 63% more than control growth cones (10.92 ± 2.011 percent of total filopodia examined, N=90, ***p<0.0001), that had only 11% of their filopodia invaded by microtubules. TACC wt-expressing growth cones also had a greater number of filopodia with microtubules (25.82 ± 2.446 N=92, ***p<0.0001) compared to controls. While not significant, TACC phospho-null growth cones had 11% more filopodia with microtubules compared to TACC wt (**Figure A.II.4F**). Thus, it appears that over-expression of the phospho-null TACC domain somehow leads to an increased number of microtubules that penetrate into filopodia, which may contribute directly or indirectly to increased pausing and retraction rates of these axons.

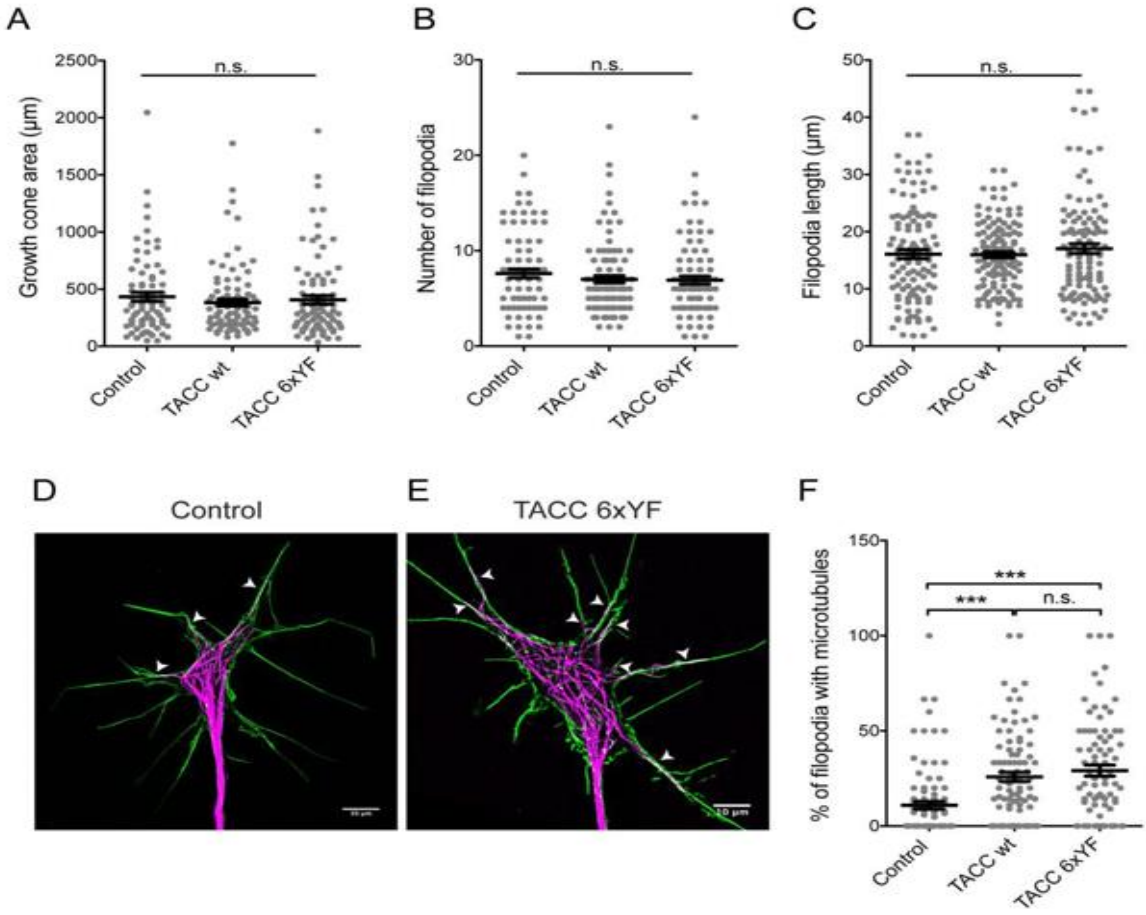

Figure A.II.4. TACC tyrosine phospho-null mutant-expressing growth cones display increased numbers of filopodia that contain microtubules. (A-C) The average growth cone area of TACC mutant (406.5 ± 37.17 □m, N=88) expressing growth cones was 13% smaller than control (432.6 ± 39.62 □m, N=77) and 6% larger than TACC wt (382.5 ± 30.17 □m, N=94) (A). TACC p-null mutant growth cones had an average of 6.9 ± 0.4130 N=93 filopodia which was 10% less than control growth cones (7.6 ± 0.4510 N=89) while TACC wt had 9% fewer filopodia than control (7.0 ± 0.3812 N=101) (B). The average filopodia length in TACC p-null mutant growth cones was 17.03 ± 0.8448□m, N=113, while it was 16.07 ± 0.7707 □m, N=119 in control growth cones, and 15.96 ± 0.5079 □m, N=126 in TACC wt expressing growth cones (C). Almost 30% of the filopodia had microtubules in the TACC p-null mutant growth cones (29.13 ± 2.932 percent of total filopodia examined, N=82, E), which is 63% more than control growth cones (10.92 ± 2.011 percent of total filopodia examined, N=90, D), that had only 11% of their filopodia invaded by microtubules. TACC wt-expressing growth cones also had a greater number of filopodia with microtubules (25.82 ± 2.446 N=92) compared to controls. While not significant, TACC p-null growth cones had 11% more filopodia with microtubules compared to TACC wt (F). Scale bar 10 µm.

TACC tyrosine phospho-null mutant-expressing axons are more responsive to repellent guidance signals

We previously tested TACC3 function downstream of Slit2 and found that growth cones overexpressing TACC3 were more resilient to bath-applied Slit2-induced growth cone collapse

compared to control growth cones [142]. While bath application of guidance proteins is useful to test how manipulation of protein levels would alter the growth cone's reaction to an applied guidance molecule, it does not convey information regarding the ability of the growth cone to make guidance choices such as steering. In order to test that, we utilized an approach where the repellent guidance protein Ephrin-A5 is coated on a glass coverslip in zigzag patterns and neural tube explants are cultured on top of these cue-coated coverslips. After 12-18 h of culturing, explants are fixed and stained for tubulin and actin to examine axon responsiveness to Ephrin-A5. The responsiveness is scored based on how many of the axons that grow out from the given explant preferred to stay on the Ephrin-A5-free (growth permissive) surface versus how many of them cross that barrier and grow on the Ephrin-A5 (non-permissive) surface.

We found that control neural tube explants (**Figure A.II.5A**), composed of a heterogeneous population of neurons, do not show a preference towards a particular surface and grow axons on both permissive (Ephrin-A5 free) and non-permissive (Ephrin-A5) surfaces equally (**Figure A.II.5D**; Control - off, 50.01 ± 2.93 N=55; Control- on, 49.99 ± 2.93, respectively, p=0.9). However, TACC wt over-expressing neural tube explants (**Figure A.II.5B**) show a preference for the permissive surfaces, as they grow 25% more axons on permissive surfaces (**Figure A.II.5D**; 57.18 ± 2.68 N=62, TACC wt – off, ***p=0.0002) compared to the Ephrin-A5 coated surface (TACC wt - on, 42.82 ± 2.68 N=62). TACC phospho-null mutant-expressing axons (**Figure A.II.5C**), on the other hand, show an even stronger preference for the permissive surface, as they grow 41.3% more axons on the permissive surface (**Figure A.II.5D**; TACC mut - off, 63.02 ± 3.03 N=42, ***p<0.0001) compared to the Ephrin-A5 coated non-permissive surface (TACC mut - on, 36.98 ± 3.03 N=42). Together, these data suggest that expression of the

TACC domain with the non-phosphorylatable tyrosine residues are less able to grow on the Ephrin surface and are thus more responsive to the Ephrin-A5 repellent guidance cue activity.

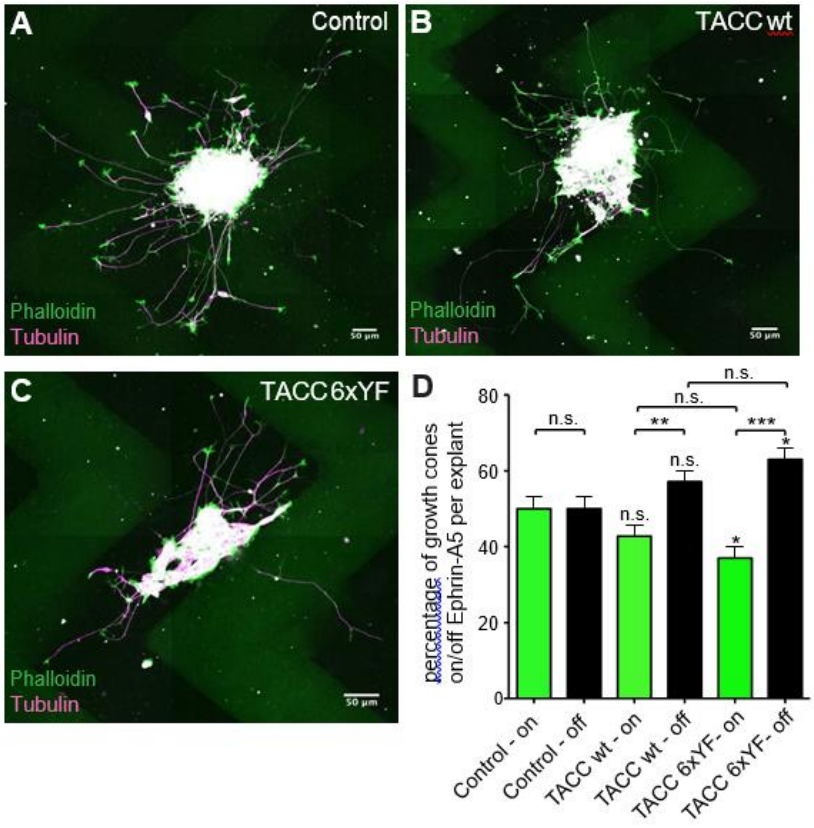

Figure A.II.5. TACC tyrosine phospho-null mutant-expressing axons are more responsive to repellent guidance signals. (A-C) Immunofluorescence images of control (A). TACC wt (B) and TACC p-null mut (C) labelled with phalloidin (green) to label growth cones and tubulin (red) to label axons showing axon responsiveness to Ephrin-A5 coated zigzag surfaces (green). (D) Quantification of the number of axons on permissive (Ephrin-A5 free) versus non-permissive (Ephrin-A5) surfaces. Control neural tube explants does not show a preference between permissive versus non-permissive surfaces and grow axons on both surfaces equally (Control - off, 50.01 ± 2.930 N=55; Control-on, 49.99 ± 2.930, respectively). TACC wt expressing neural tube explants grow 25% more axons on permissive surfaces (57.18 ± 2.683 N=62, TACC wt - off) compared to Ephrin-A5 coated surface (TACC wt - on, 42.82 ± 2.683 N=62). TACC p-null mutants grow 41.3% more axons on permissive surface (TACC mut - off, 63.02 ± 3.036 N=42) compared to Ephrin-A5 coated non-permissive surface (TACC mut - on, 36.98 ± 3.036 N=42). Scale bar 50 µm.

Discussion

In this study, we sought to examine the impact of TACC3 tyrosine phosphorylation on its interaction with microtubules and regulation of axon outgrowth and guidance. We showed that co-expressing TACC3 with Abelson kinase in HEK293 cells induces TACC3 tyrosine phosphorylation, as evident by the phospho-tyrosine signal we obtained by Western blot. Our Western blot analysis also shows that phosphorylation of TACC3 happens only in the presence of Abelson, as we do not observe any phospho-tyrosine signal when TACC3 is expressed alone or with Fyn, which is another tyrosine kinase (**Figure A.II.1A**).

Interestingly, creating single or combinatorial phospho-null mutations at tyrosine residues that we identified, as potential targets for Abelson, did not show any changes in phospho-tyrosine signal levels observed with Western blot. In an attempt to identify the source of tyrosine phosphorylation, we tested other tyrosine residues and focused specifically on the ones in the TACC domain positioned at the C-terminal of TACC3 and which is responsible for microtubule plus-end tracking and interaction with its well-studied partner, microtubule polymerase XMAP215. The TACC domain possesses 6 tyrosine residues with two of them (Y759 and Y762, aa location given based on full length protein) identified as Abelson targets from the mass-spec analysis and three of them (Y832, Y846 and Y857) predicted as putative targets for Abl via in silico analysis. Intriguingly, mutating all these tyrosines into non-phosphorylatable phenylalanine did not cause any reduction in the phospho-tyrosine signal level as evident by the Western blot (Supplementary Fig. 2A-B). In spite of the lack of any tyrosines in the TACC domain, it was intriguing to see that there was still a phospho-tyrosine signal in the Western blot. The only possible source of phosphorylatable tyrosine was GFP that is tagged to the TACC domain. Tyrosine phosphorylation of GFP has not been reported previously, to our knowledge, nor does *in silico* phosphorylation prediction identify any sites by which kinases might target GFP. However, expression of GFP with Abelson clearly showed a strong phospho-tyrosine signal (Supplementary Fig. 2C-D) suggesting that GFP might be partially contributing to the phospho-tyrosine signal that we have been observing in GFP-TACC.

The impact of phosphorylation on the interaction between +TIPs and microtubules has been studied for several +TIPs, such as CLASP [53,187–189], APC [18], ACF7 [190], EB1 [64,180,191,192]. Here, we demonstrated that tyrosine residues within the TACC domain of TACC3 are important for maintaining the interaction between TACC3 and microtubules. The TACC domain with all

tyrosine residues mutated into phenylalanine remains mostly cytoplasmic, while TACC wild-type localizes to microtubules. It should be noted that the wild-type TACC domain, in contrast to full-length TACC3 (which shows primarily plus-end binding), also shows lattice binding in addition to plus-end localization. Consistent with our previous observations [98], this suggest that N-terminus of TACC3 is important for restricting TACC3 localization to the microtubule plus-ends. +TIPs track microtubule plus-ends either autonomously, through recognition of the growing microtubule structure, or non-autonomously, through an interaction with another plus-end tracking protein such as end-binding (EB) proteins. Although the mechanism of how TACC3 tracks plus-ends is not fully resolved, EB-dependent plus-end tracking can be ruled out as TACC3 does not contain a SxIP motif (serine- any amino acid- isoleucine-proline) that is required for EB binding. It is believed that TACC3 tracks microtubule plus-ends through its interaction with XMAP215, which is mediated by the TACC domain [103,185,193]. Therefore, it is possible that the impaired interaction between microtubules and TACC phospho-null mutant could be arising due to a change in TACC3's ability to interact with XMAP215.

The TACC domain consists of two coiled-coil domains, which means that the sequence follows heptad repeats. Presence of these coiled-coil domains are responsible for TACC3's oligomerization, which is important for TACC3's function and its interaction with XMAP215 [103,129]. Using Multicoil, a coiled-coil prediction program, we looked at whether tyrosine-to-phenylalanine mutations might have altered coiled-coil formation or dimerization of TACC domain. Based on this prediction, it seems as though the TACC phospho-null mutant is still likely able to dimerize and form a coiled-coil (Supplementary Figure 3), suggesting that the interaction between XMAP215 and TACC phospho-null mutant might be retained. Although *in silico* analysis suggests that switching from phosphorylatable tyrosine to non-phosphorylatable

phenylalanine does not affect TACC3's coiled-coil structure, reduced interaction between phospho-null TACC mutants and microtubules might be explained by a change in electrostatic interactions between the two. While this could be a possibility, negative charges introduced via phosphorylation often cause dissociation of proteins from the microtubule [53,194] which is already loaded with negative charges due to negatively-charged residues at the C-terminus of tubulin. While our findings suggest that the tyrosine residues of TACC domain are important for mediating TACC3's interaction with microtubules, the exact mechanism of how they are involved in this interaction remains to be determined.

Microtubule advance within the growth cone is important for consolidating and driving growth cone forward movement [1]. Intriguingly, despite increasing microtubule growth speed and length, our data shows that TACC phospho-null mutant expressing axons of cultured neural tube explants are shorter in spite of slightly higher axon forward velocity rates compared to control. When we further examined other axon outgrowth parameters, we found that TACC phospho-null mutants tend to pause and retract more frequently compared to TACC wild-type and controls (**Figure A.II.3D**). Additionally, mutant axons tend to grow with less directionality (**Figure A.II.3F**). In an attempt to seek further explanation to axon outgrowth behavior, we examined growth cone morphology, since growth cone morphology can often predict the growth behavior of axon [186]. For example, increased growth cone size is often associated with frequently pausing or slow growing axons. Although we did not see a significant difference in growth cone size, filopodia length, or number among conditions (**Figure A.II.4A-C**), there was a significant increase in the number of filopodia with microtubules in the TACC phospho-null mutant expressing growth cones (**Figure A.II.4F**).

We know that microtubules can play an instructive role in growth cone directional motility. Having more filopodia with microtubules might generate more alternative routes for the growth cone to extend, which could result in more pausing for decision making and could also cause the growth cone to wander more, which would result in less directed movement. Additionally, there might be increased microtubule/F-actin coupling, which would enable microtubules to track more persistently along F-actin into the filopodia. In fact, increased microtubule/F-actin coupling could also explain increased retraction rates. For example, actin filaments in the growth cone are subjected to rearward translocation also known as retrograde flow, due to myosin II activity [24]. The retrograde flow of actin filaments can be attenuated when the F- actin cytoskeleton engages with receptors at point contact sites. This interaction acts as a molecular clutch that will restrain actin retrograde flow, while continuing actin polymerization will generate the force to allow membrane protrusion, thereby growth cone advance. The growth cone retracts when actin retrograde flow fails to be attenuated, which is also an indication of poor surface adhesion.

It is known that dynamic microtubules play an important role in facilitating focal adhesion dynamics by transporting molecules that are involved in focal adhesion turnover [91]. Several microtubule plus-end binding proteins have been studied for their association with adhesion sites [91,195,196]. Therefore, by facilitating microtubule protrusion into the filopodia, the TACC phospho-null mutant domain might be playing an indirect a role in adhesion dynamics. A potential role in point contact regulation can also explain avoidance of EphrinA5-coated repellent substrates. Filopodia with microtubules could be more sensitive to cues, due to the microtubule-mediated signal trafficking, thereby affecting the interaction with the underlying substrate. Moreover, as speculated earlier, having more filopodia with microtubules could generate more alternative

routes; thus, when the growth cone encounters a non-permissive substrate, it could pick one of these alternative routes and steer away from the repellent source.

In conclusion, we have demonstrated that tyrosine residues within the TACC domain, which is the domain important for mediating microtubule plus-end tracking behavior, are critical for localizing the protein to microtubules, regulating axon outgrowth parameters and making guidance decisions. Given the increased number of microtubules in the filopodia when the TACC domain is over-expressed, we hypothesize that the tyrosine residues in the TACC domain might be involved in regulating a potential TACC-mediated interaction between microtubules and F-actin. Such an interaction has not been proposed for TACC3 before, however, there are studies that might offer a potential interaction between TACC3 and the actin cytoskeleton. A proteomic screen previously identified an interaction between TACC3 and actin regulator proteins Ena/VASP [197]. Additionally, the close interactor of TACC3, XMAP215, has recently been shown to interact with actin and mediate microtubule/F-actin interaction in growth cones [149], which makes TACC3 a candidate to be involved in actin cytoskeleton interaction either direct or indirectly.

To our knowledge, TACC3 tyrosine phosphorylation has not been explored extensively before. Nelson et. al. identified two tyrosine residues, Y684 and Y753 (corresponding to residues Y725 and Y832 in X. laevis and conserved across species, Supp. Fig. 4) that showed enhanced phosphorylation when it is fused to Fibroblast Growth Factor Receptor 3 (FGFR3) [198]. It has been indicated that the FGFR3–TACC3 fusion is important for the activation of FGFR3 tyrosine kinase activity, and fusion of these proteins increases cell proliferation and tumor formation. Moreover, TACC3 in association with ch-TOG has been shown to localize to the mitotic spindles [130]. However, the FGFR3-TACC3 fusion, which pulls TACC3 away from mitotic

spindles and localizes to the spindle poles, causes mitotic defects, which might explain the involvement of these proteins in tumor formation [199]. From this perspective, it might be intriguing to investigate TACC domain tyrosine residues and TACC association with microtubules during cell division. Finally, in addition to tyrosine phosphorylation, serine/threonine phosphorylation sites within TACC3 would be worthwhile to explore, given that there are several S/T kinases that operate under guidance cues, such as GSK3, which is a well-studied S/T kinase that is already shown to phosphorylate various +TIPs and modulate microtubule dynamics. Future work can further explore whether TACC3 is targeted by S/T kinases and whether S/T phosphorylation would affect TACC3's function in a similar way, which could shed light on differential and asymmetric regulation of microtubule dynamics under various guidance signals.

Materials and Methods

Embryos

Eggs collected from Xenopus laevis were fertilized in vitro and kept between at 13-22˚C in 0.1X Marc's Modified Ringer's (MMR). All experiments were approved by the Boston College Institutional Animal Care and Use Committee and were performed according to national regulatory standards.

Culture of embryonic explants

Neural tubes of embryos staged according to Nieuwkoop and Faber were dissected at stages between 20-21 as described previously [146]. Neural tube explants were cultured on MatTek glass bottom dishes coated with poly-L-lysine (100 µg/ml) and laminin (20 µg/ml). Culture media prepared by mixing L-15 Leibovitz medium and Ringer's solution supplemented with antibiotics NT3 and BDNF to promote neurite outgrowth.

Constructs and RNA

Capped mRNAs were transcribed and purified as previously described [98,112]. TACC3 pET30a was a gift from the Richter lab, University of Massachusetts Medical School, Worcester, MA and sub-cloned into GFP pCS2+. Tyrosine phospho-null mutations were introduced into wild-type GFP-TACC3 by using overlapping extension PCR method with appropriate primers designed to substitute tyrosine residues with phenylalanine to generate GFP-TACC3 6xYF. Wild type and phospho-null mutants of TACC domain were cloned from their full-length counterparts. MACF 43 (a gift from Hoogenraad Lab) was sub-cloned into mKate2 pCS2+. Embryos either at the 2-cell or 4-cell stage were injected with the following total mRNA amount per embryo; 100 pg of GFP-MACF43 as a control for GFP-TACC3 and to analyze microtubule dynamics parameters. GFP-TACC3 full-length wild type or phospho-null mutant injected at 1000 pg. GFP-TACC wild type or phospho-null mutant were injected at 400 pg. The human c-Abl construct was originally constructed in the Kufe lab (Harvard Medical School) and gifted by Dr. Alan Howe (University of Vermont). The Fyn construct in pRK5-Entry [200]was acquired from AddGene (Cambridge, MA, USA).

Cell Culture and Transfections

HEK293 cells were maintained at 37 °C and 5% CO2 and cultured in DMEM containing L-glutamine, sodium pyruvate and 4.5 g/L glucose (MediaTech/Corning Life Sciences, Tewksbury, MA, USA). DMEM was supplemented with 5% fetal bovine serum (Hyclone, Logan, UT, USA), 5% Cosmic calf serum (Hyclone), 50 units/mL penicillin and 50 µg/mL streptomycin (Penicillin-Streptomycin, Invitrogen, Carlsbad, CA, USA). Cells were cultured to 75% of confluence and transfected with 3-6 µg GFP-TACC3 full-length (FL) with or without 2 µg c-Abl or 3.5 µg Fyn expression plasmids using calcium phosphate precipitation. The following expression constructs encoding TACC3 phospho-null and truncation mutants were co-transfected at 3 µg with c-Abl: GFP-TACC3 Y2A (Y608A, Y628A); GFP-TACC3 Y3A (Y608A, Y628A, Y759A); GFP-TACC3 Y4A (Y608A, Y628A, Y759A, Y762A). GFP-TACC domain widtype; GFP-TACC domain phospho-null mutant (Y725F, Y759F, Y762F, Y832F, Y846F, Y857F).

Cell Lysis, Immunoprecipitation and Western Blotting

HEK293 cells were lysed as previously described in lysis buffer (25 mM Tris pH 7.4, 137 mM NaCl, 10% glycerol, 1% NP-40) containing protease inhibitors (5 µg/mL Pepstatin, 10 µg/mL Leupeptin, 1 mM PMSF) and phosphatase inhibitors (1 mM NaVO3, 25 mM NaF, 10 mM Na2H2P2O7) [201]. For cell extract immunoblotting, 20-30 µg total protein extract was denatured in protein sample buffer (125 mM Tris pH 6.8, 7.5% glycerol, 2% sodium dodecyl sulfate (SDS), 5% β-mercaptoethanol, and 0.02% bromophenol blue) at 95 °C for 5 minutes and subjected to SDS-PAGE. For immunoprecipitation experiments, 1000 µg of total protein was incubated overnight at 4 °C with 2 µg α-GFP (Life Technologies/ThermoFisher Scientific, Carlsbad, CA, USA) and 20 µL of a 50% slurry of sepharose Protein A (Rockland Immunochemicals, Limerick,

PA, USA) and Protein G resin (G-Biosciences, St. Louis, MO, USA) prewashed with lysis buffer. Immune complexes were washed 3 times with lysis buffer, dried and denatured in protein sample buffer at 95 °C for 5 minutes. Denatured cell extract and immunoprecipitation samples were subjected to SDS-PAGE separation. For mass spectrometry analysis, the SDS-PAGE gel was stained with Coomassie (0.1% Coomassie brilliant blue R-250, 20% glacial acetic acid and 40% methanol) and subsequently prepared for mass spectrometry as described below. For immunoblotting experiments, the following primary antibodies were diluted in 10 mL of 1.5% BSA in TBST containing 0.0005% sodium azide and incubated at 4 °C with the membranes overnight: α-GFP (1:2000, rabbit pAb, Life Technologies); α-Abl (1:1000, rabbit pAb, Santa Cruz Biotechnology, Dallas, TX, USA); α-phosphotyrosine 4G10 (1:1000, mouse mAb, EMD Millipore, Billerica, MA, USA). The following secondary antibodies were used: α-mouse- HRP (goat IgG, 1:5000; EMD Millipore); α-rabbit-HRP (goat IgG, 1:15,000, EMD Millipore); or for immunoprecipitation experiments, α-rabbit-HRP Light Chain Specific (goat IgG, 1:10,000, Jackson ImmunoResearch Laboratories, West Grove, PA, USA). Proteins were detected using enhanced chemiluminescence (ThermoFisher Scientific, Waltham, MA, USA) and film was developed using a Medical Film Processor SRX-101A (Konica Minolta Medical and Graphic, Tokyo, Japan).

Mass Spectrometry

To identify Abl-induced phosphorylation sites on TACC3, GFP-TACC3 was transfected with or without c-Abl. GFP-TACC3 was immunoprecipitated using α-GFP and subjected to SDS-PAGE separation and Coomassie staining as described above. The region corresponding to the molecular weight of GFP-TACC3 (180 kDa) was excised and prepared for mass spectrometry as

previously described [202]. Briefly, gel regions were diced and proteins were subjected to in-gel digestion with 6 ng/μL trypsin (Promega, Madison, WI, USA) in 50 mM ammonium bicarbonate at 37 °C for 10-12 hours. The tryptic peptides were resuspended in 2.5% acetonitrile, 0.15% formic acid and separated via HPLC prior to MS/MS analysis on a linear ion trap-orbitrap (LTQ-Orbitrap) mass spectrometer (Thermo Electron, Waltham, MA, USA) controlled with Thermo Xcalibur 2.1 software. Peptides were eluted and electrosprayed (2.1 kV) into the mass spectrometry as previously described [203]. The precursor scan (scan range = 360- 1700 m/z, resolution = 3.0 x 104) was followed by ten collision-induced dissociation (CID) tandem mass spectra. CID spectra were acquired for the top ten ions in the precursor scan. A SEQUEST search of the mass spectrometry data was performed using the forward and reverse Xenopus TACC3 Uniprot sequence requiring tryptic peptides and permitting phosphorylation of serine, threonine and tyrosine (+79.9663 Da), oxidation of methionine (+15.9949 Da), and acrylamidation of cysteine (+71.0371Da). Peptides were identified with a false discovery rate of less than 1%.

Immunocytochemistry

Embryonic explant cultures were fixed with 0.2% Glutaraldehyde as described [40] and labelled with primary antibody (1:1000 diluted in blocking buffer made up by 1% non-fat dry milk in calcium and magnesium free PBS) to tyrosinated tubulin [YL1/2] (rat monoclonal, ab6160, Abcam) for 45 min at room temperature which is followed by PBS washes repeated three times and 10 min of blocking. Goat anti-rat AlexaFluor568 (1:500, ab175476, Abcam Technologies) was used as a secondary to tubulin and Phalloidin 488 (1:500, Molecular Probes) was used to label actin. Both reagents are diluted in blocking solution and applied for 45 min at room

temperature followed by PBS washes several times. 90% glycerol stock was used as a mounting media for imaging.

Stripe Assay

The stripe assay is performed as described in Knoll et al 2001 [123]. 10 ug/ml of Ephrin-A5/Fc (chimera human, Sigma, E0628) and 10 ug/ml of Fc are mixed with 2.5 ug/ ml of Anti-human IgG (Fc specific) FITC (Sigma, F9512) and Anti-human IgG (Fc specific) respectively in PBS. Solutions are incubated at room temperature for 30 min to allow for oligomerization. To coat coverslips with Ephrin-A5, a coverslip is attached to a zigzag patterned silicon matrix and Ephrin-A5 solution is injected with a micropipette through the channel in the silicon. Injected matrices are incubated at 37˚C for 30 min and then rinsed with PBS several times using the same injection method. After rinsing, coverslips are detached from the matrix and placed in a culture dish and 100 µl of second stripe solution (Fc only) is applied directly on the coverslip and incubated at 37˚C for 30 min. After incubation is over coverslips are rinsed with PBS and 20 ug / ml of 100ul laminin in PBS is applied on coverslips and incubated for 1 h. After laminin incubation, coverslips are rinsed with PBS several times. 400 µl of culture media is applied on coverslips and neural tube explants are placed on protein-coated area and cultured for 24 h prior to imaging.

Image acquisition

To assess axon outgrowth parameters, phase contrast images of axons were collected on a Zeiss Axio Observer inverted motorized microscope with a Zeiss 20×/0.5 Plan Apo phase objective.

For axon outgrowth length, snap-shots of neural tube explants were taken 12-18h post culturing. Time-lapse images were collected for 4 h with 5 min intervals and axon growth was manually tracked frame-by-frame using Fiji Manual Tracking plugin. Axon growth velocity information is provided by the Manual Tracking plugin but only the forward movement velocity was included in the analysis. Axon outgrowth forward movement, pause and retraction frequencies (as a percentage of total frames tracked) are scored manually tracking axons frame by frame. High-resolution images of cultured spinal cord explants were obtained with a CSU-X1M 5000 spinning-disk confocal (Yokogawa) on a Zeiss Axio Observer inverted motorized microscope with a Zeiss Plan-Apochromat 63×/1.40 numerical aperture lens. Images were acquired with an ORCA R2 charge-coupled device camera (Hamamatsu) controlled with Zen software. For microtubule dynamics and TACC localization experiments, images are time lapse images are acquired for 1 min with 2.0 s intervals. Structured illumination super-resolution images were collected on a Zeiss Axio Observer.Z1 for super-resolution microscope with Elyra S.1 system, utilizing an Objective Plan-Apochromat 63×/1.40 oil (DIC). Images were acquired with a PCO-Tech Inc.pco.edge 4.2 sCMOS camera. The images were obtained in a chamber at approximately 28°C and utilizing the immersion oil Immersol 518F 30°.

Image Analysis

Channel alignment and structured illumination processing were applied to the super-resolution images using the Zeiss Black program. Experiments were performed multiple times to ensure reproducibility. Graphs were made in GraphPad Prism. Statistical differences were determined using unpaired two tailed t-tests when comparing two conditions and one-way analysis of variance (ANOVA) with Tukey's post-hoc analysis when multiple conditions were compared.

Supplemental Information

For supplemental figures and movies, please find them online at:

https://onlinelibrary.wiley.com/action/downloadSupplement?doi=10.1002%2Fcm.21622&file=cm21622-sup-0001-supinfo.pdf

Appendix Chapter 3. Characterization of Xenopus laevis Guanine Deaminase reveals new insights for its expression and function in the embryonic kidney

*My role in facilitating the completion of this chapter was the following: Growth cone imaging and all MT dynamics data in Figure 2, and subcloning on constructs. However, the full manuscript is included in its entirety adapted from: (Slater et. al., 2019 – Dev. Dynamics.)

Introduction

The proper establishment of neuronal morphology is essential for the correct communication between neurons, and the cytoskeleton plays a key role in determining neuronal morphology during development. In particular, microtubules (MTs) orchestrate formation of neuronal polarity and ensure proper axon and dendrite morphology. MT dynamics are widely regulated by proteins that bind to the plus-end of the MT, called plus-end tracking proteins (+TIPs), in addition to other types of MT-binding proteins [19,33,36,115,171]. While many studies have begun to investigate MT plus-end dynamics in the developing nervous system, it is clear that much more information is needed to reveal a comprehensive picture for how MT dynamics regulate neural development.

One important MT regulator in the developing nervous system is the mammalian guanine deaminase (GDA), called Cypin (cytosolic PSD-95 interactor) [204]. Cypin has been linked to autism spectrum disorders and has been described as a risk biomarker for these disorders [205]. In addition, Cypin levels increase in rat striatal neurons in response to nigro-striatal degeneration, which models the degeneration of neurons in Parkinson's disease [206]. Multiple neurodevelopmental disorders are associated with defects in axon guidance and dendritogenesis. Furthermore, it has been shown that Cypin plays a key role in establishing neuronal morphology

by antagonizing PSD-95 function and increasing dendrite branching [204,207]. Cypin contains a domain with homology to the collapsin response mediator protein (CRMP), which binds tubulin and has a suggested role in regulating MT assembly in the growth cone [208]. In addition, Cypin can bind tubulin heterodimers and regulate MT assembly in vitro [204]. Moreover, the binding partner of Cypin, PSD-95, binds to the known +TIP, EB3, in neurons and hence regulates MT dynamics [209]. However, while Cypin has previously been proposed to regulate MT dynamics, it has not yet been determined whether Cypin can actually localize to MT plus-ends or alter MT dynamics in living cells.

Multiple +TIPs have been described and characterized using Xenopus laevis [17,52,98,112,142,183,184]. Xenopus embryos can be easily manipulated, and their primary embryonic neural cells are facile to obtain, culture, and image, as they display large growth cones (diameter of 10 microns or more), which are useful for imaging cytoskeletal dynamics [172,173]. Live cell imaging is particularly important, as some +TIPs only bind to growing MTs and, thus, their localization dynamics cannot be visualized using immunohistochemistry of fixed cells [98].

In this work, we investigated whether human GDA (Cypin) and/or Xenopus laevis GDA (GDA) can localize to MT plus ends, perhaps functioning as a +TIP, and tested whether it has a role in regulating MT dynamics. Additionally, we examined GDA expression in Xenopus laevis during embryonic development, as its expression and function had not been well characterized. We visualized exogenously-expressed Cypin and GDA for the first time in living primary embryonic neural growth cones using fluorescent confocal microscopy and found that neither of them co-localize with MT plus-ends, suggesting that GDA does not function as a +TIP. Despite the lack of MT binding, we found that expression of Cypin, but not GDA, promotes MT assembly in neuronal growth cones. Moreover, we found that the CRMP homology domain, which has been

described as important for binding tubulin and regulating MT assembly, is not fully conserved in Xenopus. By generating a chimera containing the N-terminal region from GDA plus the Cypin domain containing the CRMP homology and PDZ-binding domain, we found that this Cypin region is necessary for regulating MT dynamics. Finally, using whole-mount in situ hybridization, we observed that GDA is highly expressed in the kidneys and may be important for proper kidney function. Our results suggest that the function of GDA to regulate MT dynamics is not conserved in Xenopus.

Results

The CRMP homology domain is not conserved between human and Xenopus GDA

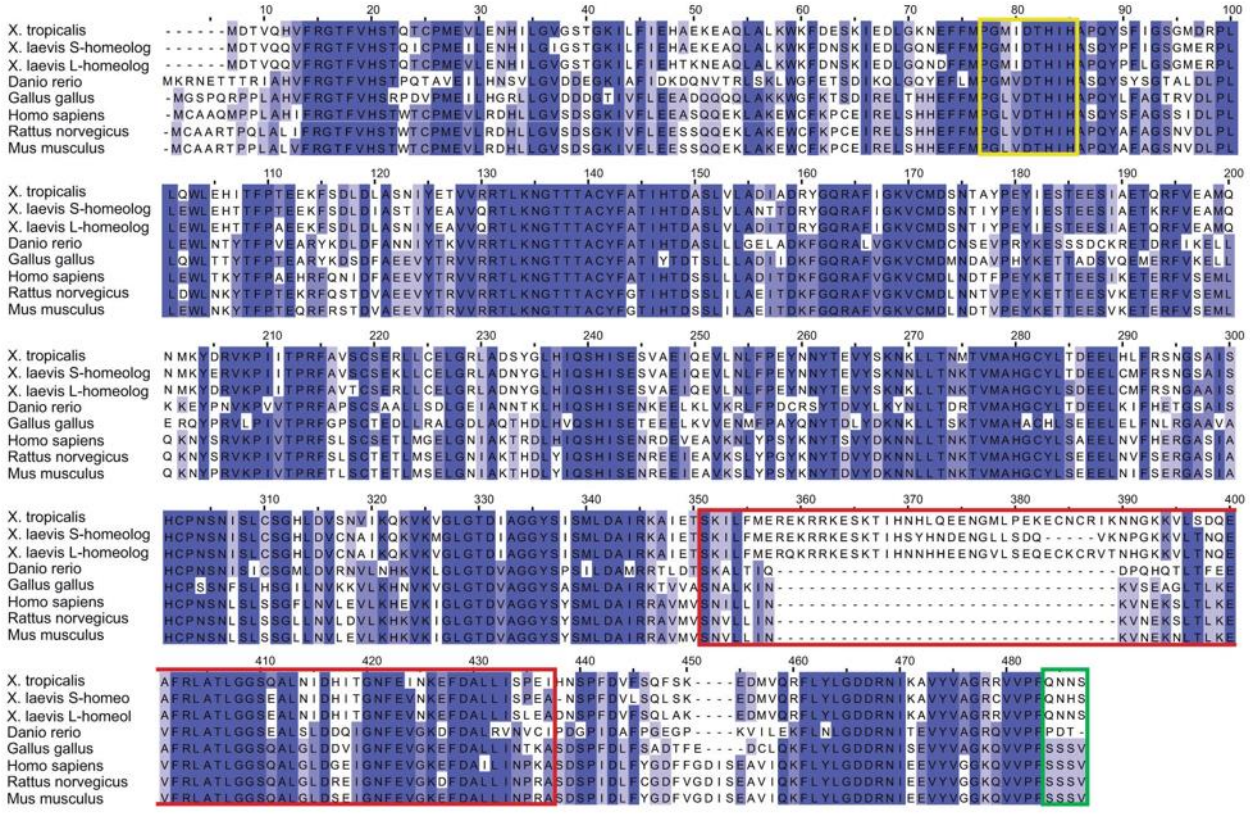

Figure A.III.1. The CRMP homology domain is not conserved between human and Xenopus GDA. Sequence alignment of X. laevis homeologs; X.tropicalis; Danio rerio; Gallus gallus; Homo sapiens; Rattus norvegicus; and Mus musculus GDA. The GDA N-terminal, including the Zn2+ binding domain (yellow square), is well conserved among all species, while the CRMP homology (red square) and the PDZ-binding domains (green square) are less conserved.

While a previous phylogeny study reported that the guanine deaminase (GDA) DNA sequence has been conserved from prokaryotes to higher eukaryotes [210], this early study did not examine the entire amino acid sequence nor did it look specifically at the CRMP domain sequence. X. laevis, X. tropicalis, Danio rerio, Gallus gallus, Homo sapiens, Mus musculus and Rattus norvegicus form part of the same related clusters of GDA sequences [210]. Here, we compared the GDA protein sequences of all the aforementioned species. X. laevis is an allotetraploid organism and has two GDA homologs, S and L; thus, we considered both homologs for protein sequence comparison. We found the following sequence homologies of each organism with human Cypin: X. laevis GDA S-homeolog 60%; X. laevis GDA L-homeolog 61%; X. tropicalis 61%; zebrafish 59%; chicken 72%; rat 91%; and mouse 91% (**Figure A.III.1**).

In addition, while all GDAs were previously described to have well-conserved zinc-binding domains, the CRMP homology and PDZ-binding domains are not completely conserved. *Gallus gallus, Homo sapiens, Mus musculus* and *Rattus norvegicus* all have a PDZ-binding domain, which is absent from *X. laevis, X. tropicalis* and *Danio rerio* (**Figure A.III.1**). Moreover, even though the CRMP homology domain was present in all the organisms, it is not well conserved. While chicken, rat, and mouse have strong conservation with human (82%, 91%, 91%, respectively), the CRMP homology domains in X. laevis GDA S and L, X. tropicalis, and zebrafish are not as similar (60%, 53%, 53%, 58% conservation with human GDA, respectively) (**Figure A.III.1**). Notably, neither the PDZ-binding domain nor the CRMP domains are conserved between amniotes and amphibians/fish.

GDA has a cytosolic distribution and does not accumulate at MT plus-ends

In order to explore the possibility that GDA may function as a +TIP and thereby bind to the plus-ends of MTs to regulate MT dynamics [1,19], we first examined whether human (Cypin) and/or X.laevis (GDA) GDA localize to MT plus-ends or not. We co-injected mRNAs coding for GFP-tagged N- or C-terminus Cypin and GDA along with mKate2- MACF43, a known marker of growing MTs that localizes to the MT plus-ends [64], into X. laevis embryos at the 2-cell stage. We prepared spinal cord explants from stages 20–24 Xenopus embryos, and we used live imaging to

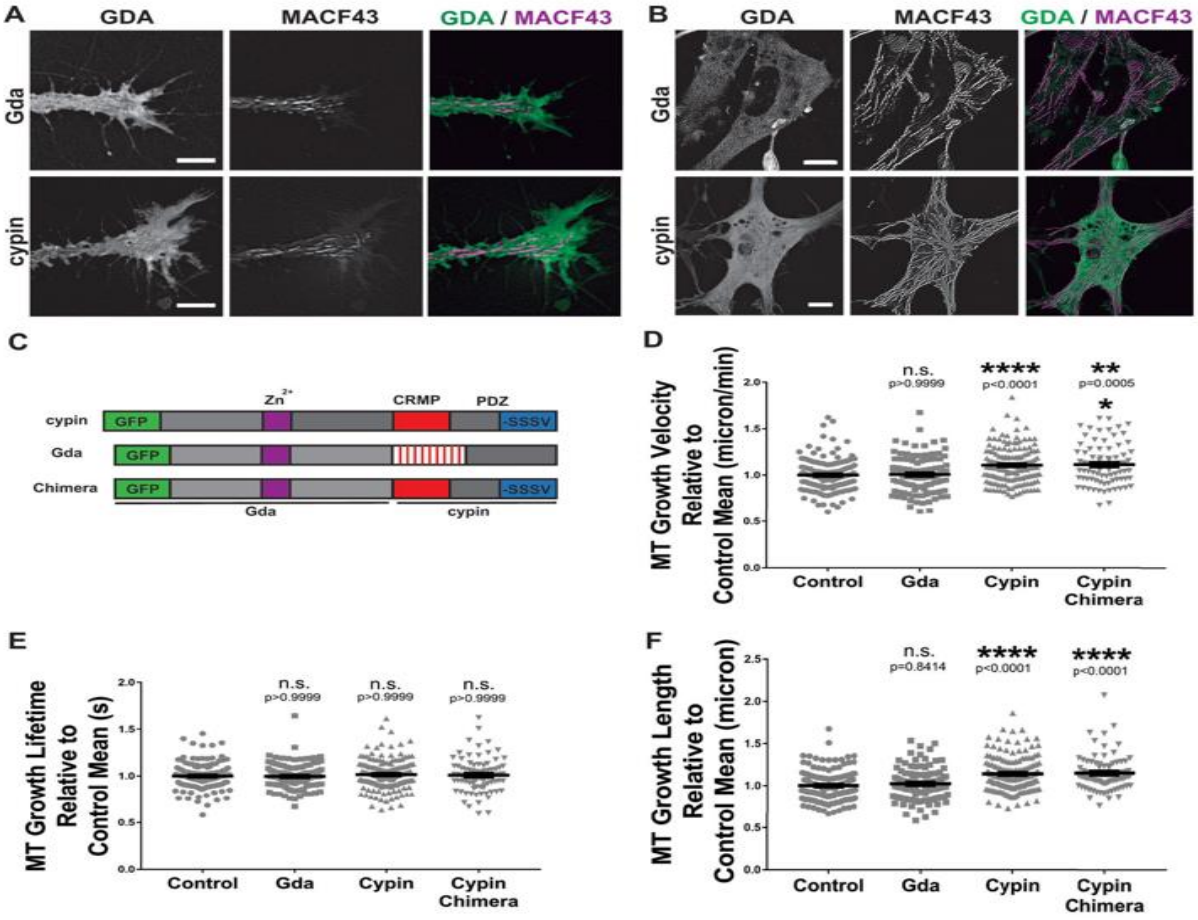

Figure A.III.2. GDAs do not localize to the MT plus-end and only Cypin promotes MT polymerization. A-B. Maximum intensity montage of 31 frames from a one-minute time-lapse image series, of Gda and Cypin (green), and mKate2-MACF43 tracks (magenta), in cultured neuronal growth cones (A) and neural-derived embryonic mesenchymal cells (B), obtained from Xenopus embryos at stage 20–24. Scale bars 8.0 µm (A) and 5 µm (B). C. Schematic representation of the GFP-tagged constructs used, showing the critical domains. D-F. Quantification of mean values of MT growth velocity (D), growth lifetime (E) and growth length (F) in neuronal growth cones upon GFP, Gda, Cypin and Cypin chimera over- expression. (See Supplementary Movie 1 for a representative movie of mKate2-MACF43.) Bars on dot plots show mean and SEM. ** $P < 0.01$; *** $P < 0.001$; **** $P < 0.0001$; n.s., not significant. A total of 138 control; 107 Gda; 154 Cypin and 83 Cypin chimera growth cones, from three independent experiments, were analyzed.

visualize the exogenously- expressed GDAs. We found that neither Cypin nor GDA localized to the MT plus-end in neuronal growth cones (**Figure A.III.2A**), nor in neural-derived mesenchymal cells (**Figure A.III.2B**), as GDAs did not co-localize with mKate2-MACF43. Rather, in all cases, GDA was diffused throughout the cytosol and did not appear to localize to MTs at all, consistent with what has been previously described for Cypin localization [204,207,209]. These data suggest that neither human nor Xenopus GDA accumulate on MTs plus-ends, and thus, GDA does not act as a +TIP in Xenopus embryonic cells.

Exogenous expression of Cypin, but not GDA, promotes MT polymerization in living cells

Considering that some proteins regulate MT dynamics through indirect mechanisms, for example, by binding tubulin heterodimers or other proteins that bind to MTs [32,38], we sought to determine whether over-expression of Cypin or GDA (**Figure A.III.2C**) could affect MT dynamics indirectly in living cells. We measured MT behavior in cultured primary embryonic neuronal growth cones obtained from Xenopus stages 20–24, by quantifying the MT growth track velocity, lifetime and length of mKate2- MACF43 comets after GDA over-expression (Supplementary Movie 1). We observed that axonal growth cones over-expressing Cypin showed an 11% increase in MT growth track velocity and a 17% increase in MT growth track length compared to those of control cells, while no change was observed in mKate2-MACF43 comet lifetime (**Figure A.III.2D-F**). Similar results were observed for both N- and C-terminal tagged GFP-Cypin (data not shown). However, we observed no changes in MT dynamics in cells over-expressing GDA compared to control cells (**Figure A.III.2D-F**). These data show that Cypin over-expression increases MT polymerization rate in living Xenopus embryonic cells, and that human and Xenopus GDAs are different in their ability to modulate MT dynamics.

Additionally, considering the differential regulation of MT dynamics by Cypin and GDA, and the striking differences between the Cypin and GDA CRMP homology and PDZ-binding domain, we decided to evaluate if this Cypin region is responsible for the effect on MT dynamics. We generated a chimera GDA containing the N-terminal half from GDA and the CRMP homology plus PDZ-binding domain from Cypin (**Figure A.III.2C**) and examined the effect of the chimera GDA on MT dynamics. We found that the chimera GDA was able to increase MT growth track velocity and MT growth track length compared to those of control, similar to Cypin (**Figure A.III.2D-F**). Our results suggest that the Cypin region containing both CRMP homology and PDZ-binding domains plays an important role in promoting MT polymerization.

Xenopus GDA is strongly expressed in the embryonic kidney and thus may play a role in kidney function

Given that our results suggested that Xenopus GDA did not function as a promoter of MT polymerization, we wondered if it was still expressed in the developing brain, like Cypin. In order to characterize GDA expression during Xenopus embryonic development, we used reverse transcription (RT) PCR and whole-mount in situ hybridization at different stages of development. First, we performed RT-PCR using cDNA from embryos at various stages including 2 cell, blastula, neurula, 3 dpf and 6 dpf, as well as cDNA from the adult brain. We found that strong GDA expression was not apparent until 3–6 dpf and persisted, although to a lesser extent, through adulthood within the brain (**Figure A.III.3A**). Whole-mount in situ hybridization showed no staining in early stages including 2-cell, blastula, and 1 dpf, confirming the RT-PCR results (**Figure A.III.2B**). However, specific accumulation of GDA expression in

two bilateral regions behind the embryonic eye became apparent at 3 dpf and remained at a high level to 6 dpf (**Figure A.III.3B**). Following the stages of Xenopus laevis development [144], and considering the localization and the tubular structures (**Figure A.III.3B**), we identified these areas to be the developing kidneys. Thus, we used the proximal tubule kidney marker, xSGLT1K

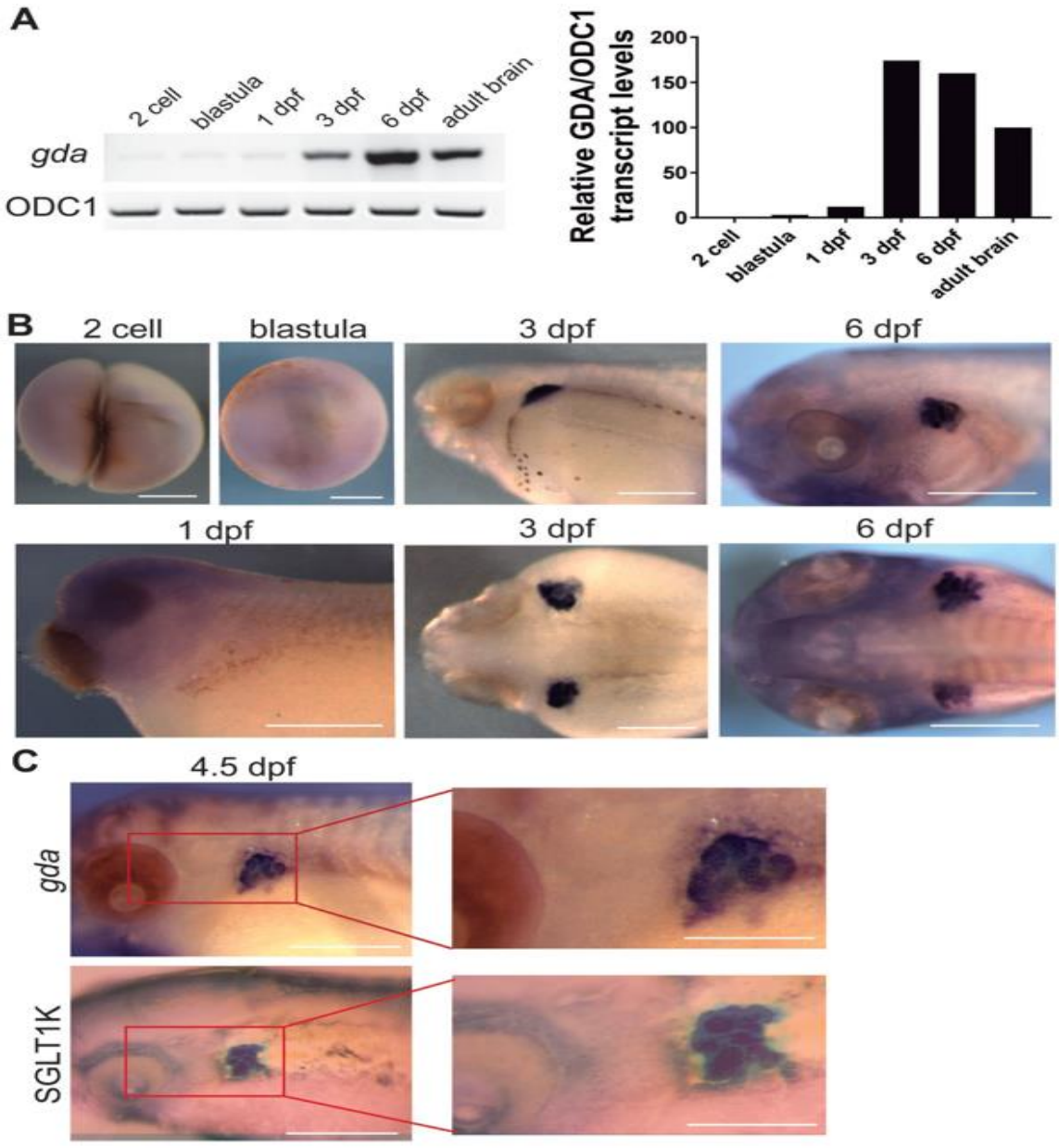

Figure A.III.3. Xenopus GDA is expressed in the developing kidney. A. RT-PCR showing Gda expression in the different developmental stages: two cell, blastula, neurula, 3 dpf, 6 dpf, and adult. ODC1 was used as an internal RT-PCR reference. B. Whole- mount in situ hybridization using an antisense probe specific to Gda in different developmental stages. Scale bar: 0.5 mm C. Whole-mount in situ hybridization using an antisense probe specific to GDA or the kidney marker xSGLT-1K in 4.5 dpf embryos. Both Gda and xSGLT-1K can be seen in a similar embryonic location. Scale bar: 0.5 mm and 0.25 mm for magnifications.

to perform in situ hybridization in 4.5 dpf embryos. Our results showed that both GDA and xSGLT1K are expressed in the same location (**Figure A.III.3C**), confirming the expression of GDA in the kidneys.

We were also interested in determining a possible function of GDA in Xenopus. Since our over-expression analysis suggested that GDA does not play a role in modulating MT dynamics, and our expression analysis showed that GDA is not present in most embryonic cells during early neural development, we reasoned that GDA could not be playing a role to promote MT polymerization in the early nervous system. Given its strong expression in the kidneys beginning at 3 dpf, we wondered if GDA might play a role in kidney development or function. However, pronephros development in Xenopus begins at stage 12.5, and kidneys become initially functional by stage 38, which corresponds to 2 dpf [211,212]. Thus, it did not seem likely that GDA was required for initial kidney development. Still, we wondered whether GDA might be important for kidney function. It has been demonstrated that an altered osmoregulatory function of the kidney leads to edema formation due to water retention [212,213] and evaluation of edema has been widely used to assess kidney function [213]. Thus, we used an antisense oligonucleotide to knock down (KD) GDA by 50% (**Figure A.III.4A**), and at 4 dpf, we analyzed edema formation in the chest as a proxy to study kidney function (**Figure A.III.4B-C**). We observed that GDA KD induced edema in 44% of tadpoles, while no edema was observed in the controls (**Figure A.III.4B-C**). This phenotype was rescued by adding back GDA mRNA to the KD condition (**Figure A.III.4E-D**), attributing these effects specifically to GDA. However, as cardiac and other developmental anomalies can also lead to edema, we also performed targeted injections at the 4-cell stage to knock down GDA function in a more restricted cell lineage.

With these targeted injections, we did not observe significant edema (not shown), suggesting that the edema formation in the GDA knockdown embryos was not necessarily due to defects in kidney function alone. We also examined gross morphology of kidney development by immunostaining for anti-kidney antibodies, 4A6 and 3G8, at 4 dpf and observed no apparent

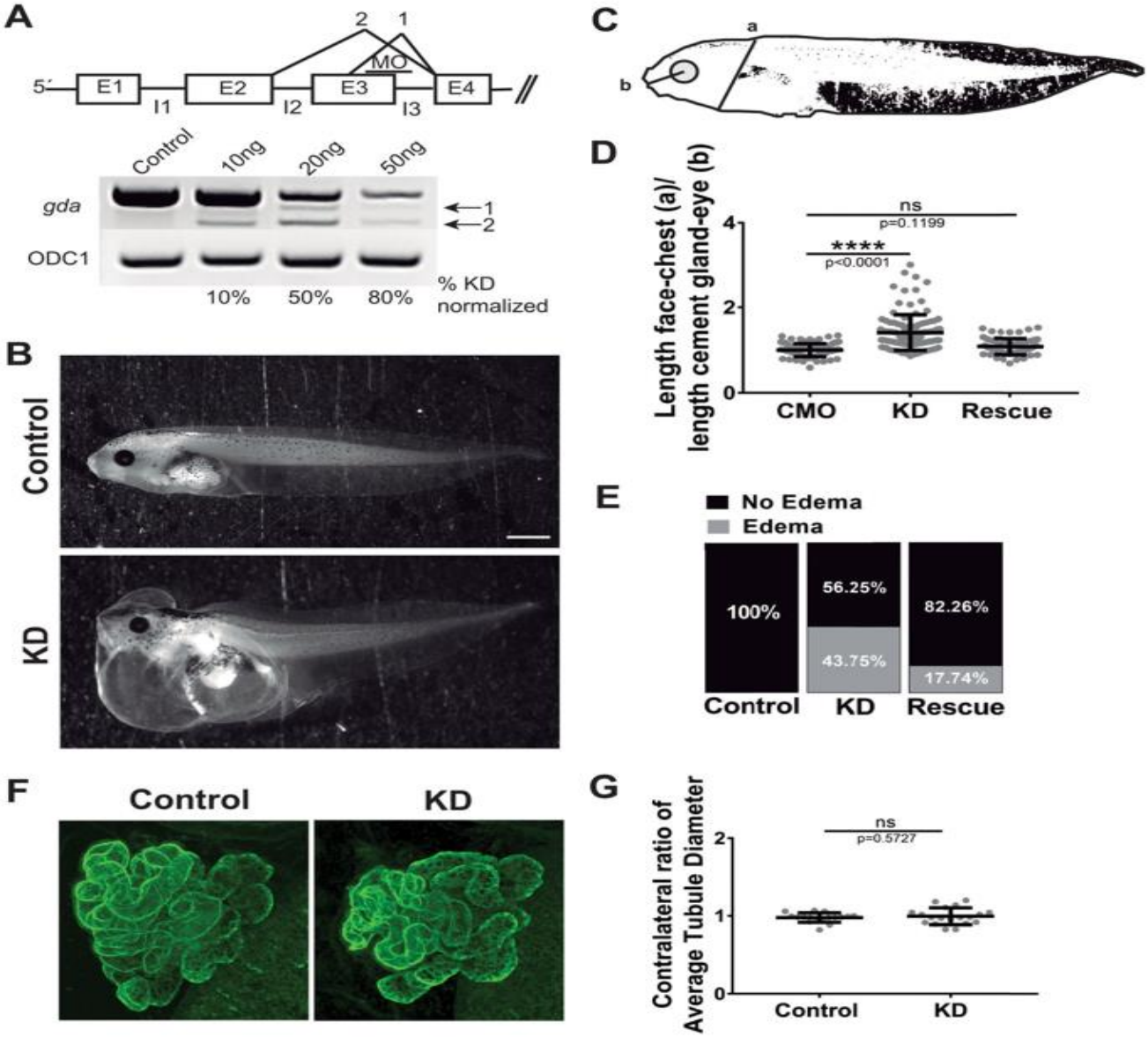

Figure A.III.4. Xenopus GDA knockdown results in edema formation but kidney morphology appears to be normal. A. Schematic representation of the MO effect on Gda RNA splicing (above) RT-PCR showing Gda knockdown (KD) when injecting increasing concentrations of MO (below). B. Representative images at 4 dpf control and Gda KD tadpoles. Scale bar: 1 mm. C. Schematic representation of a tadpole showing the measurements for edema identification. D. Quantification of the ratio: length face-to-chest (a) over length of cement gland-to-eye (b). E. Quantification of the percentage of tadpoles showing edema. F. Representative images of immunofluorescence using the kidney marker 3G8 in addition to 4A6 at 4 dpf control and Gda KD tadpoles. F. Quantification of the ratio: average tubule diameter of the Gda MO- injected side over that of the uninjected side of the same tadpole. Bars on dot plots show mean and SEM. ns: not significant. **** $P < 0.0001$.

differences with GDA knockdown compared to controls (**Figure A.III.4F-G**). Thus, these data suggest that GDA does not appear to be involved in kidney development, but it may still play a role in later kidney function in Xenopus.

Discussion

In this study, we first compared the GDA amino acid sequence from different species, which were related phylogenetically. We determined that the CRMP homology domain is not present in amphibians or fish. Additionally, we visualized fluorescently-tagged Cypin and GDA using live imaging for the first time and determined that GDA protein is cytosolic but is not enriched at the MT plus-end or the MT lattice in Xenopus embryonic cells. We also showed that over-expression of Cypin influenced MT dynamics in embryonic cells, and that this effect of GDA is not conserved among all vertebrates, since the overexpression of GDA has no effect in Xenopus cells. In addition, we showed that the CRMP homology domain and the PDZ-binding domain of Cypin are responsible for the effect on MT dynamics, as we could recapitulate the increased MT polymerization by expressing a Cypin chimera containing the N-terminal region of GDA combined with the Cypin CRMP homology and PDZ-binding domains. Finally, we characterized the spatiotemporal expression of GDA throughout Xenopus embryonic development using RT-PCR and whole-mount in situ hybridization. We show that the highest expression of GDA occurs at 3 dpf and that it is strongly expressed in the kidneys, where it may play a role in kidney function. Thus, our work provides, for the first time, a characterization of GDA expression during embryonic development along with a comparison between human and Xenopus GDA, revealing divergence in sequence and function.

A GDA evolutionary study had determined that the Rattus norvegicus, Xenopus laevis and Homo sapiens GDA proteins are part of the same sequence cluster, meaning that their sequences

are evolutionarily similar [210]. While the GDA enzymatic activity of guanine deamination into xanthine and ammonia has been conserved across many species [210], few studies have examined GDA function during embryonic development. One of the most prominent studies of GDA function has examined the role of the mammalian orthologue, Cypin, during neuronal development [204,214,215]. Importantly, GDAs contain a PDZ-binding domain that is important for interaction and clustering with other proteins [216]. The Cypin PDZ-binding domain is necessary for binding to PSD-95 protein [207], which has been described to increase dendritic branching [207] and indirectly affect MT dynamics [209].

Interestingly, while the enzymatic active site and divalent cation-binding domain are conserved among these species, the PDZ-binding domain is not present in either of the Xenopus homologs [210]. Additionally, GDAs also have a CRMP homology domain that is known to bind tubulin heterodimers [207,217]. The CRMP homology domain is necessary for inducing MT polymerization in vitro [204]. Our work is the first to evaluate the sequence homology of the CRMP homology domain between Cypin and GDA, showing that the CRMP homology domain is not fully conserved. These differences in the PDZ-binding and CRMP homology domains between Cypin and GDA likely explain the divergence in function between the proteins as it relates to their ability to regulate MT dynamics.

Our results show that exogenous expression of both GFP-tagged Cypin and GDA present a cytosolic distribution in living cells, and are not enriched at MT plus-ends, where the majority of the proteins that regulate MT plus-end dynamics are localized. Nevertheless, our observations are consistent with previous immunocytochemistry studies showing that Cypin has a cytosolic localization in rat primary hippocampal neurons [204,207,209,215]. Additionally, while GDA is obtained primarily in the soluble fractions after subcellular fractionation, it is also present in

other intracellular compartments, where it exists in isoenzymic forms [218,219]. Considering this evidence, even though GDA localization is not enriched on MTs, we cannot discard a possible GDA activity near MT lattice or plus ends, which could still allow Cypin to have an indirect effect on MT dynamics.

Using live imaging, we showed that Cypin over-expression increases the MT growth velocity and MT track length in neuronal growth cones. These results are in accordance with previous studies showing that rat Cypin promotes MT assembly and polymerization using in vitro assays [204]. Additionally, it is well known that Cypin increases dendritic arbor length [204] and that it interacts with PSD-95 [207]. Cypin interaction with PSD-95 leads to decreased dendrite branching, potentially caused by the disruption of the MT cytoskeleton [220]. Interestingly, PSD-95 was found to bind and reduce the MT binding of the known +TIP EB3, as well as reduce EB3 comet lifetime and velocity [209]. Thus, given that Cypin has been shown to oppose PSD-95 function, and that PSD-95 reduces MT polymerization, it is possible that Cypin expression in our study perturbs the ability of PSD-95 to inhibit MT polymerization.

However, we observed that expression of mammalian Cypin, but not Xenopus GDA, promotes MT polymerization. This result is consistent with the fact that the CRMP homology domain, which has been shown to bind tubulin and regulate MT assembly [208], is not fully conserved between Cypin and GDA. Additionally, the Cypin PDZ-binding domain that has been described to bind PSD-95 and is responsible for regulating MT dynamics [209] is absent from GDA. Finally, we found that by adding the Cypin CRMP homology and PDZ-binding domains to the N terminal region of Xenopus GDA, we observed MT dynamics regulation similar to that of Cypin. This result further supports the importance of the CRMP and PDZ-binding domain in regulating MT dynamics.

We found that GDA is highly expressed at 3 dpf, which corresponds to stages 41–44, a relatively late time point in Xenopus embryonic development. By this point, significant dendrite branching and elongation in Xenopus retinal ganglion cells has already occurred (stages 32–34) and the specialization into various dendritic subtypes is in process (stages 34–46) [221]. While we cannot overlook the possibility of GDA being involved in this second phase of dendrite branching and differentiation, this hypothesis is unlikely due to the fact that whole-mount in situ hybridization showed minimal GDA expression in the brain or neural tube in Xenopus. While the lack of GDA staining in the neural tube is unsurprising given that Cypin is absent from the mammalian spinal cord [207], the lack of GDA expression in the brain is striking, as Cypin is highly expressed in the developing brain in mammals. This suggests that Cypin may have evolved to serve a different function in mammals than that observed in Xenopus. In the present work, we demonstrated by in situ hybridization that GDA is expressed primarily in the kidney. This expression pattern is more restricted than that observed for Cypin, which is expressed in the human nervous system, placenta, liver, and kidney, and absent from the heart, lung, muscle, and pancreas [207]. Moreover, Cypin protein is expressed in rat kidney, liver, lung, brain, and spleen [207]. Thus, rat Cypin expression pattern contrasts with that of human Cypin, which is not expressed in the lung, suggesting that even within mammals, Cypin has a slightly different expression pattern.

To date, most studies relating to GDA function have focused on its role in maintenance of homeostasis of triphosphate nucleotides, its role as a nitrogen source, its signal transduction pathway, and, lately, on its role in neuronal development. In the present work, we showed that the peak GDA expression is at 3 dpf, which is temporally coincident with a fully functional primitive kidney. Thus, a GDA effect on kidney functioning or maturation to mesonephroi might be expected. Moreover, knockdown of Xenopus GDAs resulted in edema formation, which has

been shown to be indicative of kidney malfunction [212,213]. Nevertheless, at the Xenopus developmental time point that we performed our studies, the pronephroi has still not matured to mesonephroi, thus, it remains to be determined if GDA has an effect on kidney maturation to mesonephroi, or if the effect is restricted to kidney function. Additionally, given that edema also results from cardiac and other developmental issues, it is also possible that other organ systems are affected by reduced GDA function.

The present study shows that human Cypin and Xenopus GDA have different protein sequences and functions. In addition, our MT dynamics analysis suggests that the role of GDA in regulating MT dynamics is not conserved among species. Furthermore, GDA is expressed with high specificity in the kidneys during Xenopus development. Thus, our study suggests a novel function for GDA and warrants further study of its potential role in kidney maturation and function.

Materials and Methods

Culture of Xenopus embryonic explants

Eggs obtained from female X. laevis frogs (NASCO, Fort Atkinson, WI) were fertilized in vitro, dejellied, and cultured following standard methods [156]. Embryos were staged according to Nieuwkoop and Faber [144], and embryonic explants were dissected at stage 22–24 and cultured as described [146]. All experiments were approved by the Boston College Institutional Animal Care and Use Committee and performed according to national regulatory standards.

Guanine deaminase constructs and sequence alignment

The X. laevis GDA L homeolog (GDA) sequence was designed based on the GDA annotated sequence from the laevis genome, version 9.1 (www.xenbase.org) using the transcript model of chr1L:128,874,669..128,903,678 (+ strand), which was predicted to contain the X. laevis GDA genomic sequence. The GDA sequence was acquired from Biomatik (Biomatik, Atlanta, GA, USA) in pBluescript, and then subcloned into the GFP-pCS2+ vector to add a GFP tag to the N-terminus of GDA. The human Cypin sequence, based on NCBI reference sequence NM_004293.4, was obtained from Origen (Origen, Rockville, MD, USA) and subcloned into a GFP-pCS2+ to generate GFP-Cypin and Cypin-GFP. The Cypin-chimera was obtained by removing the GDA region, beginning with the CRMP domain, and replacing it with the human Cypin CRMP homology and PDZ-binding domain. The NCBI Reference Sequences for the GDA protein sequence comparison were the following: Xenopus laevis S homeolog (XP_018099342.1); Xenopus laevis L homeolog (NP_001083074.1); Homo sapiens (NP_001229434.1); Xenopus tropicalis (XP_004910825.1); Danio rerio (NP_001018510.1); Rattus norvegicus (NP_113964.2); Mus musculus (NP_034396.1); Gallus gallus (XP_424835.3). The GDA protein sequences were compared using Clustal Omega (www.ebi.ac.uk/Tools/msa/clustalo/; RRID: SCR_001591).

RNA and Morpholino

Capped mRNA was transcribed in vitro using the SP6 mMessage mMachine Kit (Thermo Fisher Scientific, Waltham, MA, USA). RNA was purified with LiCl precipitation and re- suspended in nuclease-free water. Constructs coding for GFP, GFP-GDA, GFP-Cypin and Cypin-GFP, Cypin-chimera, and mKate2-MACF43 (a gift from Hoogenraad Lab sub-cloned into pCS2+) were used

as templates for in vitro transcription. Embryos were injected at the two-to-four-cell stage in each dorsal blastomere (in 0.1× MMR containing 5% Ficoll) with total mRNA amount per embryo of 1000 pg of Cypin, GDA and 200 pg of mKate2-MACF43.

A morpholino (MO) was designed specific to the Xenopus GDA L homeolog with the sequence 5' TCCCCAAACCAAAGTCCTTACCACA 3' and targeted to the exon 3 – intron 3 splice junction (Fig. 4C) (Gene Tools, LLC, Philomath OR, USA). A standard control MO (5'-cctcttacctcagttacaatttata-3') (Gene Tools, LLC, Philomath OR, USA) was used as control MO. The GDA MO was injected at concentrations of 10, 20, and 50 ng per embryo in order to assess knock down of GDA (Fig. 4C). The GDA transcript levels were measured by reverse-transcription PCR, and the PCR product was sent for sequencing to ensure the introduction of a stop codon. A 50% KD was obtained when injecting 20 ng of the MO (Fig. 4A), which was used for the rest of the experiments in order to generate a partial KD phenotype.

Reverse-transcription PCR

Whole RNA was extracted from embryos at various stages and adult Xenopus brain using Trizol reagent (Invitrogen, LifeTechnologies) and reverse transcribed using SuperScript IV reverse transcriptase (Invitrogen, LifeTechnologies). PCR was then performed with HotStarTaq Plus DNA Polymerase (Qiagen, Hilden, Germany) and primers specific to Xenopus GDA: forward 5' CCCTTGTGCTGGCCGATATTAC 3' and reverse 5' GTAGCAGCCATGAGCCATCAC 3' PCR was performed on the same samples of cDNA, also using primers specific to the housekeeping gene ODC1: forward 5'GCCATTGTGAAGACTCTCTCCATTC 3' and reverse 5'TTCGGGTGATTCCTTGCCAC3' as a RT-PCR control.

Microscopy

Live images of cultured cells were obtained with a CSU-X1M 5000 spinning-disk confocal (Yokogawa, Tokyo, Japan) on a Zeiss Axio Observer inverted motorized microscope with a Zeiss 63× Plan Apo 1.4 numerical aperture lens (Zeiss, Thornwood, NY). Images were acquired with an ORCA R2 charge-coupled device camera (Hamamatsu, Hamamatsu, Japan) controlled with Zen software. For time-lapse, images were collected every 2 sec for 1 min. For two-color images, the red and green channels were imaged sequentially. The images were deconvolved using the "Iterative Deconvolve 3D" plugin within ImageJ. Lateral images of embryos at 4 days post-fertilization (dpf), for quantification of edema formation, in addition to in situ hybridization images, were obtained with a SteREO Discovery.V8 microscope using a Zeiss 1X objective for edema formation experiments and 5X or 8X objectives for in situ hybridization, and Axiocam 512 color camera (Zeiss, Thornwood, NY). Images of immunostained fluorescent kidneys at 4 dpf were obtained with a Leica TCS SP5 scanning confocal inverted microscope (Leica, Buffalo Grove, IL) using a 10X objective. Lateral images of embryos were obtained in a BABB solution on a MatTek glass bottom dish.

plusTipTracker software analysis

MT dynamics were analyzed from mKate2-MACF43 movies from embryonic mesenchymal cells using plusTipTracker, as previously described [112,145]. The same parameters were used for all movies: maximum gap length, eight frames; minimum track length, three frames; search radius range, 5–12 pixels; maximum forward angle, 50°; maximum backward angle, 10°; maximum

shrinkage factor, 0.8; fluctuation radius, 2.5 pixels; and time interval 2 sec. Only cells with a minimum number of 10 MT tracks in a 1-min time lapse were included for analysis. All raw data of automated tracking of mKate2-MACF43 comets were normalized to the same-day control means. Dot plots were made using GraphPad Prism (GraphPad Software, La Jolla, CA). To determine statistical differences, unpaired two-tailed t tests were used for comparing two conditions, after confirming normalized data distribution (GraphPad). A total of 83–154 growth cones were analyzed for each condition, from three independent experiments.

Whole-mount in situ hybridization

Embryos at various developmental stages from two-cell to 6 dpf were fixed overnight at 4°C in a solution of 4% paraformaldehyde in phosphate-buffered saline (PBS), gradually dehydrated using ascending concentrations of methanol in PBS, and stored in methanol at −20°C before in situ hybridization, which was performed as previously described [143]. Embryos were treated with proteinase K for: 1–2 min in the case of 1 dpf embryos and 3–5 min for 3–6 dpf embryos, and then bleached under a fluorescent light in 1.8× saline–sodium citrate, 1.5% H2O2, and 5% (vol/vol) formamide for 45 min before prehybridization. Probes for both GDA and the proximal tubule kidney marker, xSGLT1K (sodium glucose transporter), were used at a concentration of 0.5 μg/ml and hybridized overnight. Sglt1K construct pCMV-SPORT6, SalI/T7 was a gift from the Wessely Lab (Cleveland Clinic, Lerner Research Institute, Cleveland, OH, USA). The full-length antisense digoxigenin-labeled hybridization RNA probes were transcribed in vitro using the T7 MAXIscript kit (Thermo Fisher Scientific, Waltham, MA, USA). The probes were purified using ammonium acetate precipitation and resuspended in nuclease-free water.

Quantification of the edema formation

Embryos were injected with 20 ng of the control MO, Xenopus GDA MO or Xenopus GDA MO plus 1000 pg GDA mRNA, for rescue experiments. From lateral images of 4 dpf injected tadpoles, the formation of edema was analyzed by measuring the length from the top of the face to the bottom of the chest (face-chest), and as the size of the head can vary from tadpole to tadpole, the length from the middle of the cement gland to the middle of the eye (cement gland-eye) was used as an internal reference (**Figure A.III.4C**). The ratios of the former over the latter measurement were compared among the different conditions, to normalize the data for differences in tadpole size. The presence of edema in the embryo was defined as when the above ratio was 2×greater than standard deviation of ratios from the control MO injected embryos. Dot plots were produced using GraphPad Prism (GraphPad Software, La Jolla, CA).

Whole-mount immunostaining

Embryos were injected at the 4-cell stage in the left ventral blastomere to target the developing kidney on the left side of the embryo, leaving the right side as an uninjected internal control. Embryos were injected with 20 ng of control MO with 300 pg of GFP mRNA or 20 ng of Xenopus GDA MO with 300 pg of GFP mRNA. At 4 dpf, the embryos were fixed overnight at 4° C in a solution of 4% paraformaldehyde in phosphate-buffered saline (PBS). After 24 hours, the 4% paraformaldehyde solution was removed and embryos were dehydrated in multiple methanol washes, and subsequently rehydrated in a methanol/PBS series. The eyes and surrounding cartilage were removed from each embryo for ease of mounting when imaging. Embryos were bleached under a fluorescent lamp in a 1.8X saline-sodium citrate, 1.5% H2O2, and 5% (vol/vol) formamide solution for 30 minutes. After incubating the embryos in blocking

solution (3% bovine serum albumin, 1% Triton X-100 in PBS) for two hours, embryos were incubated overnight at 4° in 2% 4A6 and 2% 3G8 monoclonal antibodies (European Xenopus Resource Center) in blocking solution. After multiple rinses, embryos were incubated with 0.1% anti-mouse Alexa 488 overnight at 4° C. Embryos were then cleared overnight in BABB solution (33% benzyl alcohol, 66% benzyl benzoate).

Quantification of pronephric tubule diameter

The embryonic kidneys were immunostained using both 3G8 and 4A6 antibodies, specific markers of pronephric tubules and nephrostomes, respectively, in order to obtain a full picture of the kidney. The diameter of each tubule at its widest point was measured at 4 layers through the immunostained embryonic kidney: 35%, 45%, 55%, and 65% through the sample. The average of the widest diameter was obtained for each sample, then a ratio was calculated between the average tubule diameter of the injected and uninjected sides. The Xenopus GDA knockdown condition was compared with the control MO condition, and the results were presented with a dot plot produced with GraphPad Prism (GraphPad Software, La Jolla, CA).

Statistical Analysis

Statistical analyses were performed using GraphPad Prism (GraphPad Software Inc). The D'Agostino and Pearson normality test was used to determine if the data was distributed normally. For MT dynamics analyses, the unpaired Student's t-test was performed when comparing two conditions. To assess statistical significance when quantifying the edema formation, the Mann Whitney test was used, as GDA KD population did not pass the normality

test. At least 3 independent experiments were carried out for each condition. The alpha value was set at 0.05 for all statistical tests, and the P values are represented as follows: *P<0.05, **P<0.01, ***P<0.001 and ****P<0.0001. Values are expressed as mean ± standard error of the mean.

Supplemental Information

For supplementary movie data and information please visit:
https://www.ncbi.nlm.nih.gov/pmc/articles/PMC6452025/

References:

1. Lowery, L. A. & Van Vactor, D. The trip of the tip: understanding the growth cone machinery. *Nat. Rev. Mol. Cell Biol.* **10**, 332–343 (2009).
2. Forscher, P. & Smith, S. J. Actions of cytochalasins on the organization of actin filaments and microtubules in a neuronal growth cone. *J. Cell Biol.* **107**, 1505–1516 (1988).
3. Yamada, K. M., Spooner, B. S. & Wessells, N. K. Ultrastructure and function of growth cones and axons of cultured nerve cells. *Journal of Cell Biology* vol. 49 614–635 http://jcb.rupress.org/content/49/3/614.full.pdf (1971).
4. Bunge, M. B. Fine structure of nerve fibers and growth cones of isolated sympathetic neurons in culture. *J. Cell Biol.* **56**, 713–35 (1973).
5. Bray, D. & Bunge, M. B. Serial analysis of microtubules in cultured rat sensory axons. *J. Neurocytol.* **10**, 589–605 (1981).
6. Tanaka, E., Ho, T. & Kirschner, M. W. The role of microtubule dynamics in growth cone motility and axonal growth. *J. Cell Biol.* **128**, 139–55 (1995).
7. Schaefer, A. W., Kabir, N. & Forscher, P. Filopodia and actin arcs guide the assembly and transport of two populations of microtubules with unique dynamic parameters in neuronal growth cones. *J. Cell Biol.* **158**, 139–52 (2002).
8. Mitchison, T. & Kirschner, M. Cytoskeletal dynamics and nerve growth. *Neuron* **1**, 761–72 (1988).
9. Sabry, J. H. *et al.* Microtubule behavior during guidance of pioneer neuron growth cones in situ. *J. Cell Biol.* **115**, 381–395 (1991).
10. Zhou, F.-Q. & Cohan, C. S. How actin filaments and microtubules steer growth cones to their targets. *J. Neurobiol.* **58**, 84–91 (2004).
11. Bentley, D. & O'Connor, T. P. Cytoskeletal events in growth cone steering. *Curr. Opin. Neurobiol.* **4**, 43–48 (1994).
12. Lin, C. H., Thompson, C. A. & Forscher, P. Cytoskeletal reorganization underlying growth cone motility. *Curr. Opin. Neurobiol.* **4**, 640–7 (1994).
13. Marsh, L. & Letourneau, P. C. Growth of neurites without filopodial or lamellipodial activity in the presence of cytochalasin B. *J. Cell Biol.* **99**, 2041–2047 (1984).
14. Tanaka, E. M. & Kirschner, M. W. Microtubule behavior in the growth cones of living neurons during axon elongation. *J. Cell Biol.* **115**, 345–63 (1991).
15. Drechsel, D. N., Hyman, A. A., Cobb, M. H. & Kirschner, M. W. Modulation of the dynamic instability of tubulin assembly by the microtubule-associated protein tau. *Mol. Biol. Cell* **3**, 1141–1154 (1992).
16. Buck, K. B. & Zheng, J. Q. Growth cone turning induced by direct local modification of microtubule dynamics. *J. Neurosci.* **22**, 9358–67 (2002).
17. Lee, H. *et al.* The microtubule plus end tracking protein Orbit/MAST/CLASP acts downstream of the tyrosine kinase Abl in mediating axon guidance. *Neuron* **42**, 913–26

(2004).

18. Zhou, F.-Q., Zhou, J., Dedhar, S., Wu, Y.-H. & Snider, W. D. NGF-induced axon growth is mediated by localized inactivation of GSK-3beta and functions of the microtubule plus end binding protein APC. *Neuron* **42**, 897–912 (2004).

19. Bearce, E. A., Erdogan, B. & Lowery, L. A. TIPsy tour guides: how microtubule plus-end tracking proteins (+TIPs) facilitate axon guidance. *Front. Cell. Neurosci.* **9**, 241 (2015).

20. Watanabe, T. *et al.* Interaction with IQGAP1 links APC to Rac1, Cdc42, and actin filaments during cell polarization and migration. *Dev. Cell* **7**, 871–83 (2004).

21. Tsvetkov, A. S., Samsonov, A., Akhmanova, A., Galjart, N. & Popov, S. V. Microtubule-binding proteins CLASP1 and CLASP2 interact with actin filaments. *Cell Motil. Cytoskeleton* **64**, 519–30 (2007).

22. Geraldo, S., Khanzada, U. K., Parsons, M., Chilton, J. K. & Gordon-Weeks, P. R. Targeting of the F-actin-binding protein drebrin by the microtubule plus-tip protein EB3 is required for neuritogenesis. *Nat. Cell Biol.* **10**, 1181–1189 (2008).

23. Watanabe, T. *et al.* Phosphorylation of CLASP2 by GSK-3beta regulates its interaction with IQGAP1, EB1 and microtubules. *J. Cell Sci.* **122**, 2969–79 (2009).

24. Suter, D. M. & Forscher, P. Substrate-cytoskeletal coupling as a mechanism for the regulation of growth cone motility and guidance. *J. Neurobiol.* **44**, 97–113 (2000).

25. Jay, D. G. The clutch hypothesis revisited: ascribing the roles of actin-associated proteins in filopodial protrusion in the nerve growth cone. *J. Neurobiol.* **44**, 114–25 (2000).

26. Lin, C. H. & Forscher, P. Growth cone advance is inversely proportional to retrograde F-actin flow. *Neuron* **14**, 763–771 (1995).

27. Medeiros, N. A., Burnette, D. T. & Forscher, P. Myosin II functions in actin-bundle turnover in neuronal growth cones. *Nat. Cell Biol.* **8**, 215–26 (2006).

28. Dent, E. W., Gupton, S. L. & Gertler, F. B. The growth cone cytoskeleton in Axon outgrowth and guidance. *Cold Spring Harb. Perspect. Biol.* **3**, 1–39 (2011).

29. Bradke, F. & Dotti, C. G. The role of local actin instability in axon formation. *Science* **283**, 1931–4 (1999).

30. Mitchison, T. & Kirschner, M. Dynamic instability of microtubule growth. *Nature* **312**, 237–242 (1984).

31. Holy, T. E. & Leibler, S. Dynamic instability of microtubules as an efficient way to search in space. *Proc. Natl. Acad. Sci.* **91**, 5682–5685 (1994).

32. Akhmanova, A. & Steinmetz, M. O. Tracking the ends: a dynamic protein network controls the fate of microtubule tips. *Nat. Rev. Mol. Cell Biol.* **9**, 309–22 (2008).

33. Akhmanova, A. & Steinmetz, M. O. Microtubule +TIPs at a glance. *J. Cell Sci.* **123**, 3415–9 (2010).

34. Al-Bassam, J. & Chang, F. Regulation of microtubule dynamics by TOG-domain proteins XMAP215/Dis1 and CLASP. *Trends Cell Biol.* **21**, 604–14 (2011).

35. Lowery, L. A. & Van Vactor, D. The trip of the tip: understanding the growth cone

machinery. *Nat. Rev. Mol. Cell Biol.* **10**, 332–43 (2009).

36. Akhmanova, A. & Hoogenraad, C. C. Microtubule plus-end-tracking proteins: mechanisms and functions. *Curr. Opin. Cell Biol.* **17**, 47–54 (2005).

37. Galjart, N. CLIPs and CLASPs and cellular dynamics. *Nat. Rev. Mol. Cell Biol.* **6**, 487–498 (2005).

38. Akhmanova, A. & Steinmetz, M. O. Microtubule +TIPs at a glance. *J. Cell Sci.* **123**, 3415–9 (2010).

39. Williamson, T., Gordon-Weeks, P. R., Schachner, M. & Taylor, J. Microtubule reorganization is obligatory for growth cone turning. *Proc. Natl. Acad. Sci. U. S. A.* **93**, 15221–6 (1996).

40. Challacombe, J. F., Snow, D. M. & Letourneau, P. C. Dynamic microtubule ends are required for growth cone turning to avoid an inhibitory guidance cue. *J. Neurosci.* (1997) doi:10.1523/jneurosci.17-09-03085.1997.

41. Zhou, F.-Q., Waterman-Storer, C. M. & Cohan, C. S. Focal loss of actin bundles causes microtubule redistribution and growth cone turning. *J. Cell Biol.* **157**, 839–49 (2002).

42. Gordon-Weeks, P. R. Microtubules and growth cone function. *J. Neurobiol.* **58**, 70–83 (2004).

43. O'Connor, T. P. & Bentley, D. Accumulation of actin in subsets of pioneer growth cone filopodia in response to neural and epithelial guidance cues in situ. *The Journal of cell biology* vol. 123 935–48 http://www.pubmedcentral.nih.gov/articlerender.fcgi?artid=2200150&tool=pmcentrez&rendertype=abstract (1993).

44. Rodriguez, O. C. *et al.* Conserved microtubule-actin interactions in cell movement and morphogenesis. *Nat. Cell Biol.* **5**, 599–609 (2003).

45. Geraldo, S. & Gordon-Weeks, P. R. Cytoskeletal dynamics in growth-cone steering. *J. Cell Sci.* **122**, 3595–604 (2009).

46. Letourneau, P. C. Differences in the organization of actin in the growth cones compared with the neurites of cultured neurons from chick embryos. *J. Cell Biol.* **97**, 963–73 (1983).

47. Burnette, D. T., Schaefer, A. W., Ji, L., Danuser, G. & Forscher, P. Filopodial actin bundles are not necessary for microtubule advance into the peripheral domain of Aplysia neuronal growth cones. *Nat. Cell Biol.* **9**, 1360–9 (2007).

48. Schaefer, A. W. *et al.* Coordination of actin filament and microtubule dynamics during neurite outgrowth. *Dev. Cell* **15**, 146–62 (2008).

49. Lee, A. C. & Suter, D. M. Quantitative analysis of microtubule dynamics during adhesion-mediated growth cone guidance. *Dev. Neurobiol.* **68**, 1363–77 (2008).

50. Alves-Silva, J. *et al.* Spectraplakins promote microtubule-mediated axonal growth by functioning as structural microtubule-associated proteins and EB1-dependent +TIPs (tip interacting proteins). *J. Neurosci.* **32**, 9143–58 (2012).

51. Engel, U. *et al.* Abelson phosphorylation of CLASP2 modulates its association with microtubules and actin. *Cytoskeleton* **71**, 195–209 (2014).

52. Marx, A. *et al.* Xenopus cytoplasmic linker-associated protein 1 (XCLASP1) promotes axon elongation and advance of pioneer microtubules. *Mol. Biol. Cell* **24**, 1544–58 (2013).

53. Hur, E.-M. *et al.* GSK3 controls axon growth via CLASP-mediated regulation of growth cone microtubules. *Genes Dev.* **25**, 1968–81 (2011).

54. Tanaka, E. & Kirschner, M. W. The role of microtubules in growth cone turning at substrate boundaries. *J. Cell Biol.* **128**, 127–37 (1995).

55. Lanier, L. M. & Gertler, F. B. From Abl to actin: Abl tyrosine kinase and associated proteins in growth cone motility. *Curr. Opin. Neurobiol.* **10**, 80–7 (2000).

56. Wills, Z., Bateman, J., Korey, C. A., Comer, A. & Van Vactor, D. The tyrosine kinase Abl and its substrate enabled collaborate with the receptor phosphatase Dlar to control motor axon guidance. *Neuron* **22**, 301–312 (1999).

57. Koleske, A. J. *et al.* Essential roles for the Abl and Arg tyrosine kinases in neurulation. *Neuron* **21**, 1259–72 (1998).

58. Moseley, J. B. *et al.* Regulated binding of adenomatous polyposis coli protein to actin. *J. Biol. Chem.* **282**, 12661–8 (2007).

59. Koester, M. P., Müller, O. & Pollerberg, G. E. Adenomatous polyposis coli is differentially distributed in growth cones and modulates their steering. *J. Neurosci.* **27**, 12590–600 (2007).

60. Purro, S. A. *et al.* Wnt regulates axon behavior through changes in microtubule growth directionality: a new role for adenomatous polyposis coli. *J. Neurosci.* **28**, 8644–54 (2008).

61. Marshall, T. W., Lloyd, I. E., Delalande, J. M., Näthke, I. & Rosenblatt, J. The tumor suppressor adenomatous polyposis coli controls the direction in which a cell extrudes from an epithelium. *Mol. Biol. Cell* **22**, 3962–70 (2011).

62. Komarova, Y. *et al.* Mammalian end binding proteins control persistent microtubule growth. *J. Cell Biol.* **184**, 691–706 (2009).

63. Vitre, B. *et al.* EB1 regulates microtubule dynamics and tubulin sheet closure in vitro. *Nat. Cell Biol.* **10**, 415–21 (2008).

64. Honnappa, S. *et al.* An EB1-Binding Motif Acts as a Microtubule Tip Localization Signal. *Cell* **138**, 366–376 (2009).

65. Tortosa, E., Galjart, N., Avila, J. & Sayas, C. L. MAP1B regulates microtubule dynamics by sequestering EB1/3 in the cytosol of developing neuronal cells. *EMBO J.* **32**, 1293–306 (2013).

66. Sharma, V. M., Litersky, J. M., Bhaskar, K. & Lee, G. Tau impacts on growth-factor-stimulated actin remodeling. *J. Cell Sci.* **120**, 748–57 (2007).

67. Pedrotti, B. & Islam, K. Dephosphorylated but not phosphorylated microtubule associated protein MAP1B binds to microfilaments. *FEBS Lett.* **388**, 131–133 (1996).

68. Cross, D., Vial, C. & Maccioni, R. B. A tau-like protein interacts with stress fibers and microtubules in human and rodent cultured cell lines. *J. Cell Sci.* **105 (Pt 1**, 51–60 (1993).

69. Worth, D. C., Daly, C. N., Geraldo, S., Oozeer, F. & Gordon-Weeks, P. R. Drebrin contains a cryptic F-actin-bundling activity regulated by Cdk5 phosphorylation. *J. Cell Biol.* **202**, 793–806 (2013).

70. Tanabe, K. *et al.* Phosphorylation of drebrin by cyclin-dependent kinase 5 and its role in neuronal migration. *PLoS One* **9**, e92291 (2014).

71. Dun, X. *et al.* Drebrin controls neuronal migration through the formation and alignment of the leading process. *Mol. Cell. Neurosci.* **49**, 341–50 (2012).

72. Sonego, M. *et al.* Drebrin regulates neuroblast migration in the postnatal mammalian brain. *PLoS One* **10**, e0126478 (2015).

73. Kreis, P. *et al.* Phosphorylation of the actin binding protein Drebrin at S647 is regulated by neuronal activity and PTEN. *PLoS One* **8**, e71957 (2013).

74. Sharma, S., Grintsevich, E. E., Phillips, M. L., Reisler, E. & Gimzewski, J. K. Atomic force microscopy reveals drebrin induced remodeling of f-actin with subnanometer resolution. *Nano Lett.* **11**, 825–7 (2011).

75. Mikati, M. A., Grintsevich, E. E. & Reisler, E. Drebrin-induced stabilization of actin filaments. *J. Biol. Chem.* **288**, 19926–38 (2013).

76. Grintsevich, E. E. & Reisler, E. Drebrin inhibits cofilin-induced severing of F-actin. *Cytoskeleton* **71**, 472–483 (2014).

77. Leung, C. L., Sun, D., Zheng, M., Knowles, D. R. & Liem, R. K. H. Microtubule actin cross-linking factor (MACF): A hybrid of dystonin and dystrophin that can interact with the actin and microtubule cytoskeletons. *J. Cell Biol.* **147**, 1275–1285 (1999).

78. Fuchs, E. & Karakesisoglou, I. Bridging cytoskeletal intersections. *Genes Dev.* **15**, 1–14 (2001).

79. Kodama, A., Karakesisoglou, I., Wong, E., Vaezi, A. & Fuchs, E. ACF7: An essential integrator of microtubule dynamics. *Cell* **115**, 343–354 (2003).

80. Applewhite, D. A. *et al.* The spectraplakin Short stop is an actin-microtubule cross-linker that contributes to organization of the microtubule network. *Mol. Biol. Cell* **21**, 1714–1724 (2010).

81. Stroud, M. J., Kammerer, R. A. & Ballestrem, C. Characterization of G2L3 (GAS2-like 3), a new microtubule- and actin-binding protein related to spectraplakins. *J. Biol. Chem.* **286**, 24987–95 (2011).

82. Suozzi, K. C., Wu, X. & Fuchs, E. Spectraplakins: Master orchestrators of cytoskeletal dynamics. *Journal of Cell Biology* vol. 197 465–475 (2012).

83. Slep, K. C. *et al.* Structural determinants for EB1-mediated recruitment of APC and spectraplakins to the microtubule plus end. *J. Cell Biol.* **168**, 587–598 (2005).

84. Margaron, Y., Fradet, N. & Côté, J. F. ELMO recruits actin cross-linking family 7 (ACF7) at the cell membrane for microtubule capture and stabilization of cellular protrusions. *J. Biol. Chem.* **288**, 1184–1199 (2013).

85. Ka, M., Jung, E.-M., Mueller, U. & Kim, W.-Y. MACF1 regulates the migration of pyramidal neurons via microtubule dynamics and GSK-3 signaling. *Dev. Biol.* **395**, 4–18

(2014).

86. Sanchez-Soriano, N. *et al.* Mouse ACF7 and drosophila short stop modulate filopodia formation and microtubule organisation during neuronal growth. *J. Cell Sci.* **122**, 2534–42 (2009).

87. Applewhite, D. a, Grode, K. D., Duncan, M. C. & Rogers, S. L. The actin-microtubule cross-linking activity of Drosophila Short stop is regulated by intramolecular inhibition. *Mol. Biol. Cell* **24**, 2885–93 (2013).

88. Drabek, K. *et al.* Role of CLASP2 in Microtubule Stabilization and the Regulation of Persistent Motility. *Curr. Biol.* **16**, 2259–2264 (2006).

89. Van Vactor, D., Sink, H., Fambrough, D., Tsoo, R. & Goodman, C. S. Genes that control neuromuscular specificity in Drosophila. *Cell* **73**, 1137–1153 (1993).

90. Wu, X., Kodama, A. & Fuchs, E. ACF7 Regulates Cytoskeletal-Focal Adhesion Dynamics and Migration and Has ATPase Activity. *Cell* **135**, 137–148 (2008).

91. Stehbens, S. & Wittmann, T. Targeting and transport: how microtubules control focal adhesion dynamics. *J. Cell Biol.* **198**, 481–9 (2012).

92. Zaoui, K., Benseddik, K., Daou, P., Salaün, D. & Badache, A. ErbB2 receptor controls microtubule capture by recruiting ACF7 to the plasma membrane of migrating cells. *Proc. Natl. Acad. Sci. U. S. A.* **107**, 18517–18522 (2010).

93. Gard, D. L. & Kirschner, M. W. A microtubule-associated protein from Xenopus eggs that specifically promotes assembly at the plus-end. *J. Cell Biol.* **105**, 2203–2215 (1987).

94. Brouhard, G. J. *et al.* XMAP215 is a processive microtubule polymerase. *Cell* **132**, 79–88 (2008).

95. Lowery, L. A. *et al.* Parallel genetic and proteomic screens identify msps as a clasp-abl pathway interactor in Drosophila. *Genetics* **185**, 1311–1325 (2010).

96. van der Vaart, B. *et al.* SLAIN2 links microtubule plus end-tracking proteins and controls microtubule growth in interphase. *J. Cell Biol.* **193**, 1083–1099 (2011).

97. van der Vaart, B. *et al.* Microtubule Plus-End Tracking Proteins SLAIN1/2 and ch-TOG Promote Axonal Development. *Journal of Neuroscience* vol. 32 14722–14728 (2012).

98. Nwagbara, B. U. *et al.* TACC3 is a microtubule plus end-tracking protein that promotes axon elongation and also regulates microtubule plus end dynamics in multiple embryonic cell types. *Mol. Biol. Cell* **25**, 3350–62 (2014).

99. Riquelme, D. N., Meyer, A. S., Barzik, M., Keating, A. & Gertler, F. B. Selectivity in subunit composition of Ena/VASP tetramers. *Biosci. Rep.* (2015) doi:10.1042/BSR20150149.

100. Erdogan, B. *et al.* Investigating the impact of the phosphorylation status of tyrosine residues within the TACC domain of TACC3 on microtubule behavior during axon growth and guidance . *Cytoskeleton* (2020) doi:10.1002/cm.21622.

101. Widlund, P. O. *et al.* XMAP215 polymerase activity is built by combining multiple tubulin-binding TOG domains and a basic lattice-binding region. *Proc. Natl. Acad. Sci. U. S. A.* (2011) doi:10.1073/pnas.1016498108.

102. Fox, J. C., Howard, A. E., Currie, J. D., Rogers, S. L. & Slep, K. C. The XMAP215 family drives microtubule polymerization using a structurally diverse TOG array. *Mol. Biol. Cell* (2014) doi:10.1091/mbc.E13-08-0501.

103. Mortuza, G. B. *et al.* XTACC3-XMAP215 association reveals an asymmetric interaction promoting microtubule elongation. *Nat. Commun.* **5**, 5072 (2014).

104. O'Brien, A. *et al.* The Xenopus TACC Homologue, Maskin, Functions in Mitotic Spindle Assembly□. *Mol. Biol. Cell* **16**, 1–13 (2005).

105. Byrnes, A. E. & Slep, K. C. TOG-tubulin binding specificity promotes microtubule dynamics and mitotic spindle formation. *J. Cell Biol.* (2017) doi:10.1083/jcb.201610090.

106. Lu, W., Fox, P., Lakonishok, M., Davidson, M. W. & Gelfand, V. I. Initial neurite outgrowth in Drosophila neurons is driven by kinesin-powered microtubule sliding. *Curr. Biol.* **23**, 1018–23 (2013).

107. Myers, K. A. *et al.* Antagonistic forces generated by cytoplasmic dynein and myosin-II during growth cone turning and axonal retraction. *Traffic* **7**, 1333–51 (2006).

108. Buck, K. B. & Zheng, J. Q. Growth cone turning induced by direct local modification of microtubule dynamics. *J. Neurosci.* **22**, 9358–9367 (2002).

109. Slater, P. G. . *et al.* XMAP215 promotes microtubule–F-actin interactions to regulate growth cone microtubules during axon guidance in Xenopus laevis. *J. Cell Sci.* **132**, (2019).

110. Hur, E. M. *et al.* GSK3 controls axon growth via CLASP-mediated regulation of growth cone microtubules. *Genes Dev.* **25**, 1968–1981 (2011).

111. Coles, C. H. & Bradke, F. Coordinating Neuronal Actin-Microtubule Dynamics. *Current Biology* (2015) doi:10.1016/j.cub.2015.06.020.

112. Lowery, L. A. *et al.* Growth cone-specific functions of XMAP215 in restricting microtubule dynamics and promoting axonal outgrowth. *Neural Dev.* **8**, 22 (2013).

113. Vitriol, E. A. & Zheng, J. Q. Growth Cone Travel in Space and Time: The Cellular Ensemble of Cytoskeleton, Adhesion, and Membrane. *Neuron* (2012) doi:10.1016/j.neuron.2012.03.005.

114. Biswas, S. & Kalil, K. The microtubule-associated protein tau mediates the organization of microtubules and their dynamic exploration of actin-rich lamellipodia and filopodia of cortical growth cones. *J. Neurosci.* (2018) doi:10.1523/JNEUROSCI.2281-17.2017.

115. Cammarata, G. M., Bearce, E. A. & Lowery, L. A. Cytoskeletal social networking in the growth cone: How +TIPs mediate microtubule-actin cross-linking to drive axon outgrowth and guidance. *Cytoskeleton* (2016) doi:10.1002/cm.21272.

116. Neukirchen, D. & Bradke, F. Cytoplasmic linker proteins regulate neuronal polarization through microtubule and growth cone dynamics. *J. Neurosci.* **31**, 1528–1538 (2011).

117. Prokop, A. The intricate relationship between microtubules and their associated motor proteins during axon growth and maintenance. *Neural Development* (2013) doi:10.1186/1749-8104-8-17.

118. Ayaz, P., Ye, X., Huddleston, P., Brautigam, C. A. & Rice, L. M. A TOG:αβ-tubulin

complex structure reveals conformation-based mechanisms for a microtubule polymerase. *Science (80-.).* (2012) doi:10.1126/science.1221698.

119. Flor-Parra, I., Iglesias-Romero, A. B. & Chang, F. The XMAP215 Ortholog Alp14 Promotes Microtubule Nucleation in Fission Yeast. *Curr. Biol.* (2018) doi:10.1016/j.cub.2018.04.008.

120. Thawani, A., Kadzik, R. S. & Petry, S. XMAP215 is a microtubule nucleation factor that functions synergistically with the γ-tubulin ring complex. *Nat. Cell Biol.* (2018) doi:10.1038/s41556-018-0091-6.

121. Zanic, M., Widlund, P. O., Hyman, A. a & Howard, J. Synergy between XMAP215 and EB1 increases microtubule growth rates to physiological levels. *Nat. Cell Biol.* **15**, 1–8 (2013).

122. Kalil, K., Szebenyi, G. & Dent, E. W. Common mechanisms underlying growth cone guidance and axon branching. *J. Neurobiol.* (2000) doi:10.1002/1097-4695(200008)44:2<145::aid-neu5>3.3.co;2-o.

123. Knöll, B. *et al.* Graded expression patterns of ephrin-As in the superior colliculus after lesion of the adult mouse optic nerve. *Mech. Dev.* (2001) doi:10.1016/S0925-4773(01)00431-2.

124. Monnier, P. P., Sierra, A., Schwab, J. M., Henke-Fahle, S. & Mueller, B. K. The Rho/ROCK pathway mediates neurite growth-inhibitory activity associated with the chondroitin sulfate proteoglycans of the CNS glial scar. *Mol. Cell. Neurosci.* (2003) doi:10.1016/S1044-7431(02)00035-0.

125. Wizenmann, A. & Bähr, M. Growth characteristics of ganglion cell axon in the developing and regenerating retino-tectal projection of the rat. *Cell Tissue Res.* (1997) doi:10.1007/s004410050946.

126. Voelzmann, A., Hahn, I., Pearce, S. P., Sánchez-Soriano, N. & Prokop, A. A conceptual view at microtubule plus end dynamics in neuronal axons. *Brain Res. Bull.* (2016) doi:10.1016/j.brainresbull.2016.08.006.

127. Dent, E. W., Callaway, J. L., Szebenyi, G., Baas, P. W. & Kalil, K. Reorganization and movement of microtubules in axonal growth cones and developing interstitial branches. *J. Neurosci.* (1999) doi:10.1523/jneurosci.19-20-08894.1999.

128. Hendricks, M. & Jesuthasan, S. PHR regulates growth cone pausing at intermediate targets through microtubule disassembly. *J. Neurosci.* (2009) doi:10.1523/JNEUROSCI.1115-09.2009.

129. Thakur, H. C. *et al.* The centrosomal adaptor TACC3 and the microtubule polymerase chTOG interact via defined C-terminal subdomains in an Aurora-A kinase-independent manner. *J. Biol. Chem.* **289**, 74–88 (2014).

130. Lee, M. J., Gergely, F., Jeffers, K., Peak-Chew, S. Y. & Raff, J. W. Msps/XMAP215 interacts with the centrosomal protein D-TACC to regulate microtubule behaviour. *Nat. Cell Biol.* **3**, 643–9 (2001).

131. Popov, A. V., Severin, F. & Karsenti, E. XMAP215 Is Required for the Microtubule-Nucleating Activity of Centrosomes. *Curr. Biol.* **12**, 1326–1330 (2002).

132. Al-Bassam, J. *et al.* Fission yeast Alp14 is a dose-dependent plus end-tracking microtubule polymerase. *Mol. Biol. Cell* (2012) doi:10.1091/mbc.E12-03-0205.

133. Milunovic-Jevtic, A., Jevtic, P., Levy, D. L. & Gatlin, J. C. In vivo mitotic spindle scaling can be modulated by changing the levels of a single protein: the microtubule polymerase XMAP215. *Mol. Biol. Cell* (2018) doi:10.1091/mbc.E18-01-0011.

134. Reber, S. B. *et al.* XMAP215 activity sets spindle length by controlling the total mass of spindle microtubules. *Nat. Cell Biol.* (2013) doi:10.1038/ncb2834.

135. Shirasu-Hiza, M., Coughlin, P. & Mitchison, T. Identification of XMAP215 as a microtubule-destabilizing factor in Xenopus egg extract by biochemical purification. *J. Cell Biol.* (2003) doi:10.1083/jcb.200211095.

136. Humphrey, L., Felzer-Kim, I. & Joglekar, A. P. Stu2 acts as a microtubule destabilizer in metaphase budding yeast spindles. *Mol. Biol. Cell* (2018) doi:10.1091/mbc.E17-08-0494.

137. McConnell, R. E. *et al.* A requirement for filopodia extension toward Slit during Robo-mediated axon repulsion. *J. Cell Biol.* (2016) doi:10.1083/jcb.201509062.

138. Ezratty, E. J., Partridge, M. A. & Gundersen, G. G. Microtubule-induced focal adhesion disassembly is mediated by dynamin and focal adhesion kinase. *Nat. Cell Biol.* (2005) doi:10.1038/ncb1262.

139. Burnette, D. T. *et al.* Myosin II Activity Facilitates Microtubule Bundling in the Neuronal Growth Cone Neck. *Dev. Cell* (2008) doi:10.1016/j.devcel.2008.05.016.

140. Schaefer, A. W. *et al.* Coordination of Actin Filament and Microtubule Dynamics during Neurite Outgrowth. *Dev. Cell* (2008) doi:10.1016/j.devcel.2008.05.003.

141. Adikes, R. C., Hallett, R. A., Saway, B. F., Kuhlman, B. & Slep, K. C. Control of microtubule dynamics using an optogenetic microtubule plus end-F-actin cross-linker. *J. Cell Biol.* (2018) doi:10.1083/jcb.201705190.

142. Erdogan, B. *et al.* The microtubule plus-end-tracking protein TACC3 promotes persistent axon outgrowth and mediates responses to axon guidance signals during development. *Neural Dev.* (2017) doi:10.1186/s13064-017-0080-7.

143. Sive, H. L., Grainger, R. M. & Harland, R. M. Early Development of Xenopus Laevis: A Laboratory Manual. *Spring* (2000).

144. Nieuwkoop P., F. J. *Normal Table of Xenopus Laevis (Daudin): A Systematical & Chronological Survey of the Development from the Fertilized Egg till the End of Metamorphosis*. *Http://Www.Xenbase.Org/Anatomy/Alldev.Do* (1994).

145. Applegate, K. T. *et al.* plusTipTracker: Quantitative image analysis software for the measurement of microtubule dynamics. *J. Struct. Biol.* **176**, 168–84 (2011).

146. Lowery, L. A., Faris, A. E. R., Stout, A. & Van Vactor, D. Neural Explant Cultures from Xenopus laevis. *J. Vis. Exp.* e4232 (2012) doi:10.3791/4232.

147. Kinoshita, K., Arnal, I., Desai, A., Drechsel, D. N. & Hyman, A. A. Reconstitution of physiological microtubule dynamics using purified components. *Science (80-.).* (2001) doi:10.1126/science.1064629.

148. Nithianantham, S. *et al.* Structural basis of tubulin recruitment and assembly by

microtubule polymerases with tumor overexpressed gene (TOG) domain arrays. *Elife* **7**, (2018).

149. Slater, P. G. *et al.* XMAP215 promotes microtubule–F-actin interactions to regulate growth cone microtubules during axon guidance in Xenopus laevis. *J. Cell Sci.* **132**, (2019).

150. Srivastava, J. & Barber, D. Actin co-sedimentation assay; for the analysis of protein binding to F-actin. *J. Vis. Exp.* (2008) doi:10.3791/690.

151. Van Breugel, M., Drechsel, D. & Hyman, A. Stu2p, the budding yeast member of the conserved Dis1/XMAP215 family of microtubule-associated proteins is a plus end-binding microtubule destabilizer. *J. Cell Biol.* (2003) doi:10.1083/jcb.200211097.

152. Al-Bassam, J., Van Breugel, M., Harrison, S. C. & Hyman, A. Stu2p binds tubulin and undergoes an open-to-closed conformational change. *J. Cell Biol.* **172**, 1009–1022 (2006).

153. Wang, H. W. & Nogales, E. Nucleotide-dependent bending flexibility of tubulin regulates microtubule assembly. *Nature* (2005) doi:10.1038/nature03606.

154. Van Troys, M., Vandekerckhove, J. & Ampe, C. Structural modules in actin-binding proteins: Towards a new classification. *Biochimica et Biophysica Acta - Molecular Cell Research* (1999) doi:10.1016/S0167-4889(98)00152-9.

155. Rostkova, E., Burgess, S. G., Bayliss, R. & Pfuhl, M. Solution NMR assignment of the C-terminal domain of human chTOG. *Biomol. NMR Assign.* (2018) doi:10.1007/s12104-018-9812-9.

156. Gutzmann, J. H. & Sive, H. Epithelial relaxation mediated by the myosin phosphatase regulator Mypt1 is required for brain ventricle lumenexpansion and hindbrain morphogenesis. *Development* (2010) doi:10.1242/dev.042705.

157. Srivastava, J. & Barber, D. Actin co-sedimentation assay; for the analysis of protein binding to F-Actin. *J. Vis. Exp.* (2008) doi:10.3791/690.

158. Gard, D. L. & Kirschner, M. W. Microtubule assembly in cytoplasmic extracts of Xenopus oocytes and eggs. *J. Cell Biol.* **105**, 2191–201 (1987).

159. Telley, I. A., Bieling, P. & Surrey, T. Reconstitution and quantification of dynamic microtubule end tracking in vitro using TIRF microscopy. *Methods Mol. Biol.* **777**, 127–45 (2011).

160. Jaiswal, R. *et al.* Drosophila Homologues of Adenomatous Polyposis Coli (APC) and the Formin Diaphanous Collaborate by a Conserved Mechanism to Stimulate Actin Filament Assembly. *J. Biol. Chem.* **288**, 13897–13905 (2013).

161. Okada, K. *et al.* Adenomatous polyposis coli protein nucleates actin assembly and synergizes with the formin mDia1. *J. Cell Biol.* **189**, 1087–96 (2010).

162. Bartolini, F. *et al.* The formin mDia2 stabilizes microtubules independently of its actin nucleation activity. *J. Cell Biol.* **181**, 523–36 (2008).

163. Stepanova, T. *et al.* Visualization of microtubule growth in cultured neurons via the use of EB3-GFP (end-binding protein 3-green fluorescent protein). *J. Neurosci.* **23**, 2655–64 (2003).

164. Purro, S. A. *et al.* Wnt regulates axon behavior through changes in microtubule growth directionality: a new role for adenomatous polyposis coli. *J. Neurosci.* **28**, 8644–8654 (2008).

165. Dunsch, A. K., Linnane, E., Barr, F. A. & Gruneberg, U. The astrin-kinastrin/SKAP complex localizes to microtubule plus ends and facilitates chromosome alignment. *J. Cell Biol.* **192**, 959–968 (2011).

166. Cao, D. *et al.* Signaling Scaffold Protein IQGAP1 Interacts with Microtubule Plus-end Tracking Protein SKAP and Links Dynamic Microtubule Plus-end to Steer Cell Migration. *J. Biol. Chem.* **290**, 23766–23780 (2015).

167. Maier, B., Kirsch, M., Anderhub, S., Zentgraf, H. & Kramer, A. The novel actin/focal adhesion-associated protein MISP is involved in mitotic spindle positioning in human cells. *Cell Cycle* **12**, 1457–1471 (2013).

168. Leung, L. & Holt, C. E. Imaging axon pathfinding in Xenopus in vivo. *Cold Spring Harb. Protoc.* **2012**, 984–991 (2012).

169. Preciado López, M. *et al.* In vitro reconstitution of dynamic microtubules interacting with actin filament networks. *Methods Enzymol.* **540**, 301–320 (2014).

170. Xia, P. *et al.* Superresolution imaging reveals structural features of EB1 in microtubule plus-end tracking. *Mol. Biol. Cell* **25**, 4166–4173 (2014).

171. Lasser, M., Tiber, J. & Lowery, L. A. The role of the microtubule cytoskeleton in neurodevelopmental disorders. *Frontiers in Cellular Neuroscience* (2018) doi:10.3389/fncel.2018.00165.

172. Erdogan, B., Ebbert, P. T. & Lowery, L. A. Using Xenopus laevis retinal and spinal neurons to study mechanisms of axon guidance in vivo and in vitro. *Seminars in Cell and Developmental Biology* (2016) doi:10.1016/j.semcdb.2016.02.003.

173. Slater, P. G., Hayrapetian, L. & Lowery, L. A. Xenopus laevis as a model system to study cytoskeletal dynamics during axon pathfinding. *Genesis* (2017) doi:10.1002/dvg.22994.

174. Wurdak, H. *et al.* Erratum: A small molecule accelerates neuronal differentiation in the adult rat (Proceedings of the National Academy of Sciences of the United Stated of America (2010) 107 (16542-16547) DOI: 10.1073/pnas.1010300107)). *Proceedings of the National Academy of Sciences of the United States of America* (2010) doi:10.1073/pnas.1016908108.

175. Stein, E. & Tessier-Lavigne, M. Hierarchical organization of guidance receptors: Silencing of netrin attraction by slit through a Robo/DCC receptor complex. *Science (80-.).* (2001) doi:10.1126/science.1058445.

176. Piper, M. *et al.* Signaling mechanisms underlying Slit2-induced collapse of Xenopus retinal growth cones. *Neuron* (2006) doi:10.1016/j.neuron.2005.12.008.

177. Myers, J. P., Robles, E., Ducharme-Smith, A. & Gomez, T. M. Focal adhesion kinase modulates Cdc42 activity downstream of positive and negative axon guidance cues. *J. Cell Sci.* (2012) doi:10.1242/jcs.100107.

178. Long, J. B. *et al.* Multiparametric Analysis of CLASP-Interacting Protein Functions

during Interphase Microtubule Dynamics. *Mol. Cell. Biol.* (2013) doi:10.1128/mcb.01442-12.

179. Stehbens, S. J. *et al.* CLASPs link focal-adhesion-associated microtubule capture to localized exocytosis and adhesion site turnover. *Nat. Cell Biol.* (2014) doi:10.1038/ncb2975.

180. Mimori-Kiyosue, Y. *et al.* CLASP1 and CLASP2 bind to EB1 and regulate microtubule plus-end dynamics at the cell cortex. *J. Cell Biol.* (2005) doi:10.1083/jcb.200405094.

181. Wen, Y. *et al.* EB1 and APC bind to mDia to stabilize microtubules downstream of Rho and promote cell migration. *Nat. Cell Biol.* **6**, 820–830 (2004).

182. Zumbrunn, J., Kinoshita, K., Hyman, A. A. & Näthke, I. S. Binding of the adenomatous polyposis coli protein to microtubules increases microtubule stability and is regulated by GSK3β phosphorylation. *Curr. Biol.* **11**, 44–49 (2001).

183. Lucaj, C. M. *et al.* Xenopus TACC1 is a microtubule plus-end tracking protein that can regulate microtubule dynamics during embryonic development. *Cytoskeleton* (2015) doi:10.1002/cm.21224.

184. Rutherford, E. L. *et al.* Xenopus TACC2 is a microtubule plus end-tracking protein that can promote microtubule polymerization during embryonic development. *Mol. Biol. Cell* (2016) doi:10.1091/mbc.E16-03-0198.

185. Peset, I. *et al.* Function and regulation of Maskin, a TACC family protein, in microtubule growth during mitosis. *J. Cell Biol.* **170**, 1057–66 (2005).

186. Ren, Y. & Suter, D. M. Increase in Growth Cone Size Correlates with Decrease in Neurite Growth Rate. *Neural Plast.* (2016) doi:10.1155/2016/3497901.

187. Kumar, P. *et al.* GSK3beta phosphorylation modulates CLASP-microtubule association and lamella microtubule attachment. *J. Cell Biol.* **184**, 895–908 (2009).

188. Kumar, P. *et al.* Multisite phosphorylation disrupts arginine-glutamate salt bridge networks required for binding of cytoplasmic linker-associated protein 2 (CLASP2) to end-binding protein 1 (EB1). *J. Biol. Chem.* (2012) doi:10.1074/jbc.M111.316661.

189. Watanabe, T. *et al.* Phosphorylation of CLASP2 by GSK-3beta regulates its interaction with IQGAP1, EB1 and microtubules. *J. Cell Sci.* **122**, 2969–79 (2009).

190. Wu, X. *et al.* Skin stem cells orchestrate directional migration by regulating microtubule-ACF7 connections through GSK3β. *Cell* **144**, 341–352 (2011).

191. Honnappa, S., John, C. M., Kostrewa, D., Winkler, F. K. & Steinmetz, M. O. Structural insights into the EB1-APC interaction. *EMBO J.* **24**, 261–269 (2005).

192. Wen, Y. *et al.* EB1 and APC bind to mDia to stabilize microtubules downstream of Rho and promote cell migration. *Nat. Cell Biol.* (2004) doi:10.1038/ncb1160.

193. Kinoshita, K. *et al.* Aurora A phosphorylation of TACC3/maskin is required for centrosome-dependent microtubule assembly in mitosis. *J. Cell Biol.* **170**, 1047–1055 (2005).

194. Iimori, M. *et al.* A mutation of the fission yeast EB1 overcomes negative regulation by phosphorylation and stabilizes microtubules. *Exp. Cell Res.* (2012)

doi:10.1016/j.yexcr.2011.11.006.

195. Zhang, Z. *et al.* Structural basis for the recognition of Asef by adenomatous polyposis coli. *Cell Res.* **22**, 372–86 (2012).

196. Zhang, Y. *et al.* Proto-oncogenic Src phosphorylates EB1 to regulate the microtubule-focal adhesion crosstalk and stimulate cell migration. *Theranostics* (2016) doi:10.7150/thno.16356.

197. Hubner, N. C. *et al.* Quantitative proteomics combined with BAC TransgeneOmics reveals in vivo protein interactions. *J. Cell Biol.* (2010) doi:10.1083/jcb.200911091.

198. Nelson, K. N. *et al.* Oncogenic gene fusion FGFR3-TACC3 Is regulated by tyrosine phosphorylation. *Mol. Cancer Res.* (2016) doi:10.1158/1541-7786.MCR-15-0497.

199. Sarkar, S., Ryan, E. L. & Royle, S. J. FGFR3-TACC3 cancer gene fusions cause mitotic defects by removal of endogenous TACC3 from the mitotic spindle. *Open Biol.* (2017) doi:10.1098/rsob.170080.

200. Mariotti, A. *et al.* EGF-R signaling through fyn kinase disrupts the function of integrin α6β4 at hemidesmosomes: Role in epithelial cell migration and carcinoma invasion. *J. Cell Biol.* (2001) doi:10.1083/jcb.200105017.

201. St. Clair, R. M. *et al.* PKC induces release of a functional ectodomain of the guidance cue semaphorin6A. *FEBS Lett.* (2019) doi:10.1002/1873-3468.13561.

202. Cheerathodi, M., Vincent, J. J. & Ballif, B. A. Quantitative comparison of CrkL-SH3 binding proteins from embryonic murine brain and liver: Implications for developmental signaling and the quantification of protein species variants in bottom-up proteomics. *J. Proteomics* (2015) doi:10.1016/j.jprot.2015.04.033.

203. St. Clair, R. M. *et al.* Fyn-dependent phosphorylation of PlexinA1 and PlexinA2 at conserved tyrosines is essential for zebrafish eye development. *FEBS J.* (2018) doi:10.1111/febs.14313.

204. Akum, B. F. *et al.* Cypin regulates dendrite patterning in hippocampal neurons by promoting microtubule assembly. *Nat. Neurosci.* (2004) doi:10.1038/nn1179.

205. Braunschweig, D. *et al.* Autism-specific maternal autoantibodies recognize critical proteins in developing brain. *Transl. Psychiatry* (2013) doi:10.1038/tp.2013.50.

206. Fuller, H. R., Hurtado, M. L., Wishart, T. M. & Gates, M. A. The rat striatum responds to nigro-striatal degeneration via the increased expression of proteins associated with growth and regeneration of neuronal circuitry. *Proteome Sci.* (2014) doi:10.1186/1477-5956-12-20.

207. Firestein, B. L. *et al.* Cypin: A cytosolic regulator of PSD-95 postsynaptic targeting. *Neuron* (1999) doi:10.1016/S0896-6273(00)81120-4.

208. Schmidt, E. F. & Strittmatter, S. M. The CRMP family of proteins and their role in Sema3A signaling. *Advances in Experimental Medicine and Biology* (2007) doi:10.1007/978-0-387-70956-7_1.

209. Sweet, E. S. *et al.* PSD-95 alters microtubule dynamics via an association with EB3. *J. Neurosci.* (2011) doi:10.1523/JNEUROSCI.1205-10.2011.

210. Fernández, J. R., Byrne, B. & Firestein, B. L. Phylogenetic analysis and molecular evolution of guanine deaminases: From guanine to dendrites. *J. Mol. Evol.* (2009) doi:10.1007/s00239-009-9205-x.

211. Vize, P. D., Jones, E. A. & Pfister, R. Development of the Xenopus pronephric system. *Dev. Biol.* (1995) doi:10.1006/dbio.1995.1302.

212. Wessely, O. & Tran, U. Xenopus pronephros development-past, present, and future. in *Pediatric Nephrology* (2011). doi:10.1007/s00467-011-1881-2.

213. Krneta-Stankic, V., DeLay, B. D. & Miller, R. K. Xenopus: leaping forward in kidney organogenesis. *Pediatric Nephrology* (2017) doi:10.1007/s00467-016-3372-y.

214. Chen, M. *et al.* A novel role for snapin in dendrite patterning: Interaction with cypin. *Mol. Biol. Cell* (2005) doi:10.1091/mbc.E05-02-0165.

215. Chen, H. & Firestein, B. L. RhoA regulates dendrite branching in hippocampal neurons by decreasing cypin protein levels. *J. Neurosci.* (2007) doi:10.1523/JNEUROSCI.0872-07.2007.

216. Sheng, M. & Sala, C. PDZ Domains and the Organization of Supramolecular Complexes. *Annu. Rev. Neurosci.* (2001) doi:10.1146/annurev.neuro.24.1.1.

217. Fukata, M. *et al.* Rac1 and Cdc42 capture microtubules through IQGAP1 and CLIP-170. *Cell* **109**, 873–85 (2002).

218. KUMAR, S., TEWARI, K. K. & KRISHNAN, P. S. GUANINE-DEAMINASE ACTIVITY IN RAT BRAIN AND LIVER. *Biochem. J.* (1965) doi:10.1042/bj0950797.

219. Kumar, S., Josan, V., Sanger, K. C. S., Tewari, K. . & Krishnan, P. S. Studies on guanine deaminase and its inhibitors in rat tissue. *Biochem. J.* (1967) doi:10.1042/bj1020691.

220. Charych, E. I. *et al.* Activity-independent regulation of dendrite patterning by postsynaptic density protein PSD-95. *J. Neurosci.* (2006) doi:10.1523/JNEUROSCI.2379-06.2006.

221. Mcfarlane, S. & Lom, B. The Xenopus retinal ganglion cell as a model neuron to study the establishment of neuronal connectivity. *Dev. Neurobiol.* (2012) doi:10.1002/dneu.20928.